ROTORDYNAMIC COEFFICIENTS FOR A LOAD-BETWEEN-PAD, FLEXIBLE-PIVOT TILTING PAD BEARING AT HIGH LOADS

A Thesis

by

JOHN ERIC HENSLEY

Submitted to the Office of Graduate Studies of
Texas A&M University
in partial fulfillment of the requirements for the degree of

MASTER OF SCIENCE

August 2006

Major Subject: Mechanical Engineering

ROTORDYNAMIC COEFFICIENTS FOR A LOAD-BETWEEN-PAD, FLEXIBLE-PIVOT TILTING PAD BEARING AT HIGH LOADS

A Thesis

by

JOHN ERIC HENSLEY

Submitted to the Office of Graduate Studies of
Texas A&M University
in partial fulfillment of the requirements for the degree of

MASTER OF SCIENCE

Approved by:

Chair of Committee,	Dara W. Childs
Committee Members,	S. Bart Childs
	John Vance
Head of Department,	Dennis O'Neal

August 2006

Major Subject: Mechanical Engineering

ABSTRACT

Rotordynamic Coefficients for a Load-Between-Pad, Flexible-Pivot Tilting Pad Bearing at High Loads. (August 2006)
John Eric Hensley, B.S., Texas A&M University
Chair of Advisory Committee: Dr. Dara W. Childs

The dynamic and static performance of a flexure-pivot tilting pad bearing is presented at a load between pad configuration for various load and speed combinations. A similar work performed on the same bearing at lower loads ranging from 0-1 MPa (0-150 psi) by Al-Ghasem was tested, whereas the current work investigates effects in the load range between 1-2.2 MPa (150-320 psi). The bearing design parameters include: 4 pads with pad arc angle 72º and 50% pivot offset, pad axial length 0.0762 m (3 in), pad radial clearance 0.254 mm (0.010 in), bearing radial clearance 190.5 μm (0.0075 in), preload 0.25, and shaft nominal diameter of 0.11684 m (4.600 in). An important distinction between the two sets of tests is the difference in experimental bearing radial clearance, which for this case measured 208 μm (0.00082 in), and for Al-Ghasem's was 165.1 μm (0.0065 in). The rotordynamic coefficients are determined experimentally using a test rig equipped with motion and load sensors. The rig is modeled using Newton's laws, which is converted from the time to frequency domain using Fourier Transform to give complex dynamic stiffnesses. From the resulting complex dynamic stiffnesses the associated real and imaginary components are plotted as a function of excitation frequency and curve fitted via linear regression to give the rotordynamic coefficients. The primary objectives were to determine whether the real component of the complex dynamic stiffnesses could be better modeled with or without the mass coefficient and to contrast the rotordynamic coefficients with an analytical model. Only in the load range of 1 to 2.2 MPa were the unloaded direct mass coefficients near or at 0, which would allow for a [K][C] model to be used. The remaining real components are better represented with the mass term. The analytical model generally overpredicted the stiffness, damping and mass coefficients, especially for the direct components; the trends were generally consistent.

DEDICATION

For my Grandfather,
James A. Corbett

who loved learning and encouraged the same.

ACKNOWLEDGEMENTS

I am grateful for the opportunity to work for Dr. Dara Childs who has provided me with challenging work. His example, support, and guidance are greatly appreciated and will serve me well in the years to come.

I would also like to thank Dr. John Vance and Dr. S. Bart Childs for participating in my advisory committee. I appreciate the assistance of Dr. Luis San Andres and Avijit Bhattacharya with the XLTRC program. I am also thankful for Eddie Denk's assistance during the experimental testing portion of this thesis work. I thank the Texas A&M University Turbomachinery Research Consortium for the funding of this work and my education.

My colleagues likewise are worthy of praise, especially Clint Carter and Bader Jughaiman for their assistance and cooperation. Clint Carter served me well as a brother, coworker, and friend, while Bader Jughaiman was a considerable help with many technical problems. Adnan Al-Ghasem's thesis is the benchmark of this present work.

Thanks also to my parents, Grant and Sherryl Hensley, who taught me by example and word to work before I play so that work has become, in a way, playing. My sister Laura has been an invaluable friend during these past eighteen months.

I am pleased to give praise to my God who expresses Himself in the three persons, being the Father, the Son, and the Holy Spirit. I am grateful for the Father's election of my soul, the Son's securing of it on the cross, and the Spirit's perseverance of it. He has protected me from many sins, and is the one who has surrounded me with so many wise counselors.

TABLE OF CONTENTS

Page

LIST OF FIGURES

Page

Page

LIST OF TABLES

Page

Page

NOMENCLATURE

A	Cross sectional area of flexure pivot [μm^2]
a_x, a_y	Measured stator acceleration in the x and y directions [m/s^2]
A_x, A_y	Fourier transformation of a_x and a_y
c_{ij}	Dimensionless damping coefficient = C_{ij} $(C_p\ \omega/W)$
C_b	Radial bearing clearance [m]
C_p	Radial pad clearance [m]
C_P	Oil specific heat [$J/(kg.K^o)$]
C_c	Corrected damping [kN.s/m]
C_{ij}	Damping coefficient [kN.s/m]
D	Inside bearing diameter [m]
D_x, D_y	Fourier transformation of Δx and Δy
E	Modulus of elasticity [MPa]
e_{xDE}, e_{xNDE}	Bearing displacement in the x direction at the DE and NDE sides [m]
e_{yDE}, e_{yNDE}	Bearing displacement in the y direction at the DE and NDE sides [m]
e_x, e_y	Average bearing displacement in the x and y directions [m]
f_{bx}, f_{by}	Bearing reaction force in the x and y directions [N]
f_x, f_y	Measured excitation force in the x and y directions [N]
F_x, F_y	Fourier transformation of f_x and f_y,
H_{ij}	Average dynamic stiffness vector of the 10 tests [MN/m]
i, j	Subscripts representing x and y
$\boldsymbol{j}$	$\sqrt{-1}$
k_1	Radial stiffness [MN/m]
k_{1C}	Radial stiffness from damping relation [MN/m]
k_{1K}	Radial stiffness from stiffness relation [MN/m]
K_c	Corrected stiffness [MN/m]
k_{ij}	Dimensionless stiffness coefficient = K_{ij} (C_p/W)
K_{ij}	Stiffness coefficient [MN/m]
L	Length of flexure pivot [μm]

ΔL	Change in pad thickness [μm]
L_o	Original pad thickness [μm]
m_{ij}	Dimensionless added mass coefficient = $M_{ij}\ (C_p\ \omega^2/W)$
M_{ij}	Added mass coefficient [kg]
M_s	Stator mass [kg]
n	Dynamic stiffness vector length
N	Rotor speed [Hz]
p	Bearing unit loading = $W/(LD)$ [kPa]
P	Power loss [W]
P_{in}	Inlet Pressure [Pa]
$\dot{Q}$	Oil volumetric flowrate [m^3/s]
R_b	Bearing radius [m]
R_p	Pad radius [m]
R_s	Shaft radius [m]
S	Sommerfeld number = $\mu\ N\ L\ D\ (D/2C_p)^2/W$
ΔT	Temperature difference [°C]
T_o	Average oil outlet temperature [K^o]
T_{in}	Oil inlet temperature [K^o]
$T_{average}$	Average oil inlet and outlet temperature [K^o]
U_{ij}	Uncertainty in dynamic stiffness (H_{ij}) [MN/m]
W	Applied static load in the positive y-direction [N]
Δx, Δy	Measured relative displacement between the rotor and the bearing in the x and y directions, respectively [m]
x, y	Displacement direction

Greek symbols

α	Coefficient of thermal expansion [μm/(m-°C)]
ρ	Oil density [kg/m^3]
μ	Oil viscosity [Pa.s]
ε	Eccentricity ratio = $(e_x^2 + e_y^2)^{0.5}/C_p$
ϕ	Attitude angle = $tan^{-1}(e_y/e_x)\ 180/\pi$ [degree]
ω	Rotor speed [rpm]
Ω	Excitation frequency [Hz]
ω_s	Onset speed of instability [rpm]

Abbreviations

DE	Drive end
EXP	Experiment
Im( )	Imaginary part ( )
LBP	Load between pads
LOP	Load on pad
NDE	Non-drive end
NS	Bulk-Flow Navier Stokes
Re( )	Real part ( )
rpm	Revolution per minute
RY	Reynolds Equation
TH	Theory (bulk-flow unless mentioned otherwise)
TPJB	Tilting-pad journal bearing
WFR	Whirl frequency ratio

INTRODUCTION

The analysis of Tilting Pad (TP) journal bearings has become an issue of importance as the push to run centrifugal operating machines at higher speeds has increased. The threshold of instability is increased with the use of tilting pad bearings over fixed geometry bearings, due to the reduction or often the elimination of cross coupling. When the rotor moves both along and orthogonal to the direction of loading, cross coupling is said to occur [1], which is unique to rotating equipment. The cross coupling is "generated by the fluid rotation in the annulus between the rotating shaft and the housing" [2]. The TP bearing has become the standard for "rotordynamically sensitive and critical rotating equipment" [2], despite the added complexity and expense. A conventional 4 pad TP bearing is depicted below in Figure 1.

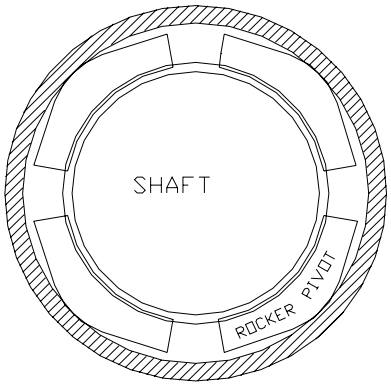

Figure 1: Tilting Pad Bearing [3]

The pivot of TP bearings may vary; Figure 1 is an illustration of a rocker pivot. Unlike many TP bearings, the flexure pivot (FP) bearings shown in Figure 2 have an inherent stiffness at the support web. The stiffness value of a rocker pivot for instance is negligible or near zero. The support web thickness of a FP bearing is designed to both support the load of the rotor and also promote stability for operation. If the stiffness of the support is such that no flexure occurs as an effect of the rotor's movement, then the bearing's stability is drastically reduced [4].

This thesis follows the style and format of the ASME Journal of Tribology.

A benefit of the flexure pivot design to other tilting pad designs is the absence of pivot wear and pad pivot contact stresses. The support web absorbs stresses that are well below its fatigue limit ensuring "long service life" [5]. Another benefit of the FP bearing over the TP bearing is the removal of tolerance stack up in the design, as the bearing is machined in one piece. Since the tolerance stack up is removed, this also lends the bearings' use to smaller turbomachines where tolerances are of particular concern. The machining process used to manufacture such a bearing for low volume situations is electrical discharge machining. For high volume needs, the bearing is manufactured via casting, extrusion or forging. Figure 2 illustrates a five pad flexure pivot pad bearing.

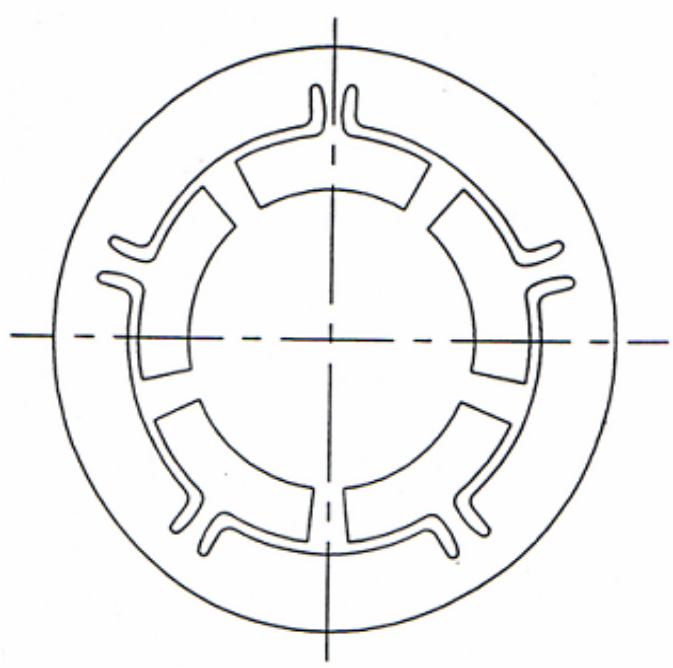

Figure 2: Flexure Pivot Pad Bearing [5]

To reasonably calculate the critical speed and unbalance response, the effect of bearing flexibility and damping must be determined [6]. The first method for calculating the stiffness and damping coefficients of a TP bearing was performed by Lund, which is known as the pad assembly method. This analysis was later suggested to be insufficient as it did not take into account the effects of the unloaded pads, which is especially important at higher Sommerfeld numbers [7]. Another revision introduced into the

method by the same author [7] was the use of finite elements instead of finite-differences to compute the hydrodynamic pressure field. A further change was implemented where the real parts of the eigenvalues were retained in the reduction of the coefficients[8]. The inclusion of the real part of the system eigenvalues accounts for the growing or decaying vibration amplitude. This analysis reduced the number of necessary stiffness and damping coefficients from $2*(5*N_{PAD}+4)$ to an equivalent eight. Having only eight coefficients enables the designer to better characterize a rotor-bearing system's stability in conjunction with optimization schemes previously developed. The greater number of coefficients for a tilting pad bearing are introduced as a result of the various pad degrees of freedom at each pad, as opposed to the simplicity of the fixed geometry bearing. Figure 3 depicts a hydrodynamic rotor bearing combination with eight linearized dynamic coefficients and Eq. (1) below gives the stiffness and damping matrix model without mass.

$$-\begin{bmatrix} f_{bx} \\ f_{by} \end{bmatrix} = \begin{bmatrix} K_{xx} & K_{xy} \\ K_{yx} & K_{yy} \end{bmatrix} \begin{bmatrix} \Delta x \\ \Delta y \end{bmatrix} + \begin{bmatrix} C_{xx} & C_{xy} \\ C_{yx} & C_{yy} \end{bmatrix} \begin{bmatrix} \Delta \dot{x} \\ \Delta \dot{y} \end{bmatrix} \tag{1}$$

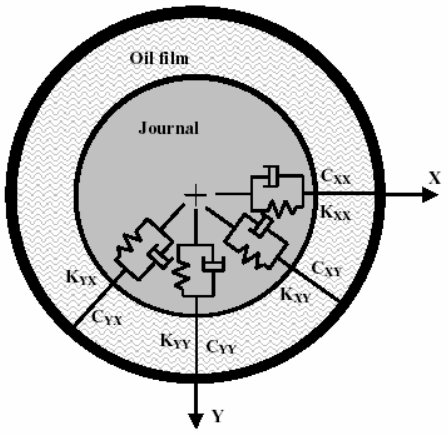

Figure 3: Linearized Dynamic Coefficients [1]

A later reduction was presented by Chen for the general method of calculating bearing dynamic coefficients for flexible-pad journal bearings [9]. In the computation of the coefficients the flexibility of the support web and mass/inertia effects are included. The numerical results of the computation were confirmed to be in good alignment with experimental results.

To determine the dynamic coefficients, integration of the fluid film hydrodynamic pressure profile is necessary, which is accomplished by solving the Reynolds equation. The Reynolds equation is a simplification of the Bulk-Flow Governing equation, where temporal and advective acceleration terms are neglected in the momentum transport equations. Computer codes used to calculate dynamic coefficients generally rely on the Reynolds equation, thus neglecting fluid inertia effects. A work accomplished by Reinhardt and Lund [9] argues that neglecting inertial forces is theoretically justified for small values of the Reynolds number. For journal bearings, turbulence is experienced at a Reynolds number between 1,000 and 1,500, but the inertial forces may become noticeable in the intermediate range above 100. Their work showed that mass terms could be significant for small, compact rotors.

Experimental results provided by Rodriguez and Childs [10] showed that the bearing dynamic stiffness is strongly dependent upon the excitation frequency. This influence modeled with the linearized coefficients previously mentioned with the addition of an added-mass matrix model. They showed that the bearing dynamic characteristics can be properly modeled with frequency-independent stiffness, damping, and added-mass matrices. They also stated that the added-mass coefficient matrix accounts for the combined effects of, "the dynamics introduced by the pads' degrees of freedom" and "the effects of the inertial forces generated by the lubricant film." The matrix model with mass is provided below in Eq. (2).

$$-\begin{bmatrix} f_{bx} \\ f_{by} \end{bmatrix} = \begin{bmatrix} K_{xx} & K_{xy} \\ K_{yx} & K_{yy} \end{bmatrix} \begin{bmatrix} \Delta x \\ \Delta y \end{bmatrix} + \begin{bmatrix} C_{xx} & C_{xy} \\ C_{yx} & C_{yy} \end{bmatrix} \begin{bmatrix} \Delta \dot{x} \\ \Delta \dot{y} \end{bmatrix} + \begin{bmatrix} M_{xx} & M_{xy} \\ M_{yx} & M_{yy} \end{bmatrix} \begin{bmatrix} \Delta \ddot{x} \\ \Delta \ddot{y} \end{bmatrix} \tag{2}$$

A similar work provided by Al-Ghasem and Childs [11] was performed on the same FP tilting pad bearing, yet the bearing configuration was altered from load-on-pad to load-between-pad. The same methodology was used where the direct added mass terms were found to be around 32 kilograms experimentally; similar mass magnitudes were found in Rodriguez's results. The experimental data given by [10] and [11] was also compared to

predictions resulting from the Reynolds equation, as well as the Bulk-Flow Governing equation. The bulk-flow model proved to match the data more accurately, which is stated to be due to the fluid inertial forces. Both models however give good results out to precession frequencies equal to the running speed.

Much analysis has been performed on the tilting pad bearing, and results for the flexible pivot pad bearing have become more common since its patent in 1991. DeChoudhury [12] tested both a flexible and tilt pad bearing for the purpose of comparison, where power losses were shown to be less for the flexible pivot pad. Zeidan and Paquette [13] provide a thorough analysis of both flexible and tilting pad bearings. Nicholas [4] explains the positives and negatives of both the tilting pad and flex pad bearings. Experimental work is also done by changing the support web thickness to view its effect on the coefficients and logarithmic decrement. San Andres [14] tested flexure-pad hybrid bearings, and the results showed that stability characteristics were then improved with the use of this bearing over the fixed geometry configuration. San Andres also stated that the load requirements of present and future cryogenic pumps are met by the newer technology bearing.

The primary research goal is to experimentally measure the stiffness and damping coefficients of a flexure pivot bearing, and to determine their relation to the excitation frequency. Limited work has been done to study the effect of the excitation frequency upon the coefficients. Parsell's work [15] in 1983 predicted that the frequency of the excitation force is an important factor in determining the dynamic bearing characteristics. Tests are regularly performed at synchronous vibrations, because the principal source of excitation in actual rotating machines is the synchronous vibration caused by unbalance of the shaft according to Ha and Yang [16]. Ha and Yang however, performed a test explicitly to study the effects of the excitation frequency at nonsynchronous frequencies and discovered slight changes in the damping and stiffness values. The tests were performed at shaft speeds ranging from 1,200 to 3,600 rpm (20 to 60 Hz), and excitation frequencies ranging from 25 to 50 Hz, which are small compared to the works of Rodriguez and Al-Ghasem. The shaft speed and excitation frequency ranges for testing

should be tested at higher speeds due to the high-speed application of tilting pad bearings. Al-Ghasem performed tests in ranges of 20 to 290 Hz and 4,000 to 12,000 rpm, while Rodriguez provided results for ranges of 20 to 320 Hz and 6,000 to 16,000 rpm. This test provides similar results for the higher frequency and shaft speed ranges, ranging between 20 and 220 Hz and 6,000 to 13,000 rpm respectively.

Another unique alteration to previous work is the reintroduction of the added-mass coefficients to model the dynamic results. This approach was carried out in the separate tests of Al-Ghasem and Rodriguez, where its initial investigation is credited to Reinhardt and Lund [9]. Barret et al., [8] advocates the use of the frequency dependent [K]-[C] model for tilting pad bearings; the [K]-[C] model has been more commonly used in the past. The accuracy of the frequency-independent [M]-[K]-[C] model will also be tested for the same bearing used in Al-Ghasem's and Rodriguez's tests yet at higher loads.

DESCRIPTION OF THE TEST RIG

Overview

A depiction of the test rig that was used for this work is provided in Figure 4. The test rig was originally designed by Kaul [17] for oil seals, yet has been modified to test bearings.

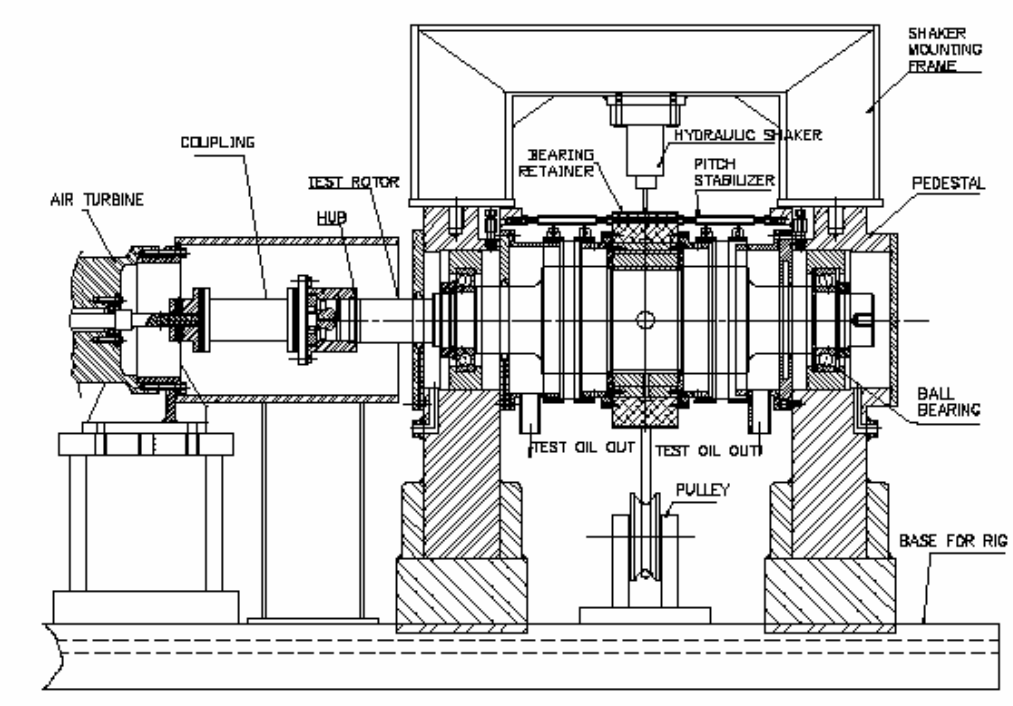

Figure 4: Test Section of Test Rig [1]

The steel base which is welded together by mild steel plates supports the main test section and air turbine. The rotor is then supported by two pedestals spaced approximately 381 mm (15 inches) apart, where it sits on two corresponding pedestal housed ball bearings. The stator in this test rig is what moves during experiments, while the rotor is stationary. An oil mist system is used to supply lubricant to the ball bearings during operation. The air turbine is then coupled to the rotor by a hi-speed flexible coupling, which can provide 65 kw (90 hp) to power the rotor to its maximum speed of 17,000 rpm. The rotor diameter is measured at 0.1168 m (4.599 in).

Instrumentation

The bearing stator houses the bearing and most of the measurement equipment used for testing. Some of these include the non-contacting eddy current proximity probes, which measure the relative position of the stator to the rotor in two directions at two planes. The planes are located orthogonal to the length of the rotor at the drive end and non-drive end. Four proximity probes are present; each pair of probes is placed at the drive end and non-drive end. This allows for control of pitch and yaw, which is maintained with six pitch stabilizers used to align the stator along the rotor. The absolute acceleration is measured with piezoelectric accelerometers, which are also located in the stator along the *x* and *y* axes of Figure 5. A static load can be applied up to 22 kN (5,000 lbf) with a pneumatic piston and cable/pulley assembly. The load is measured by a load cell attached to the cable. Figure 5 shows the static loader assembly as viewed from the non-drive end of the test rig set up.

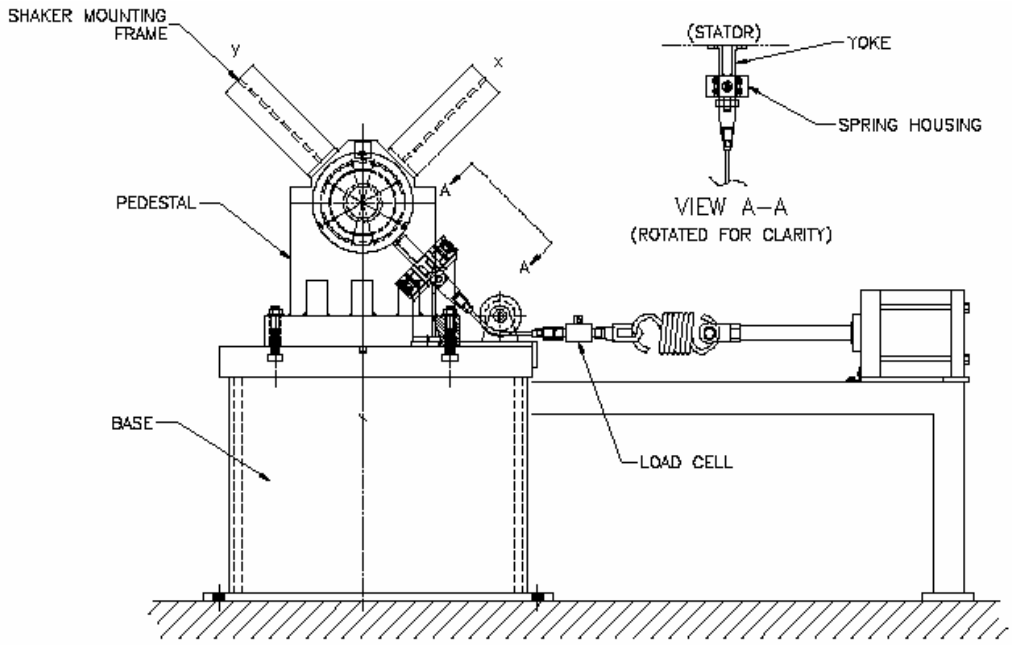

Figure 5: Static Loader Configuration (NDE View) [1]

Shaft speed is measured with a tachometer at the non-drive end of the shaft, and inlet/outlet pressure and temperature probes are attached to the stator. Thermocouples

measure the temperature in the oil inlet chamber and the downstream end caps. Oil pressure at the inlet and outlet locations are measured with pressure transducers.

Figure 6 shows the circumferential locations for the thermocouples as viewed from the drive end of the tester for the pad temperatures. When loaded, the rotor moves in the loading direction indicated relative to the stator. These thermocouples are situated on the bearing at the drive end of the tester whereas an additional 5 thermocouples were placed adjacent to pad 4 on the non-drive end.

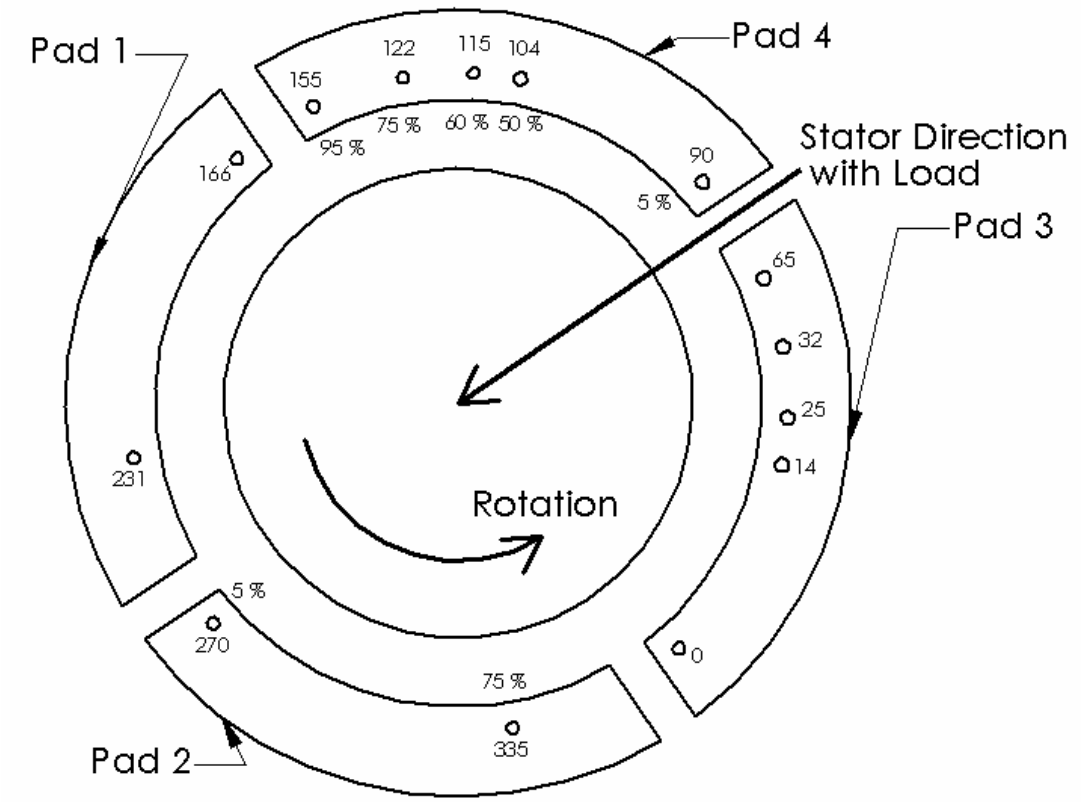

Figure 6: Flex-Pad Thermocouple Placement (DE View)

Shaker-Stinger Configuration

Static loads can also be applied with the shakers but they are strictly used for dynamic loading. The *x*-direction shaker can supply a maximum load of 4.45 kN (1,000 lb) in tension and compression; while the *y*-direction shaker pulls up to 4.45 kN (1,000 lb) in

tension, and 11.1 kN (2,500 lb) in compression. The *x* and *y* shakers can both provide excitation frequencies up to 1,000 Hz. Loads are measured with load cells, which are placed between the shaker heads and the stingers. Figure 7 below illustrates the shaker-stinger configuration as viewed from the non-drive end side.

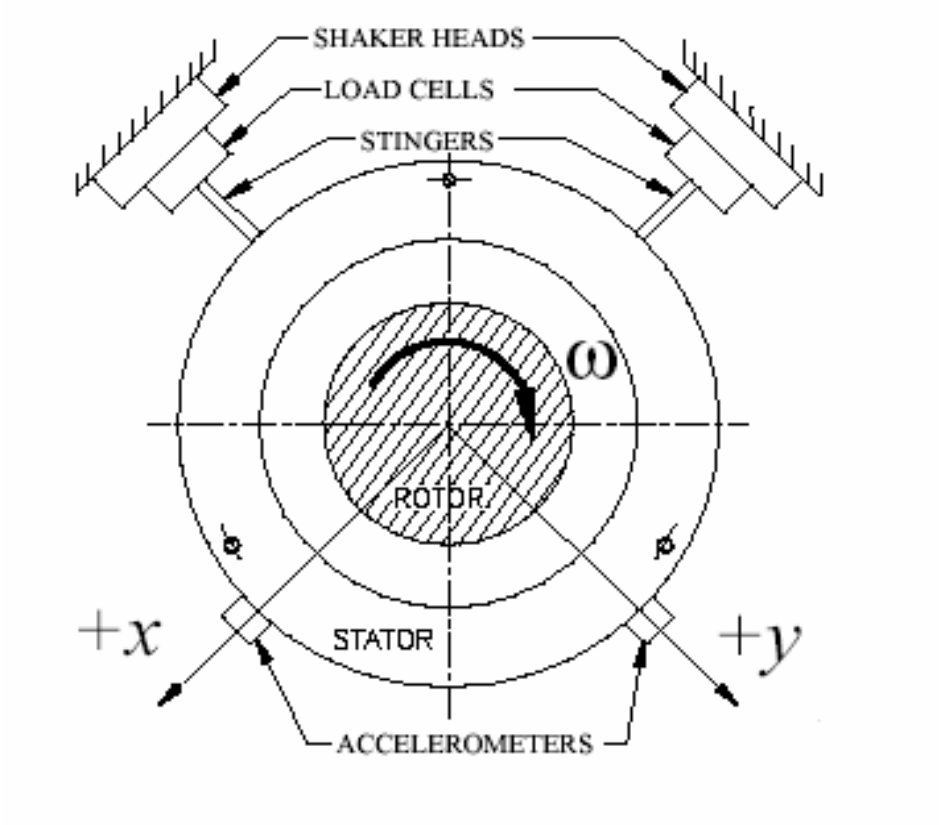

Figure 7: Shaker-Stinger Configuration (NDE View) [18]

Bearing Geometry

The design parameters of the bearing and the lubricant are provided below in Table 1.

Table 1: Flexure-Pivot Bearing Design Parameters and Lubricant Description

Number of pads	4
Configuration	LBP
Pad arc angle	72^o
Pivot offset	50%
Rotor diameter	116.8095 ± 0.0051 mm (4.5988 ± 0.0002 in)
Pad axial length	76.2 ± 0.0254 mm (3 ± 0.001 in)
Radial pad clearance(C_p)	0.254 ± 0.0127 mm (0.010 ± 0.0005 in)
Radial bearing clearance(C_b)	0.1905 ± 0.0127 mm (0.0075 ± 0.0005 in)
Preload	0.25
Pad rotational stiffness	1694.8 N.m/rad (15000 lb.in/rad)
Pad polar inertia	$7.448x10^{-5}$ kg.m^2($6.59x10^{-4}$ lbm.s^2.in)
Pad mass	1.226 kg (2.70 lbm)
Web thickness	2.1251 mm (0.0837 in)
Web height	7.4379 mm (0.2928 in)
Lubricant type	ISO VG32

Figure 8 is a drawing of the stator assembly including the bearing stator, two end caps, and FP tilt pad bearing.

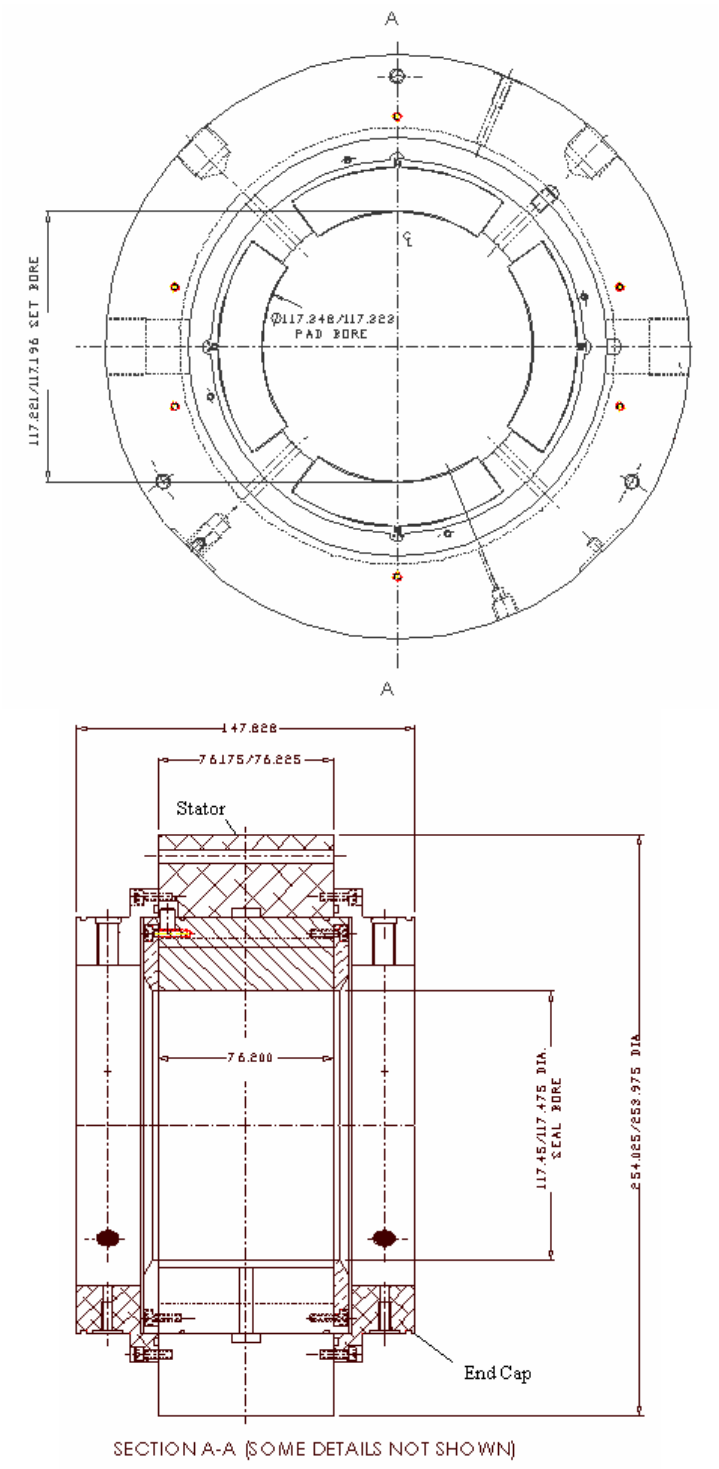

Figure 8: Bearing-Stator Assembly [3]

THEORETICAL BACKGROUND

Parameter Identification

Childs and Hale [18] explain how the rotordynamic coefficients are determined from the measurements obtained. The coordinate system used for the experimental parameter identification is pictured in Figure 9.

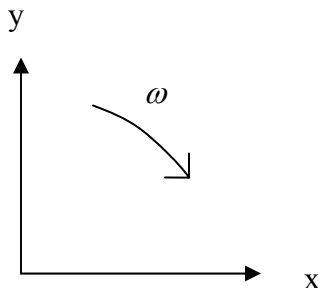

Figure 9: Test Coordinate System (NDE View)

The stator mass M_s equations of motion may be written as:

$$M_s\begin{bmatrix}\ddot{x}_s\\ \ddot{y}_s\end{bmatrix}=\begin{bmatrix}f_x\\ f_y\end{bmatrix}-\begin{bmatrix}f_{bx}\\ f_{by}\end{bmatrix} \tag{3}$$

where $\ddot{x}_s, \ddot{y}_s$ are the measured components of the stator's acceleration, f_x, f_y are the measured input excitation forces, and f_{bx}, f_{by} are the bearing reaction force components. The following relationship is the linearized force-displacement model for bearings where the rotordynamic coefficients include stiffness K_{ij}, damping C_{ij}, and added-mass M_{ij}. $\Delta x, \Delta y$ define the relative motion between the rotor and the stator.

$$-\begin{bmatrix}f_{bx}\\ f_{by}\end{bmatrix}=\begin{bmatrix}K_{xx} & K_{xy}\\ K_{yx} & K_{yy}\end{bmatrix}\begin{bmatrix}\Delta x\\ \Delta y\end{bmatrix}+\begin{bmatrix}C_{xx} & C_{xy}\\ C_{yx} & C_{yy}\end{bmatrix}\begin{bmatrix}\Delta\dot{x}\\ \Delta\dot{y}\end{bmatrix}+\begin{bmatrix}M_{xx} & M_{xy}\\ M_{yx} & M_{yy}\end{bmatrix}\begin{bmatrix}\Delta\ddot{x}\\ \Delta\ddot{y}\end{bmatrix} \tag{4}$$

Substituting Eq. (3) into Eq. (4), the following equation is developed:

$$\begin{bmatrix}f_x-M_s\ddot{x}_s\\ f_y-M_s\ddot{y}_s\end{bmatrix}=-\begin{bmatrix}K_{xx} & K_{xy}\\ K_{yx} & K_{yy}\end{bmatrix}\begin{bmatrix}\Delta x\\ \Delta y\end{bmatrix}-\begin{bmatrix}C_{xx} & C_{xy}\\ C_{yx} & C_{yy}\end{bmatrix}\begin{bmatrix}\Delta\dot{x}\\ \Delta\dot{y}\end{bmatrix}-\begin{bmatrix}M_{xx} & M_{xy}\\ M_{yx} & M_{yy}\end{bmatrix}\begin{bmatrix}\Delta\ddot{x}\\ \Delta\ddot{y}\end{bmatrix} \tag{5}$$

$\Delta x(t), \Delta y(t)$ on the right hand side of Eq. (5) are measured functions of time; hence, the left-hand vector is a known quantity. The Fourier Transform $\Im$ is used to determine the rotordynamic coefficients in the frequency domain as:

$$\begin{bmatrix} \boldsymbol{F}_x - M_s \boldsymbol{A}_x \\ \boldsymbol{F}_y - M_s \boldsymbol{A}_y \end{bmatrix} = - \begin{bmatrix} \boldsymbol{H}_{xx} & \boldsymbol{H}_{xy} \\ \boldsymbol{H}_{yx} & \boldsymbol{H}_{yy} \end{bmatrix} \begin{bmatrix} \boldsymbol{D}_x \\ \boldsymbol{D}_y \end{bmatrix} \tag{6}$$

The relationship between the dynamic bearing stiffness $\boldsymbol{H_{ij}}$ and coefficients of Eq. (5) are:

$$\begin{aligned} &\boldsymbol{H}_{ij} = (K_{ij} - \Omega^2 M_{ij}) + \boldsymbol{j}(\Omega C_{ij}), \\ &\mathrm{Re}(H_{ij}) = K_{ij} - \Omega^2 M_{ij}, \mathrm{Im}(H_{ij}) = \Omega C_{ij} \end{aligned} \tag{7}$$

The subscripts i and j alternately represent x and y, Ω is the excitation frequency and $\boldsymbol{j} = \sqrt{-1}$. The four unknowns of interest are $\boldsymbol{H}_{xx}, \boldsymbol{H}_{xy}, \boldsymbol{H}_{yx}, \boldsymbol{H}_{yy}$, which are solved using the two equations provided in equation set (6) by testing in both the x and y directions. Shaking the stator alternately in the orthogonal directions about the steady state rotor position, yields four equations to solve the parameters of interest provided in Eq. (8):

$$\begin{bmatrix} \boldsymbol{F}_{xx} - M_s \boldsymbol{A}_{xx} & \boldsymbol{F}_{xy} - M_s \boldsymbol{A}_{xy} \\ \boldsymbol{F}_{yx} - M_s \boldsymbol{A}_{yx} & \boldsymbol{F}_{yy} - M_s \boldsymbol{A}_{yy} \end{bmatrix} = - \begin{bmatrix} \boldsymbol{H}_{xx} & \boldsymbol{H}_{xy} \\ \boldsymbol{H}_{yx} & \boldsymbol{H}_{yy} \end{bmatrix} \begin{bmatrix} \boldsymbol{D}_{xx} & \boldsymbol{D}_{xy} \\ \boldsymbol{D}_{yx} & \boldsymbol{D}_{yy} \end{bmatrix} \tag{8}$$

Curve Fitting

Once the complex-dynamic stiffness matrix ($\boldsymbol{H}$) is determined, the rotordynamic coefficients can be calculated. The rotordynamic coefficients take the form of Eq. (7), where they are calculated through the use of a straight line regression [1]. To determine the stiffness (K_{ij}) and mass (M_{ij}) coefficients a linear regression is taken of the real component of the dynamic stiffness (H_{ij}). To turn the quadratic equation into a linear one, Ω^2 is treated as the domain character while the dynamic stiffness is set as the range. Similarly, the damping (C_{ij}) coefficients are calculated by applying the linear regression with the imaginary component of the dynamic stiffness plotted against Ω. The following equations describe the linear regression used to estimate the rotordynamic coefficients [19].

$$\hat{y} = \beta_0 + \beta_1 x \quad \text{(linear regression line)} \tag{9}$$

$$\beta_1 = \frac{\sum_{i=1}^{N} y_i x_i - N(\bar{y})(\bar{x})}{\sum_{i=1}^{N} x_i^2 - N(\bar{y})(\bar{x})^2} \quad \text{(slope)} \tag{10}$$

$$\beta_0 = \bar{y} - \beta_1 \bar{x} \quad \text{(intercept)} \tag{11}$$

N represents the data pairs (x_i,y_i) used for the regression, while $\hat{x}$, and $\hat{y}$ are the means of x and y respectively. The uncertainty calculations are determined using:

$$\Delta\beta_1 = t \times \sqrt{\frac{\hat{\sigma}^2}{S_{xx}}} \quad \text{(uncertainty of the slope)} \tag{12}$$

$$\Delta\beta_0 = t \times \sqrt{\hat{\sigma}^2 \left(\frac{1}{N} + \frac{\bar{x}^2}{S_{xx}} \right)} \quad \text{(uncertainty of the intercept)} \tag{13}$$

where $S_{xx} = \sum_{i=1}^{N} x_i^2 - N\bar{x}^2$, and $\hat{\sigma}^2 = \frac{\sum_{i=1}^{N} (y_i - \hat{y}_i)^2}{N-2}$. These relations are used for the theoretical and experimental data to determine the rotordynamic coefficients using the standard confidence level of 95%.

EXPERIMENTAL PROCEDURE

Test Conditions

To gather the data of interest, tests are performed at different static load and rotational speed combinations. Successful static and dynamic data were captured at unit loads between 0.7 MPa (100 psi) and 2.2 MPa (320 psi), and rotational speeds ranging from 6,000 to 13,000 rpm. The marks provided in Table 2 indicate the successful combinations tested. The higher loads for the speeds of 6,000 and 8,000 rpm were not conducted due to concerns that the rotor would contact the stator.

Table 2: Rotor Speed and Applied Load Combinations

Speed [rpm]	Nominal Bearing Unit Load [kPa / psi]					
	690 / 100	1034 / 150	1379 / 200	1655 / 240	1931 / 280	2206 / 320
6000	X		X	X		
8000		X	X	X	X	
10000			X	X	X	X
12000	X		X	X	X	X
13000				X	X	X

To gather the dynamic data, the shakers are alternately excited at the specified conditions. Using a pseudo-random excitation with a waveform calculated for the bearing. The measurement and data acquisition devices record the data. The data are then compiled in Microsoft Excel where the previously explained equation sets are used to calculate both the complex dynamic stiffness and rotordynamic coefficients. Note that at each test combination, 10 tests are performed and then averaged, which serves to define the amount of variability in the resulting dynamic stiffnesses.

Baseline

Before pumping any oil into the test rig assembly a shake test is performed to determine the measured influences affecting the rig under dry conditions. The measured influences include items such as the pitch stabilizers, and hose connections, which supply small forces to the test rig assembly. This test is known as the “dry shake”, where the

rotational speed is zero and no oil is supplied to the bearing. Determining the baseline dynamic stiffnesses is important because the coefficients of the particular bearing are of interest not the mentioned factors that supply the small forces. To calculate the rotordynamic coefficients, the baseline dynamic coefficients are subtracted from the average dynamic stiffnesses. From the resulting dynamic stiffness values the coefficients may then be determined using the procedure previously discussed.

The imaginary and real components of the baseline dynamic stiffness are pictured in Figures 10 through 12. Figure 10 pictures the real part of the direct baseline dynamic stiffness, while the real part of the cross coupled baseline dynamic stiffnesses are present in Figure 11. Figure 12 illustrates the trends of the imaginary components of the baseline dynamic stiffnesses, both direct and cross-coupled. The primary source of external stiffness is attributed to the pitch stabilizers, which was previously recorded as 2.6 MN/m in the *x* and *y* directions [1], [3]. The resulting baseline direct stiffness for the real direct terms becomes 2.96 MN/m and 2.65 MN/m for the *x* and *y* directions respectively in the 0 to 220 Hz range.

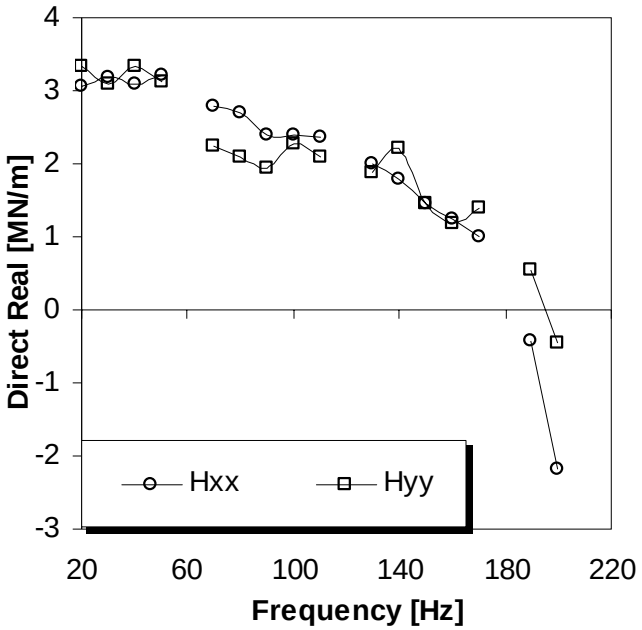

Figure 10: Baseline Real Direct Dynamic Stiffnesses

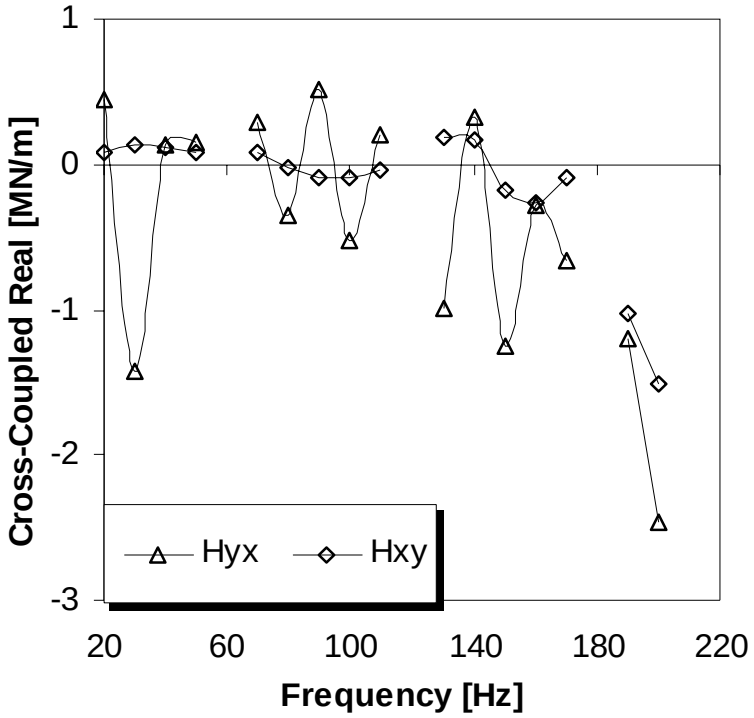

Figure 11: Baseline Real Cross-Coupled Dynamic Stiffnesses

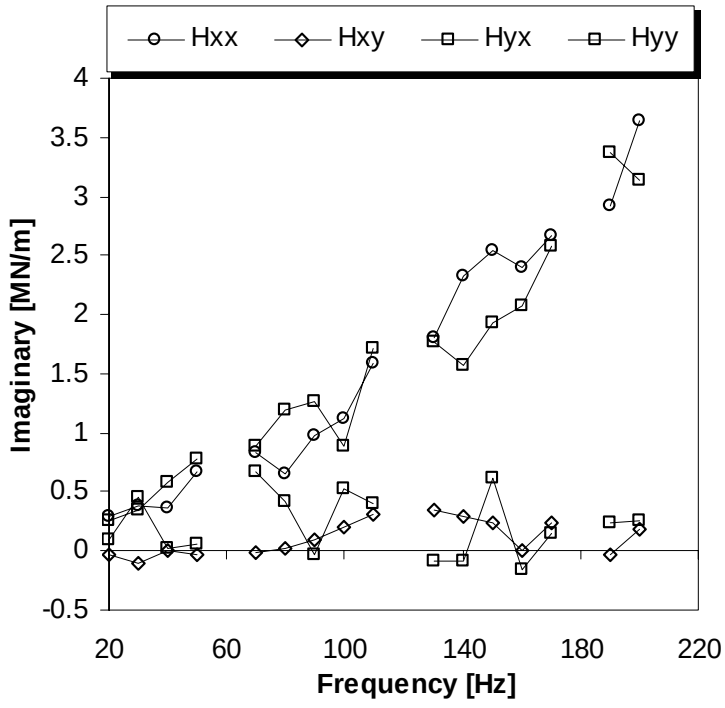

Figure 12: Baseline Imaginary Dynamic Stiffnesses

DYNAMIC RESULTS

Dynamic Stiffness

A sample of the determination for the bearing rotordynamic coefficients is provided in this section for a test condition at 12,000 rpm and a static unit load of 1.7 MPa (240 psi). To accomplish this, the least-squares linear regression is used in conjunction with the dynamic stiffness data. Associated with the dynamic stiffness data at each frequency in Figure 13 are uncertainty bars, which portray the degree of repeatability for the ten consecutive tests performed.

Figure 13 pictures the real part of the direct dynamic stiffness Re($\boldsymbol{H_{xx}}$) and Re($\boldsymbol{H_{yy}}$), which are fitted by a line of the form $y_i = a + bx_i$, where $x_i = \Omega^2$. Evaluating Eqs. (10) and (12) for $\mathrm{Re}(\boldsymbol{H_{ij}}) = K_{ij} - M_{ij}x_i$, where $x_i = \Omega^2$ and $y_i = \mathrm{Re}(\boldsymbol{H_{ij}})$ the resultant is M_{xx}=-1.34 ± 5.44 kg, and similarly M_{yy}=25.25 ± 5.34 kg. M_{xx} for this case and others close to zero with comparable uncertainties were concluded to be equal to 0. Equations (11) and (13) similarly result in K_{xx}=147.22 ± 4.85 MN/m and K_{yy}=191.17 ± 4.76 MN/m. Note that the quality of the curve fit is described by the uncertainties of the rotordynamic coefficients.

In Figure 13, Re($\boldsymbol{H_{yy}}$) is shown to decrease with increasing frequency, while Re($\boldsymbol{H_{xx}}$) remains nearly constant. These trends are present for all conditions tested excluding the 12,000 rpm and 0.7 MPa (100 psi) case. Since both functions can be fitted as $\mathrm{Re}(\boldsymbol{H_{ij}}) = K_{ij} - M_{ij}\Omega^2$, the stiffness coefficients $\boldsymbol{K_{ij}}$ are frequency independent. If Re($\boldsymbol{H_{xx}}$) were modeled simply with K_{xx}, then it could be argued that frequency dependence is present in the load range from 1 to 2.2 MPa for this term.

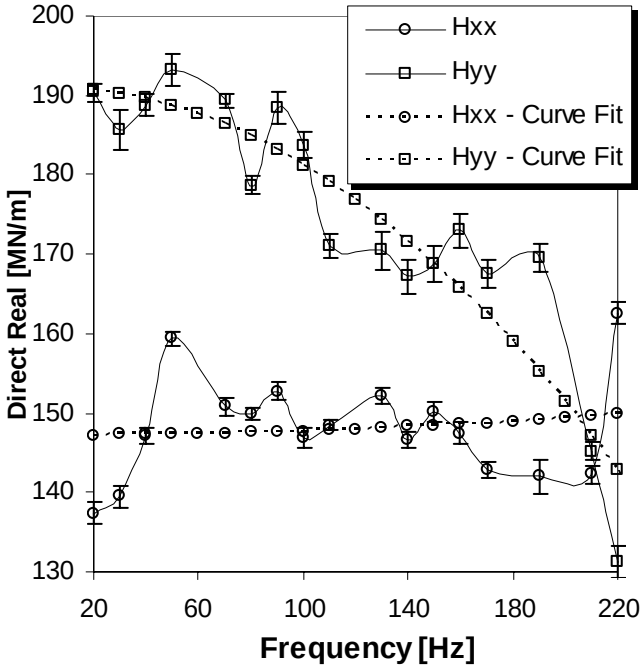

Figure 13: Real Direct Dynamic Stiffnesses at 12,000 rpm and 1.7 MPa

Frequency independence is shown to be present at a test condition of 12,000 rpm and 0.7 MPa (100 psi) for both directions in Figure 14, where the trends are more similar to the findings of Al-Ghasem. The resulting K_{xx} and K_{yy} at this condition were 58.8 and 66.5 MN/m for the current work, and 93.25 and 109 MN/m for Al-Ghasem's respectively. In Al-Ghasem's thesis the bearing is stated to have been crushed as the experimental measurements of the radial bearing clearance were 330.2 μm (13 mils) in one direction and 431.8 μm (17 mils) in its orthogonal. Note that the bearing had been removed from its casing for another test between the period of use by Al-Ghasem and the present one. In the current investigation the measured diametral bearing clearance was measured to be 416 μm (16.4 mils) for both directions, which is an increase of 110 % over the nominal diametral bearing clearance of 381 μm (15 mils) from Table 1, and the average value of both directions provided in Al-Ghasem's test. The reduced stiffnesses in this test is expected to be due to the larger bearing clearance In Figure 14 direct real plots are pictured below for both the present investigation and that conducted previously by Al-Ghasem.

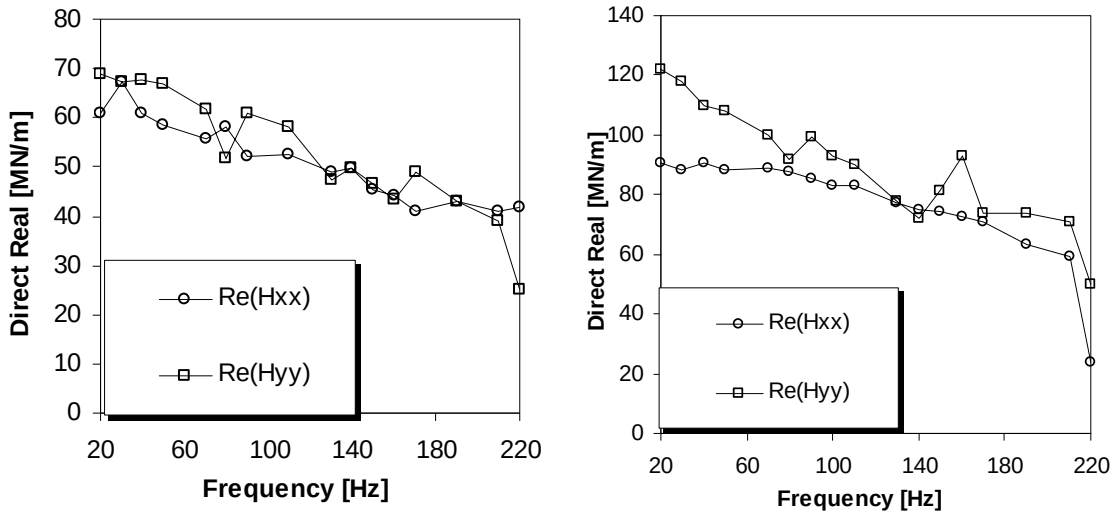

Figure 14: Real Direct Dynamic Stiffnesses at 12,000 rpm and 0.7 MPa for Tests Performed by Hensley (Left) and Al-Ghasem (Right)

Figure 15 presents the real part of the cross-coupled dynamic stiffnesses. These results are similar to those presented in the past. Slight increases in the real cross coupled impedances as the excitation frequency is increased are common. The magnitude tends to increase with increasing load, which was also observed by Al-Ghasem. Using similar procedures to calculate the direct coefficients the cross-coupled stiffness and added-mass coefficients yield:

$$K_{xy} = -33.76 \pm 2.13 \text{ MN/m} \qquad M_{xy} = -22.22 \pm 2.43 \text{ kg}$$
$$K_{yx} = 0.31 \pm 9.23 \text{ MN/m} \qquad M_{yx} = -14.98 \pm 10.37 \text{ kg} \tag{14}$$

Scatter is present for the Re(H_{yx}) term as it is plotted against excitation frequency in Figure 15 with a R_{yx}^2 value of 0.3485. The poor curve fit was observed for conditions at 1.4 to 2.2 MPa, 12,000 rpm and 1.7 to 2.2 MPa, 13,000 rpm, which resulted in unacceptable coefficients.

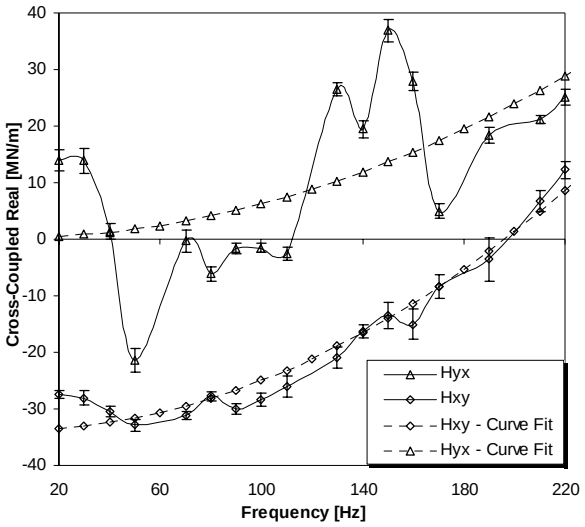

Figure 15: Real Cross-Coupled Dynamic Stiffnesses at 12,000 rpm and 1.7 MPa

Figure 16 presents the imaginary part of the direct and the cross-coupled dynamic stiffnesses. Note that the direct component magnitudes exceed those of the cross coupled ones by a significant amount. The cross coupled imaginary coefficients differ from one another for this case as the H_{xy} term increases with excitation frequency and the H_{yx} term decreases. Viewing Figure 16, scatter is evident for the H_{yx} term, which gives a R_{yx}^2 value of 0.3758. Where the curve fit of the cross coupled imaginary components (Im(H_{xy}) and Im(H_{yx})) gave a coefficient of determination less than 0.5 the related rotordynamic coefficient was not considered acceptable. It may also be viewed in Figure 16 that the H_{xy} impedance does not intersect at a y-intercept of 0. In some cases the curve fit was acceptable, yet where the impedance did not approach the 0 value for the intercept the fit was not accepted. The resulting curve fit of Im(H_{xy}) was considered to be acceptable for the 6,000 and 8,000 rpm excluding the 1.4 MPa load for both speeds. Cases including 0.7 and 1.7 MPa at 6,000 rpm; 1 and 1.4 MPa at 8,000 rpm; and 1.9 and 2.2 MPa at 13,000 rpm were considered to be acceptable curve fits of Im(H_{yx}).

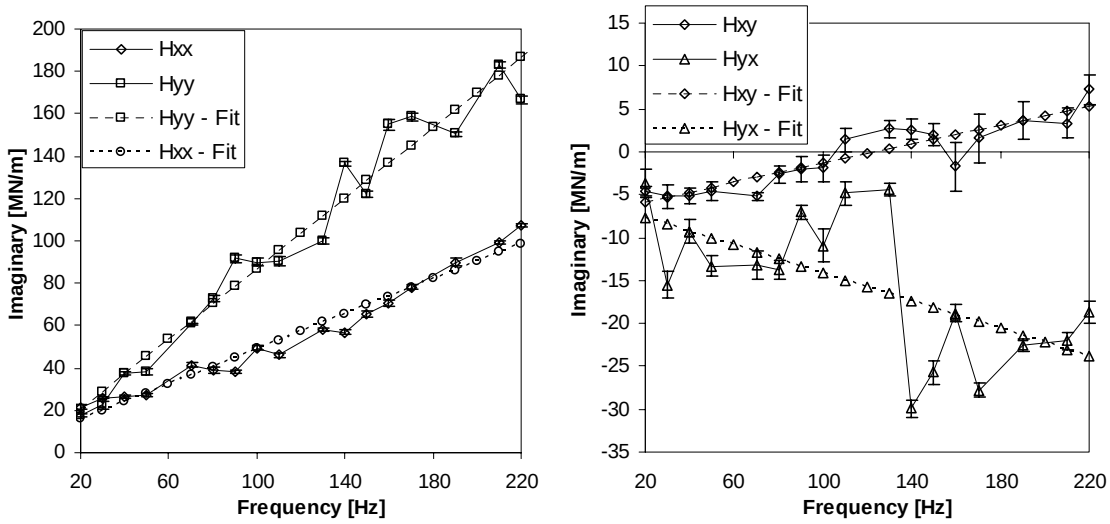

Figure 16: Imaginary Dynamic Stiffnesses at 12,000 rpm and 1.7 MPa

The damping coefficients (C_{xx}, C_{yy}, C_{xy}, C_{yx}) are identified from the slope of the imaginary part of the dynamic stiffnesses, where the intercept terms forced to go through zero in all cases. Eqs. (10) and (12) are evaluated for $x_i = \Omega_i$ and $y_i = \mathrm{Im}(H_{xxi})$ for $\mathrm{Im}(\boldsymbol{H_{ij}}) = \Omega C_{ij}$ resulting in:

C_{xx}= 65.93±6.56 C_{xy}= 8.85 ± 2.06
C_{yx}= -12.87 ±8.39 C_{yy}=132.06 ± 13.67 (kN-s/m) (15)

XLTRC ^{2}-XLTFPBrg

For the analytical computation of the rotordynamic coefficients a code produced by San Andres [20] titled XLTRC^2-XLTFPBrg was used. The program allows for the computation of both static and dynamic parameters using the Bulk-Flow Governing equation, which includes mass conservation, axial and circumferential momentum, and energy equations. The Reynolds equation is used to predict the pressure field at the fluid film region, and the resulting dynamic coefficients. The largest Reynolds number for each test condition is provided below in Table 3 with the greatest value at 173 for a rotational speed of 13,000 rpm. These results confirm that the fluid acts in a laminar manner as the provided values are below the critical Reynolds number of 2,000 [21] for all test combinations.

Table 3: Greatest Reynolds Number per Rotational Speed

Rotor Speed (rpm)	6,000	8,000	10,000	12,000	13,000
Reynold's number ($\rho C_p \omega R_b / \mu$)	61.9	90.0	123.4	157.7	173.3

The program allows for computation of the rotordynamic coefficients with the Reynolds equation (no fluid inertia) and the Bulk-Flow Governing equation (with fluid inertia). In Figure 17 the experimental data for the 12,000 rpm and 1.9 MPa case is compared to both analytical models for the dynamic real coefficients. The differences between the results of the analytical models are generally minute. Since the analytical tool often overpredicts the experimental results the bulk flow relationship was selected where overprediction is less severe. The cross coupled real components are routinely under predicted by the analytical models. Despite the fact that the bearing operates in a laminar manner the bulk flow relationship was used rather than the Reynolds equation. This was chosen as the bulk flow model better approximates the experimental data both in this thesis work and that accomplished by Al-Ghasem.

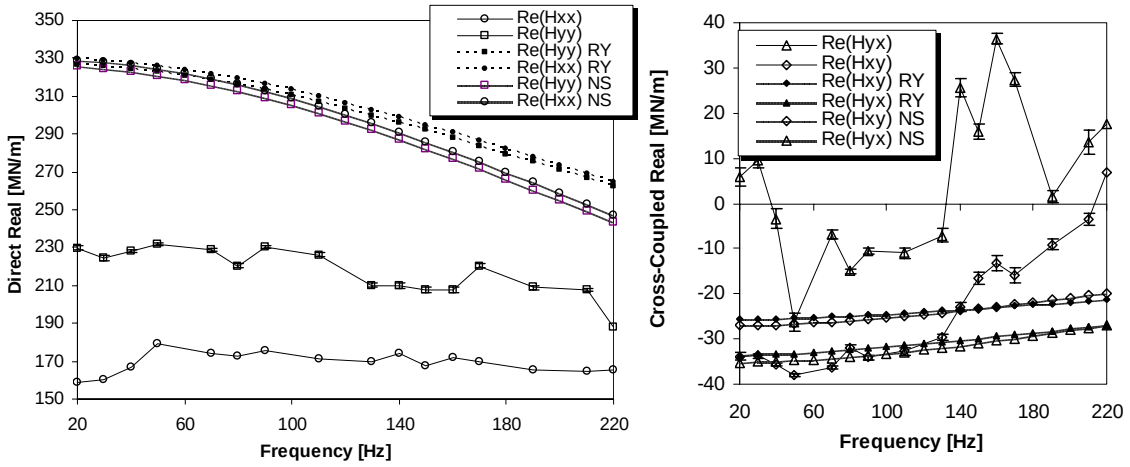

Figure 17: Direct Real and Cross-Coupled Real Dynamic Stiffnesses at 12,000 rpm and 1.9 MPa

The input data required for running the code include the bearing and shaft geometries, as well as the pad inertia and stiffness. Also necessary was the supply pressure and temperature, which was then used to calculate the properties of the ISO 32 lubricant used.

The inlet pressure and temperature values measured during testing were used as inputs for the code. Initial guesses for the algorithm were also required as well as the type of loading configuration being used (LBP or LOP). The load applied to the bearing is altered per tested condition, and the excitation frequency range is defined as an input for the code.

Different types of analyses were made available through the program, which included the selection of different thermal options, as well as the presence of fluid inertia. Among the thermal options, only two could be considered which were titled (1) Adiabatic Solid Surfaces, and (2) Isothermal Journal and Bearing. The first option assumes no heat transfer through the shaft and bearing, while the second treats the oil temperature as being equal to the supply temperature throughout the flow path. For the present work the adiabatic option was used because it agreed better with the measurement, which differs from Al-Ghasem's work where the constant temperature alternative was selected.

In the following section, which details the resulting dynamic coefficients, the theoretical points are computed at the nominal radial bearing clearance of 190.5 μm (7.5 mils). These were calculated at the associated experimental loads, supply pressures, and supply temperatures as listed in Table 4.

Table 4: Experimental Load, Supply Temperature, and Supply Pressure Used for High Load Analytical Prediction

ω [rpm]	W [N]	P_{in} [Pa]	T_{in} [K°]
6000	5900.9	183533.2	315.9
6000	12267.6	203645.5	315.9
6000	14689.7	202992.9	315.9
8000	8770.1	189237.7	315.4
8000	12215.6	203851.5	315.4
8000	14471.6	209499.3	315.4
8000	17256.1	211287.8	315.4
10000	12235.9	193628.8	316.01
10000	14909.4	198722.1	316.01
10000	17168.5	204109.7	316.01
10000	20060.5	209211	316.01
12000	5850.2	165181.3	318.02
12000	11970.9	182233.7	318.02
12000	14718.5	191321.3	318.02
12000	17156.2	191523.8	318.02
12000	20078.3	195697.5	318.02
13000	12018.5	178574.1	315.76
13000	14700.9	182778.4	315.76
13000	17188.8	185437.2	315.76
13000	20059.3	190992.7	315.76

The effect of the bearing clearance for the range of interest on the analytical loaded direct dynamic stiffness (K_{yy}) is small as can be observed in Figure 18. The smallest value observed by Al-Ghasem amounts to 165.1 μm (6.5 mils), the nominal value is 190.5 μm (7.5 mils), and the measured clearance for the current investigation was 208 μm (8.2 mils). Convergence in the XLTRC program did not occur for the measured bearing clearance of 208 μm (8.2 mils) for higher loads. Therefore for consistency the nominal value was used in the program to determine all of the resulting rotordynamic coefficients.

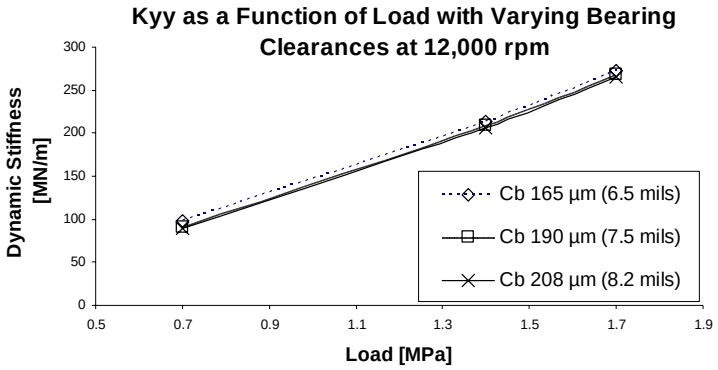

Figure 18: Kyy as a Function of Load with Varying Bearing Clearances at 12,000 rpm

Another concern related to the change in clearance was considered as a result of temperature difference at the loaded pad. The supply temperature and average of the pad temperatures from the highest load and speed condition of 2.2 MPa and 13,000 rpm were taken to define the temperature difference. The average pad temperature was taken to represent that at the rotor side of the pad, where the adjacent side was considered to be at the supply temperature. This gave a temperature difference of 30 ºC, and a resulting pad thickness change of 7.62 μm (0.3 mils). This thickness change is small and therefore considered not to be a major factor in altering the bearing clearance during operation. Eq. 16 was used to determine this value with the thermal expansion coefficient of steel, and an original pad thickness of 19.05 mm (0.75 inches).

$$\Delta L = \alpha L_0 \Delta T \tag{16}$$

Al-Ghasem's analytical results are included in addition to those of the present investigation. Al-Ghasem's analytical values were computed with a radial bearing clearance of 165.1 μm (6.5 mils), where the supply temperature entered into the program was the leading edge temperature of the loaded pad. The thermocouple location of this temperature was present at the 5% mark of pad 4 as described for the present case pictured in Figure 6. The present investigation uses the actual supply temperatures to analytically compute the rotordynamic coefficients rather than the 5% location temperatures of the pad.

Rotordynamic Coefficients

The frequency independent rotordynamic coefficients are plotted against rotational speed and unit bearing load. The coefficients are provided as a function of rotational speed or unit bearing load for the matching speed or load. Rotational speeds pictured include 6,000, 8000, 10000, 12000, and 13000 rpm, while the bearing unit loads are 0.7, 1, 1.4, 1.7, 1.9, and 2.2 MPa. Uncertainty bars are included in each of the following plots, they are only noticeable or significant for the mass coefficient plots.

As the rotor interacts with the bearing the pivot of each pad not only rocks, but also reacts radially. Since the analytical code does not account for this effect, the resulting analytical direct loaded damping (C_{yy}) and stiffness coefficients (K_{yy}) were placed in series with the radial stiffness to determine whether this would explain the discrepancy between the measured and analytical results. In Figure 19, k_1 represents the radial stiffness, while c and k represent the analytical direct damping (C_{yy}) and stiffness coefficients (K_{yy}) respectively.

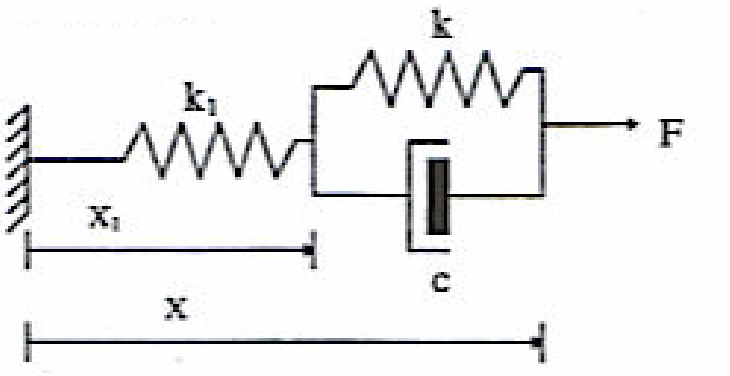

Figure 19: Radial Stiffness in Series with the Direct Loaded Spring and Damper [22]

Once the radial stiffness is set in series with the analytical values, the corrected terms may be determined with equation set 17 [22]. Using the stiffness correction relationship of equation set 17, the corrected stiffness is set equal to the experimental results and the necessary radial stiffness is calculated (k_{1K}). The necessary radial stiffness for bringing the analytical and experimental results into alignment based off of the stiffness correction relation ranges from 502 to 901 MN/m as listed in Table 5. When the damping correction relationship in equation set 17 was used to determine the radial stiffness, values between 2440 to 2831 MN/m were produced (k_{1C}). These radial stiffness values differ significantly from the stiffness estimated from the *AE/L* (Eq. 17) result, which gives a value of 6,314.6 MN/m. The cross sectional area for the steel flexure pivot is 136.5 μm^2 (211.5 mil^2), with a length of 4.47 mm (176 mils). The corrected damping shown in Table 5 was calculated using the radial stiffness from the stiffness correction relationship. It may be observed from Table 5 that the corrected damping is on average 62% of the experimental damping terms. This shows that when the stiffness is corrected the damping is over corrected. Also since the radial stiffness estimates do not agree this model is therefore considered to be insufficient to account for the differences between the measured and analytical results.

$$K_c = \frac{K_{yy}k_1}{K_{yy}+k_1},\ C_c = \frac{C_{yy}k_1^{\,2}}{(K_{yy}+k_1)^2},\ k_1 = \frac{AE}{L} \tag{17}$$

Table 5: Radial Stiffness Investigation Results

12,000 [RPM]								
Load [Mpa]	K_{yy} TH. [MN/m]	K_{yy} EXP. [MN/m]	K_c [MN/m]	k_{1K} [MN/m]	C_{yy} TH. [kN.s/m]	C_{yy} EXP. [kN.s/m]	C_c [kN.s/m]	k_{1C} [MN/m]
1.4	209.08	147.6	147.6	501.96	132.94	115.28	66.25	2830.46
1.7	268.74	191.07	191.07	661.11	161.72	132.06	81.75	2520.68
1.9	323.97	232.24	232.24	820.22	187.59	148.38	96.40	2604.46
2.2	392.85	273.61	273.61	901.44	220.35	163.48	106.89	2440.39

Direct and cross-coupled stiffness coefficients are plotted against load in Figures 20 and 21 for each rotational speed tested. The analytical direct coefficients (K_{xx} and K_{yy}) overpredict the experimental ones, yet the trends are consistent with one another. Another notable distinction is that the experimental results show orthotropy between the loaded (K_{yy}) and unloaded (K_{xx}) direct coefficients, whereas this is not present with the analytically produced coefficients. The loaded and unloaded direct coefficients show the same value for each of the conditions listed. The cross coupled coefficients (K_{xy} and K_{yx}) give values to 30 MN/m for the analytical cases and decrease steadily with increasing speed to around -40 MN/m. K_{yx} tends to be greater than K_{xy} for both the analytical and experimental conditions. As load is increased the cross coupled analytical coefficients slightly increase, while a slight decrease occurs for the experimental coefficients. These results are consistent with the findings of Al-Ghasem [3].

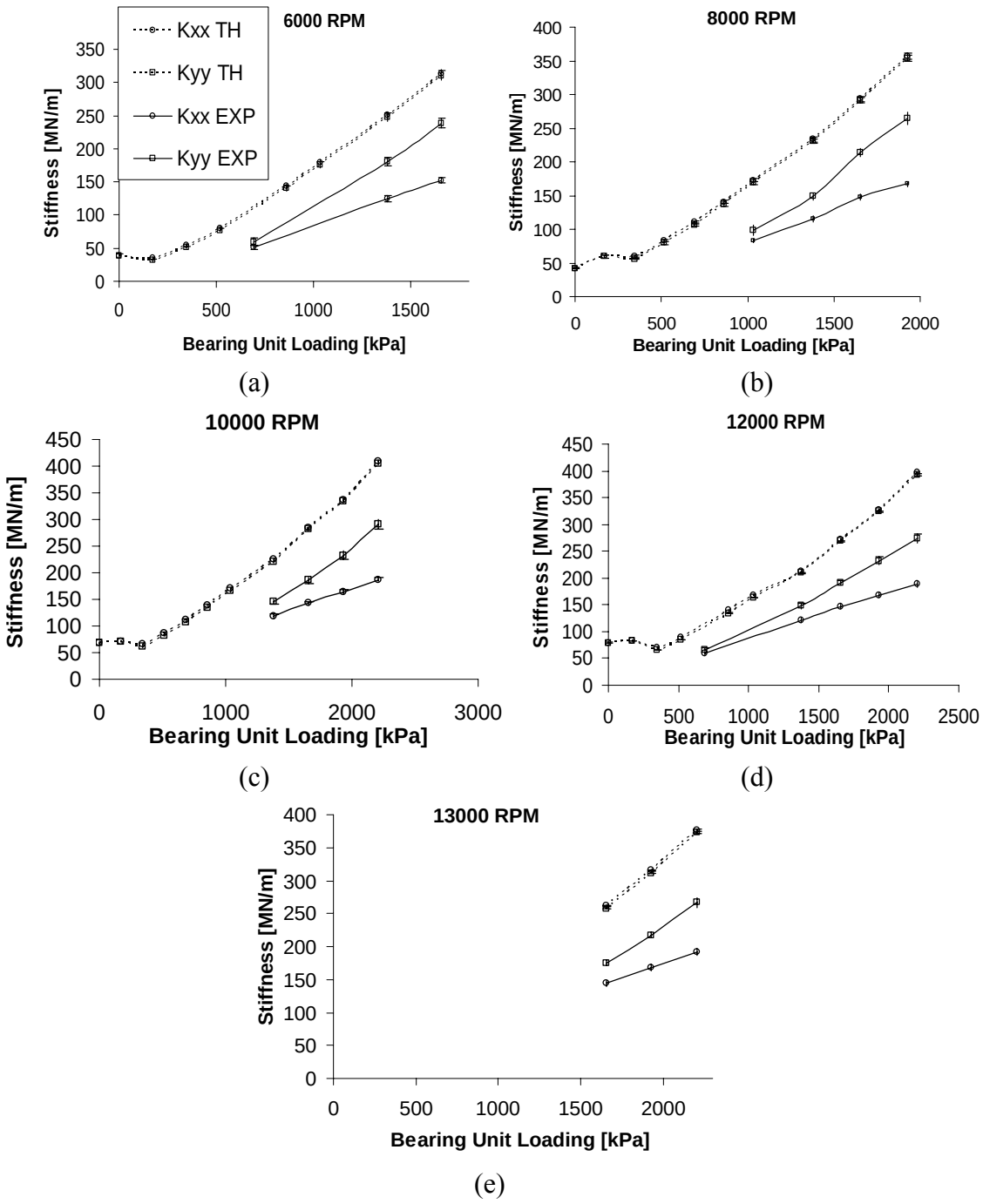

Figure 20: Direct Stiffness Coefficients in [MN/m] vs. Bearing Unit Load [kPa] for Rotor Speeds: (a) 6,000 rpm, (b) 8,000 rpm, (c) 10,000 rpm, (d) 12, 000 rpm, (e) 13,000 rpm

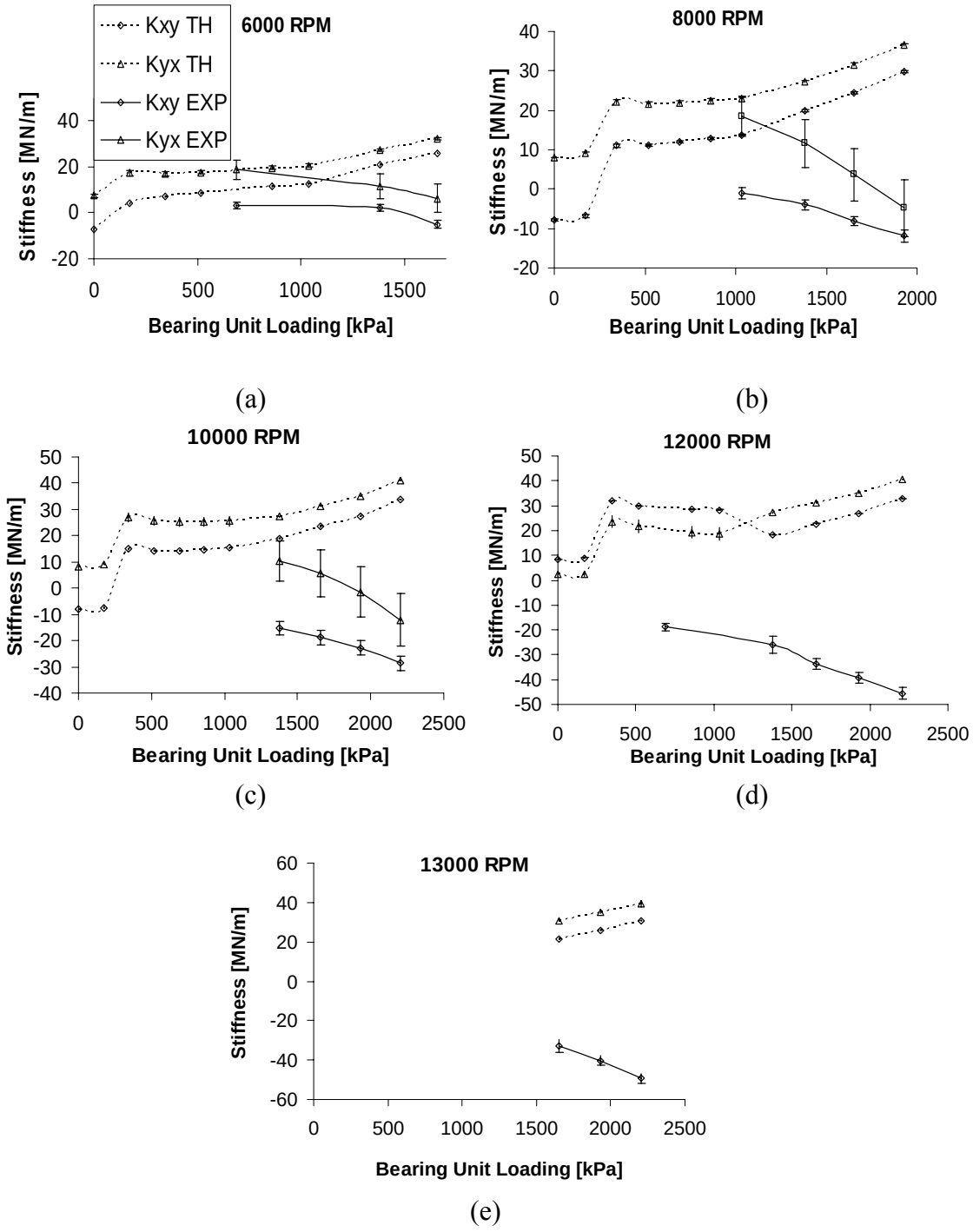

Figure 21: Cross-Coupled Stiffness Coefficients in [MN/m] vs. Bearing Unit Load [kPa] for Rotor Speeds: (a) 6,000 rpm, (b) 8,000 rpm, (c) 10,000 rpm, (d) 12, 000 rpm, (e) 13,000 rpm

Direct and cross-coupled damping coefficients are plotted against bearing unit loads in Figures 22 and 23 respectively for the different rotational speeds tested. The direct loaded damping coefficient C_{yy} is shown to increase for each speed, where the unloaded direct term remains nearly constant over the tested load range. The magnitude of the loaded term is greater than that of the unloaded for the experimental results, whereas no orthotropy is shown for the analytical results. The direct coefficients (C_{xx} and C_{yy}) and cross-coupled coefficients (C_{xy} and C_{yx}) are overpredicted by the analytical tool. As the unit load is increased the experimental cross-coupled coefficients drop below zero, while the analytical results remain nearly constant between 10 and 25 kN.s/m for each speed.

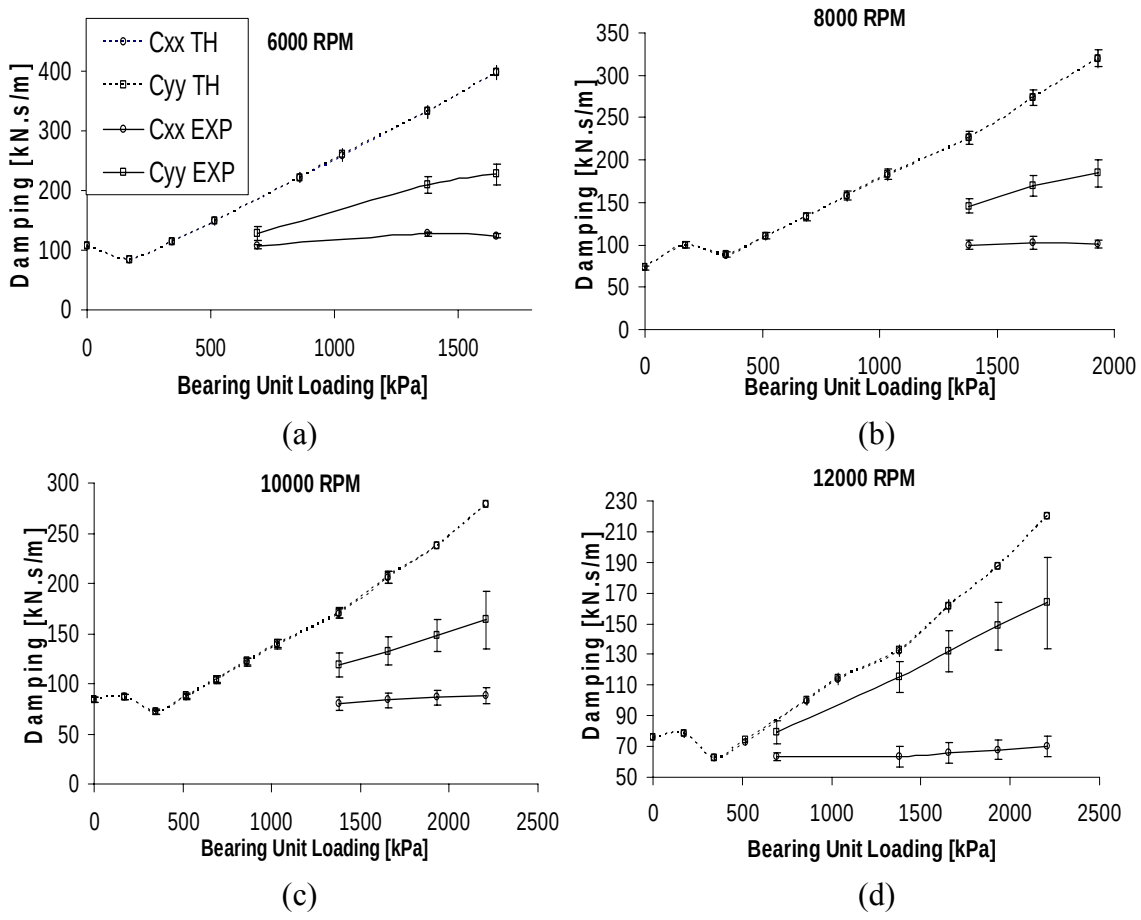

Figure 22: Direct Damping Coefficients in [kN.s/m] vs. Bearing Unit Load [kPa] for Rotor Speeds: (a) 6,000 rpm, (b) 8,000 rpm, (c) 10,000 rpm, (d) 12,000 rpm, (e) 13,000 rpm

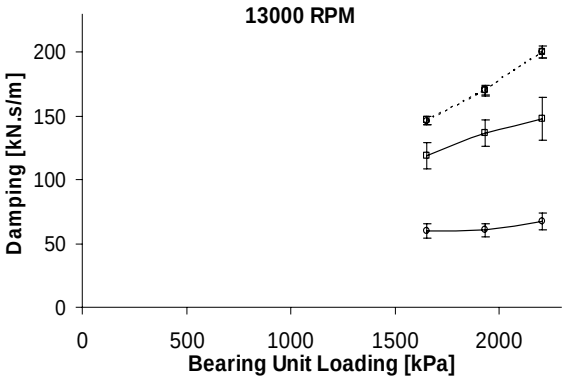

(e)

Figure 22: Continued

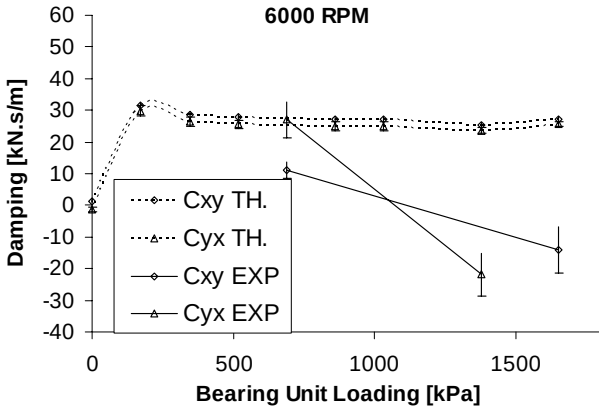

(a)

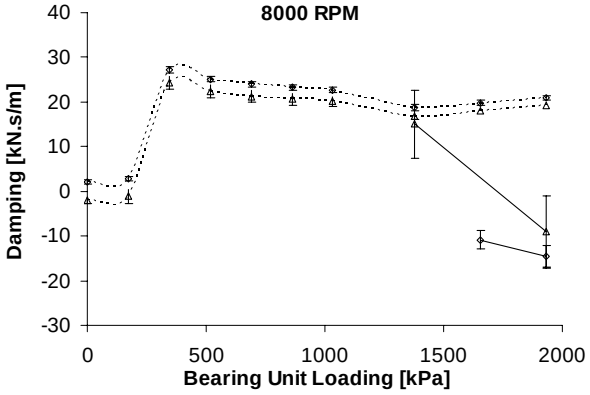

(b)

Figure 23: Cross-Coupled Damping Coefficients in [kN.s/m] vs. Bearing Unit Load [kPa] for Rotor Speeds: (a) 6,000 rpm, (b) 8,000 rpm

Direct and cross-coupled mass coefficients are plotted against bearing unit loads in Figures 24 and 25 respectively for the different rotational speeds tested. The direct loaded mass coefficients (M_{xx} and M_{yy}) are shown to increase with increasing unit load both experimentally and analytically. The direct analytical results however overpredict the experimental ones, and increasingly so as unit load is increased. The unloaded mass coefficient (M_{xx}) remains near zero for the experimental results, and decreases beneath it as load is increased. This is dissimilar to the analytical result, which shows equivalence with the loaded coefficient (M_{yy}). The cross coupled experimental coefficients (M_{xy} and M_{yx}) decrease with increasing load below zero, while the M_{xy} value exceeds M_{yx} more noticeably at the higher loads. The analytical values remain nearly constant around 5 kg over the range tested.

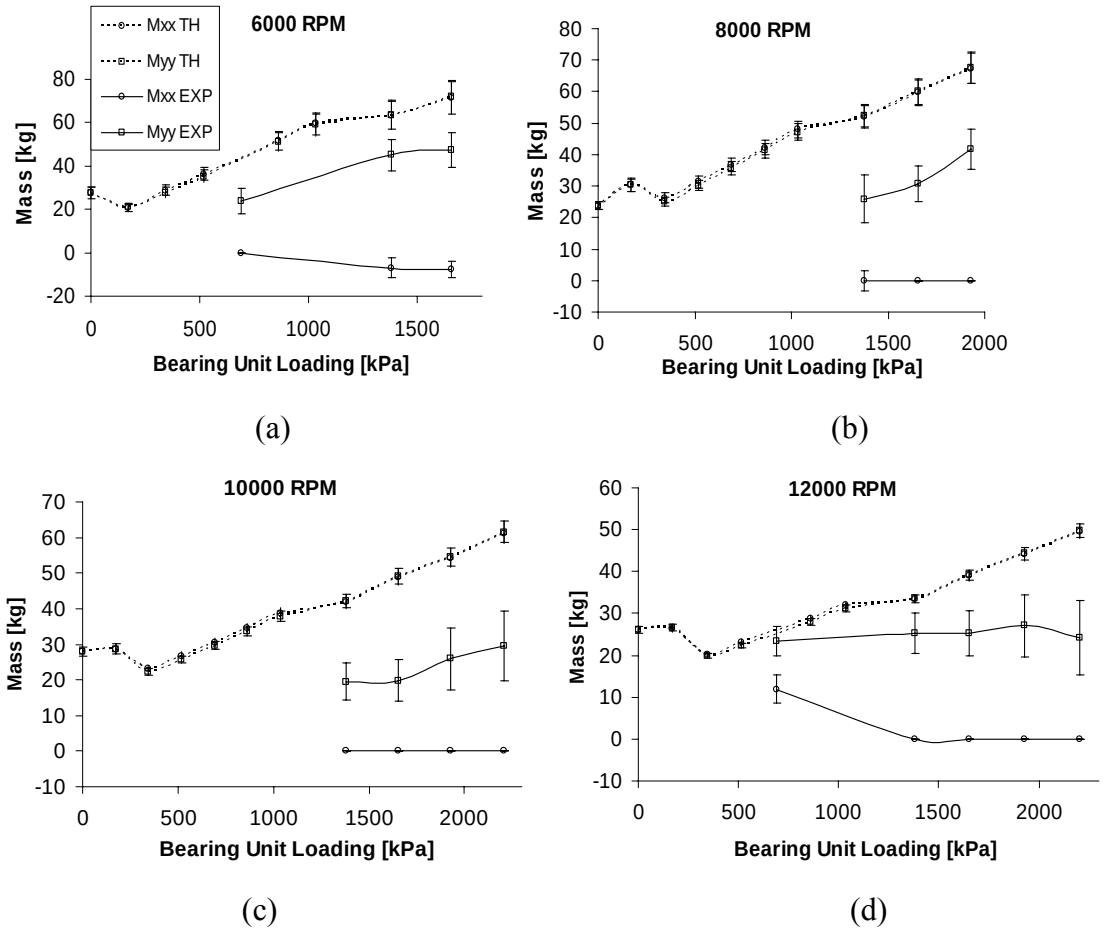

Figure 24: Direct Mass Coefficients [kg] vs. Bearing Unit Loads [kPa] for Different Rotor Speeds: (a) 6,000 rpm, (b) 8,000 rpm, (c) 10,000 rpm, (d) 12,000 rpm, (e) 13,000 rpm

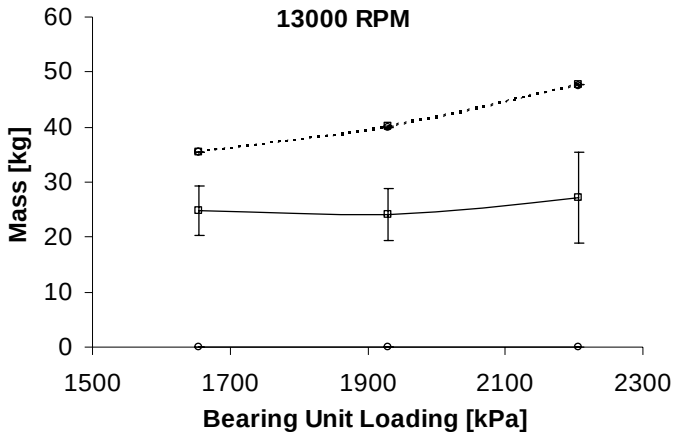

(e)

Figure 24: Continued

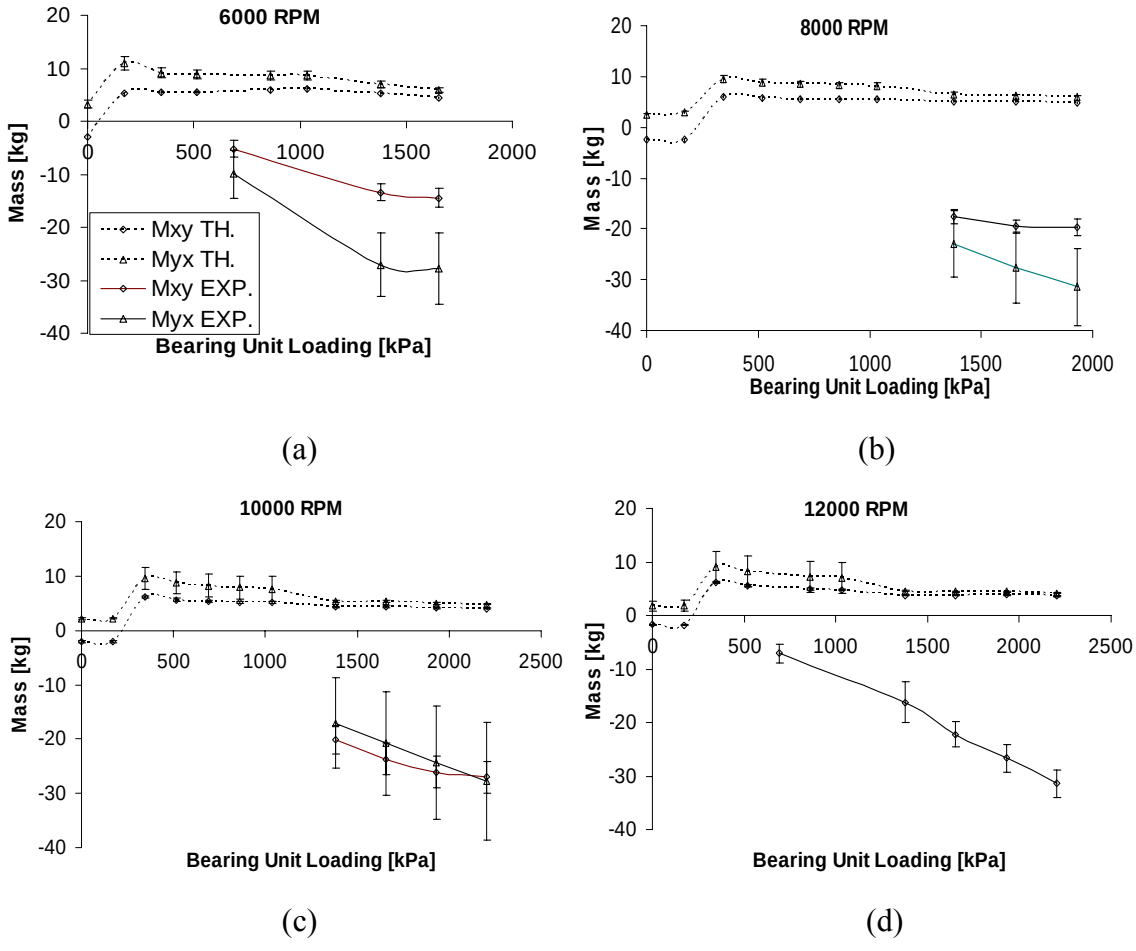

(a) (b)

(c) (d)

Figure 25: Cross-Coupled Mass Coefficients [kg] vs. Bearing Unit Loads [kPa] for Different Bearing Unit Loads: (a) 6,000 rpm, (b) 8,000 rpm, (c) 10,000 rpm, (d) 12,000 rpm, (e) 13,000 rpm

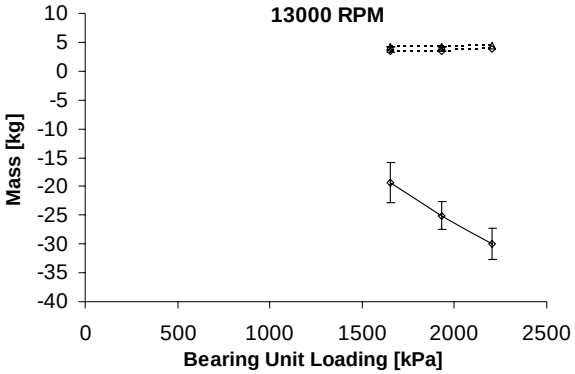

(e)

Figure 25: Continued

Stiffness, damping and mass coefficients are plotted against load at a rotational speed of 8,000 rpm in Figure 26, which includes the experimental results of both the present investigation and that performed by Al-Ghasem. The orthotropy observed at higher loads experimentally for each of the coefficients by Al-Ghasem between the direct coefficients continues on into the present study experimentally. The cross coupling values for the stiffness continue negatively with increasing load from Al-Ghasem's into the current one where K_{yx} is greater than K_{xy}. The cross coupled coefficients remain near zero which is expected for a flexure pivot pad bearing. The cross coupling effects for the damping and mass are similar to that of the stiffness. One notable event is that the unloaded direct mass coefficient (M_{xx}), and the unloaded damping coefficient (C_{xx}) do not follow the trends of the analytical result unlike the remaining coefficients. M_{xx} continues negatively with with increasing load, and C_{xx} evens out nearly constant with load.

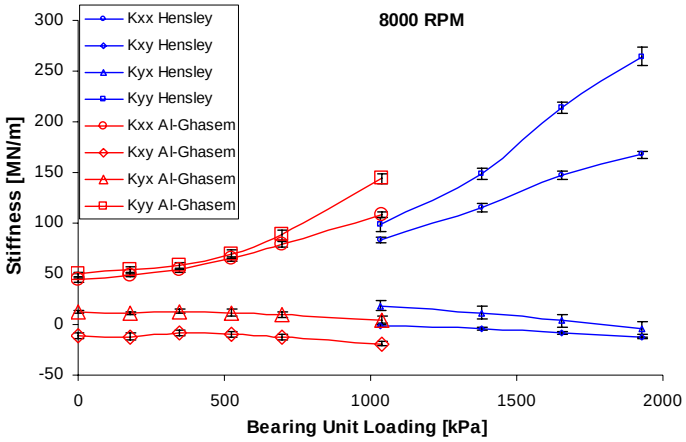

(a)

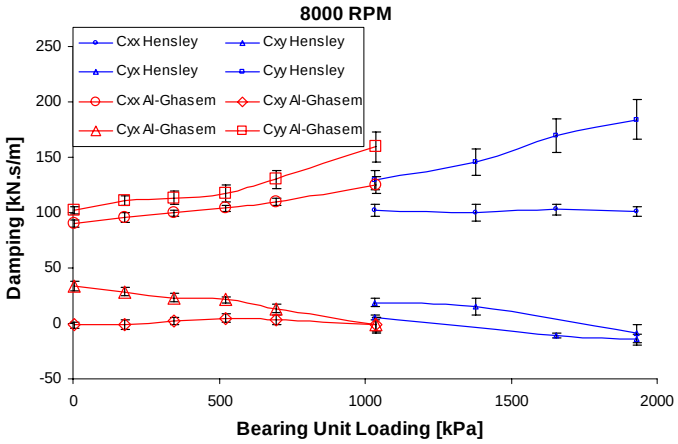

(b)

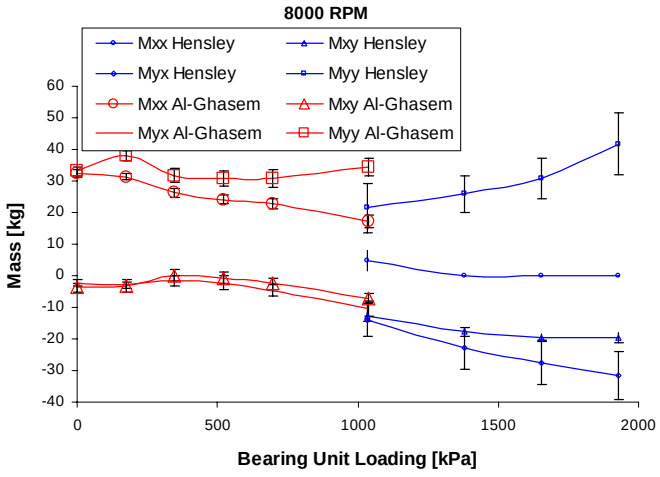

(c)

Figure 26: Comparison Including Experimental Results from Al-Ghasem (AD.) and Hensley (EXP.) of the (a) Stiffness, (b) Damping, and (c) Mass Coefficients at 8,000 RPM

Whirl Frequency Ratio

The whirl-frequency ratio is defined as the ratio between the rotor whirl frequency, and the onset speed of instability. Lund [6] provides a formula based on the rotordynamic coefficients to determine the whirl frequency for a rigid shaft supported by two identical plain journal bearings. Eq. 18 is used to provide the whirl-frequency ratio ignoring the fluid inertia and not taking into account the mass coefficients.

$$WFR^2 = \left(\frac{\Omega}{\omega_s}\right)^2 = \frac{(K_{eq} - k_{xx})(K_{eq} - k_{yy}) - k_{xy}k_{yx}}{c_{xx}c_{yy} - c_{xy}c_{yx}} \tag{18}$$

where,

$K_{eq} = \dfrac{c_{xx}k_{yy} + c_{yy}k_{xx} - c_{yx}k_{xy} - c_{xy}k_{yx}}{c_{xx} + c_{yy}}$, $k_{ij}\big|_{i,j=x,y} = \dfrac{C_p}{W}K_{ij}$ is the dimensionless stiffness and $c_{ij}\big|_{i,j=x,y} = \dfrac{C_p\omega}{W}C_{ij}$ is the dimensionless damping. The fluid inertia effects on the WFR are accounted for by San Andres [23]. These formulas account for the fluid inertia below, and are brought together in Eq. 19 for a result. This relationship was used to produce Figure 27 below.

$$a + b(WFR)^2 + c(WFR)^4 = 0 \tag{19}$$

where,

$a = k_{xx}k_{yy} - k_{xy}k_{yx} + K_{eq}^2 - (k_{xx} + k_{yy})K_{eq}$

$b = (k_{xx} + k_{yy})K_{eqm} + (m_{xx} + m_{yy})K_{eq} - 2K_{eq}K_{eqm} - Term$

$Term = k_{xx}m_{yy} + k_{yy}m_{xx} + c_{xx}c_{yy} - k_{xy}m_{yx} - k_{yx}m_{xy} - c_{xy}c_{yx}$

$c = K_{eqm}^2 + (m_{xx}m_{yy} - m_{xy}m_{yx}) - (m_{xx} + m_{yy})K_{eqm}$

$m_{ij}\big|_{i,j=x,y} = \dfrac{C_p\omega^2}{W}M_{ij}$

$K_{eqm} = \dfrac{c_{yy}m_{xx} + c_{xx}m_{yy} - c_{xy}m_{yx} - c_{yx}m_{xy}}{c_{yy} + c_{xx}}$

The WFR for plain journal bearings is generally 0.5, but the tested combinations below for the flexure pivot pad bearing give lower values. As load is increased from 0 to 1.7

MPa (240 psi) the WFR decreases from around 0.2 to 0. Load conditions from 0 to 1 MPa were calculated using the rotordynamic coefficients available in Al-Ghasem's thesis work [18]. As rotational speed increases the WFR tends increase slightly for the speed range between 6 and 12 krpm. All experimental tests conducted at and above 1.7 MPa (240 psi) gave WFR values of 0, suggesting an infinite onset speed of instability for operation at these conditions.

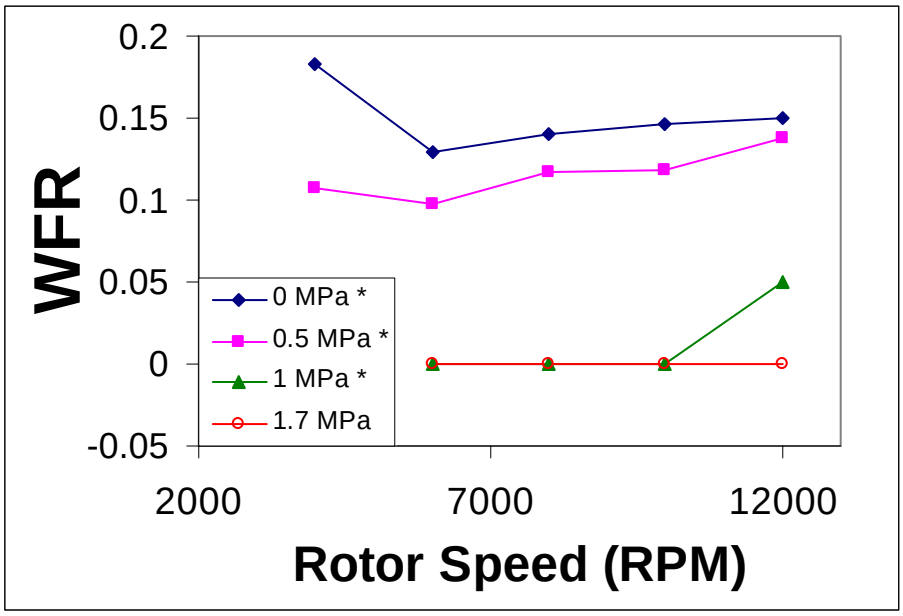

Figure 27: Whirl Frequency Ratio vs. Rotor Speed [rpm] for Different Bearing Unit Loads: (a) 0 MPa, (b) 0.5 MPa, (c) 1 MPa, (d) 1.7 MPa

STATIC RESULTS

Static Performance

Static (or steady-state) performance data presented in this section includes local stiffness, bearing load capacity (load/projection area), pad metal temperatures and estimated power losses [24]. The flow rate was maintained within a range of $8.92*10^{-4}$ to $9.14*10^{-4}$ m^3/s (14.14, 14.49 gpm), while the inlet temperate was kept within 40.96 to 46.67 °C (105.73 to 116 °F). This range contains the resulting values for all conditions of loading and rotational speed.

During a typical test, the shaft is brought up to the listed test conditions of rotational speed, oil inlet temperature, and oil flow rate. Alignment is gauged using the measurements of the proximity probes, and the pitch stabilizers are adjusted to account for this. After reaching the steady state condition and applying the required static load, the oil inlet and outlet temperatures, pad temperatures, static load and bearing oil flow rate data are taken several times and then averaged.

Figure 28 pictures the local and dynamic stiffnesses for the loads tested at 12,000 rpm for both Al-Ghasem and Hensley. The local stiffness is the slope of the curve where load is plotted against the displacement in the y-direction. The dynamic stiffnesses provided in the comparison are selected at the 20 [Hz] excitation frequency, which represents the 0-intercept for this case. The comparison provided shows good agreement for the test performed by Al-Ghasem previously and for the current investigation suggesting a reliable test for both cases. Also included in the figure is the inverse of the direct loaded flexibility coefficient, which is represented as Adjusted K_{yy}. To get to the flexibility coefficient the inverse of the stiffness matrix is performed, giving the direct loaded flexibility coefficient as $\frac{K_{xx}}{(K_{xx}K_{yy} - K_{yx}K_{xy})}$. The inverse of this term is equal to the slope of the load as a function of displacement in the y-direction, which represents the

local stiffness. Since the cross coupling (K_{xy}, K_{yx}) is small for this test, the difference between the dynamic stiffness (K_{xy}) and the inverse of the loaded flexibility coefficient is also small.

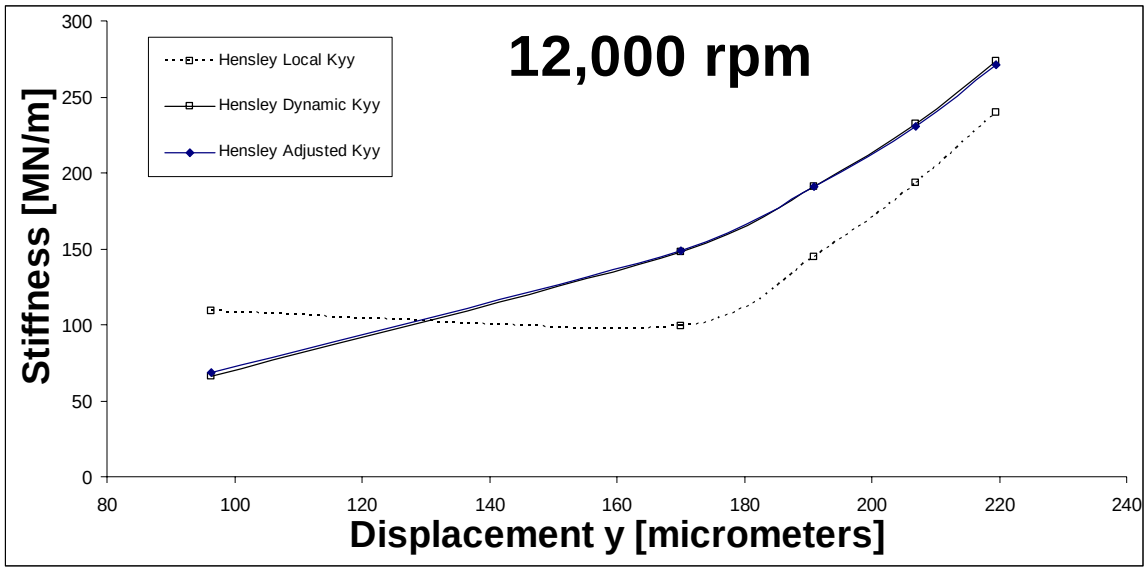

Figure 28: Local and Dynamic Stiffnesses at 12,000 rpm

Figure 29 shows the bearing centerline loci as a function of the static load 12,000 rpm. Here the measured coordinates (e_x, e_y) are divided by the radial pad clearance, which is 254 μm (10 mils). As the load is applied the eccentricity in the y-direction grows while decreasing in the x-direction. The growing eccentricity in the y-direction is due to the load applied with the static loader, and that in the x-direction is due to the cross-coupling effect. The load range plotted from Al-Ghasem's data is 0 to 1 MPa, while the data of Hensley's runs from 0.7 to 2.3 MPa for this speed.

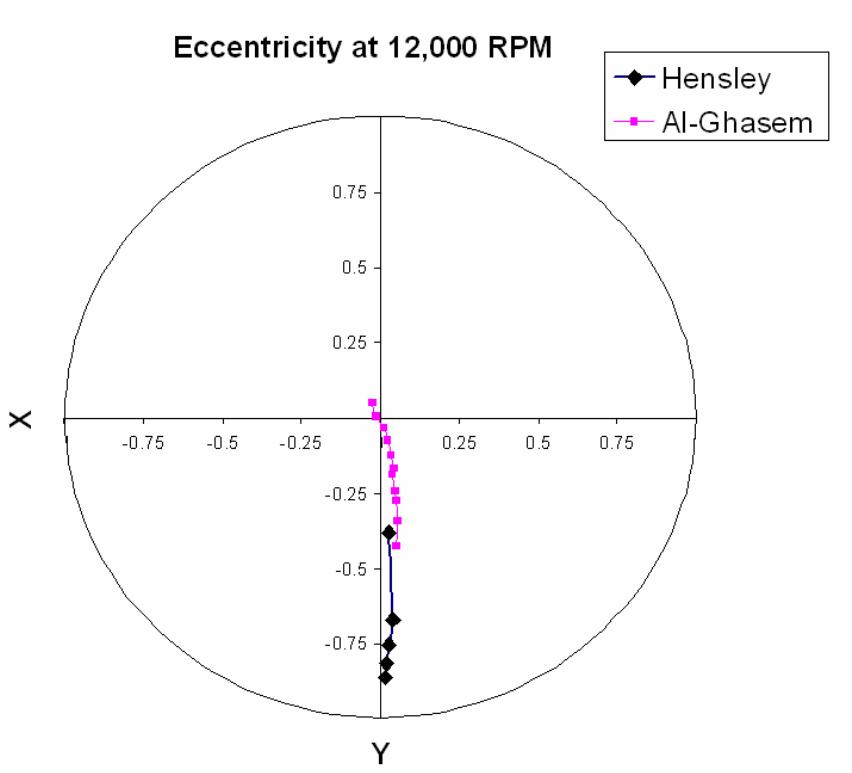

Figure 29: Static Centerline Locus of Al-Ghasem, Hensley and Theoretical Eccentricities at 12,000 RPM

The position of the bearing may be described with the eccentricity ratio ε and the attitude angle ϕ, as defined in the equation set 20 below:

$$\varepsilon_x = {e_x}/{C_p}\ ,\ \varepsilon_y = {e_y}/{C_p}$$

$$\varepsilon = \sqrt{(\varepsilon_x)^2 + (\varepsilon_y)^2} \qquad (20)$$

$$\phi = \tan^{-1}\left(\frac{\varepsilon_x}{\varepsilon_y}\right)\frac{180}{\pi} \qquad [\text{deg}]$$

Figures 30, 31, and 32 show the eccentricity ratio, attitude angle, and the estimated power loss as a function of the bearing load, respectively. The eccentricity ratio shows a nearly linear increase with increasing load. As higher loads are reached the eccentricity begins to level out, this may be due to the stiffening of the fluid film between the rotor and pad.

The theoretical, and experimental results of the eccentricity ratio for the present investigation are included with Al-Ghasem's experimental values in Figure 30. The continuation of the trend from Al-Ghasem into the present case is good.

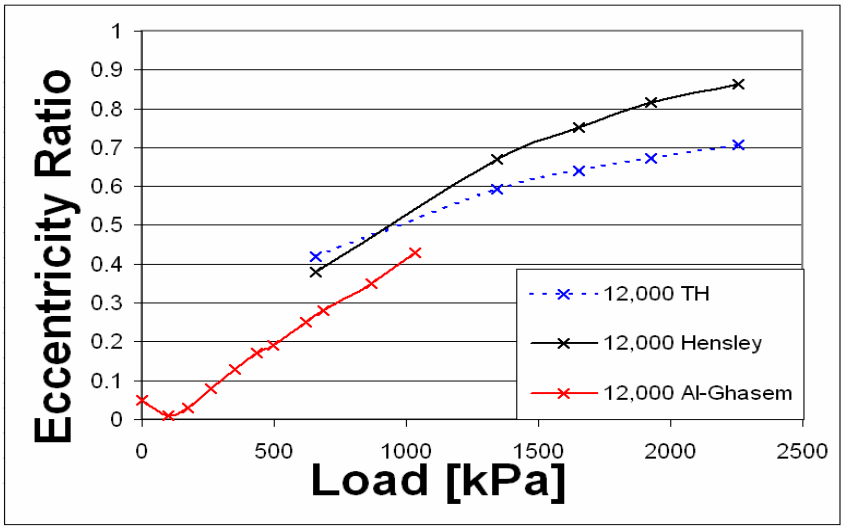

Figure 30: Eccentricity Ratio vs. Bearing Unit Load

In Figure 31 the attitude angle is plotted as a function of load. As load is increased the attitude angle continues to decrease more gradually. This trend is consistent with and expected based on Al-Ghasem's work at lower loads.

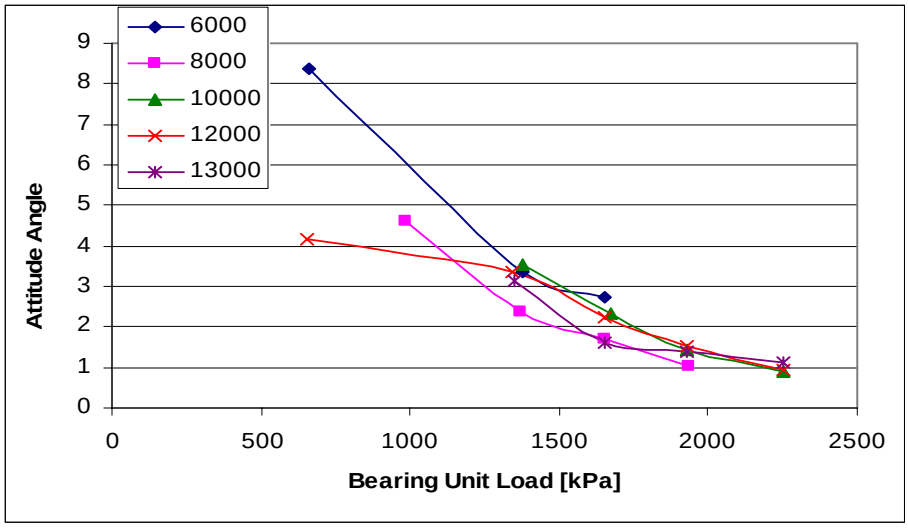

Figure 31: Attitude Angle vs. Bearing Unit Load

The estimated power loss remains nearly constant for each operating speed over the tested bearing unit load range as pictured in Figure 32. Greater magnitudes of power loss are experienced at the higher operating speeds. The power loss was calculated based on the change in bulk temperature of the lubricant, given in Eq. 21.

$$P = \rho \dot{Q} C_p (T_{out} - T_{in}) \tag{21}$$

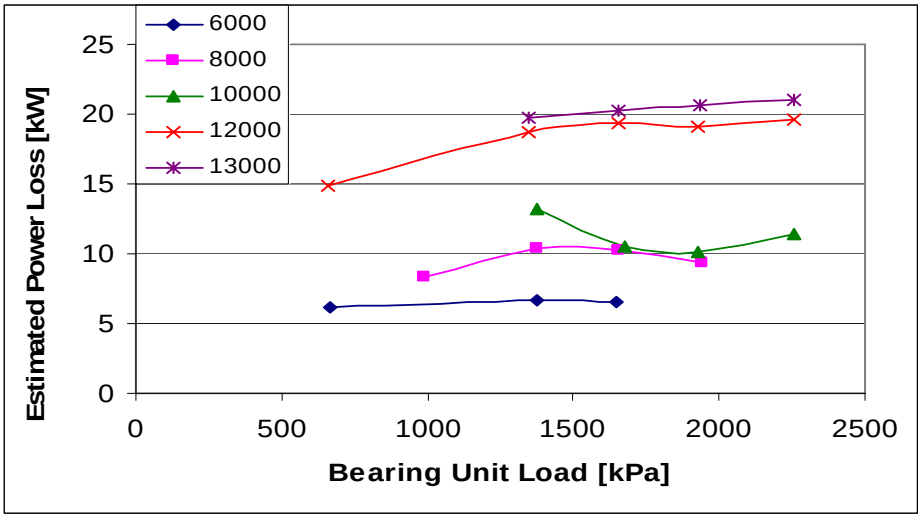

Figure 32: Estimated Power Loss vs. Bearing Unit Load

Pad Temperatures

Figure 33 shows the circumferential locations for the thermocouples as viewed from the drive end of the tester. When loaded the rotor moves in the loading direction indicated relative to the stator. These thermocouples are situated on the bearing at the drive end of the tester whereas an additional 5 thermocouples were placed adjacent to pad 4 on the non-drive end.

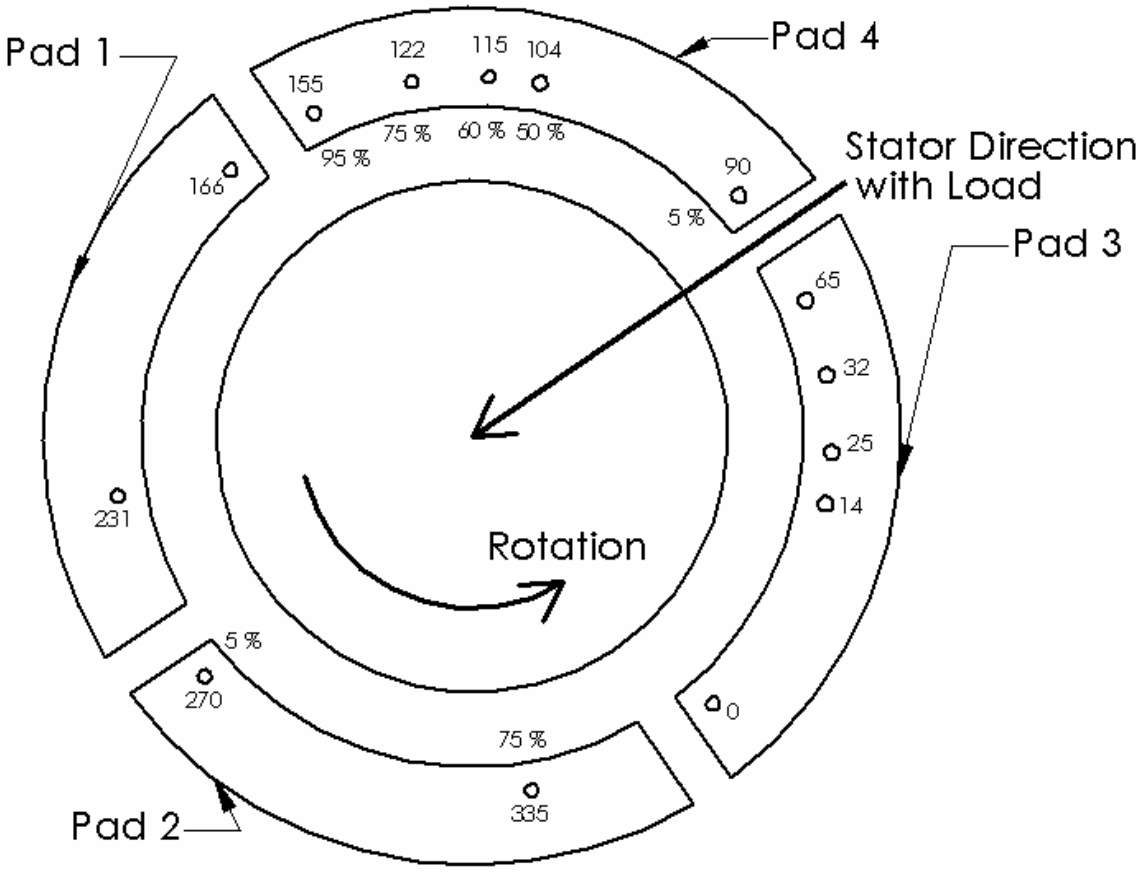

Figure 33: Thermocouple Locations (DE View)

Figure 34 provides an example temperature profile plot at a load of 19.6 kN and a bearing unit load of 2.2 MPa for different rotor speeds at different angles around the circumference of the bearing as listed. The remaining loads tested at 6.1, 12.3, 14.7, and 17.2 kN are also pictured in Figure 35, and show similar trends as that of the highest load yet at different magnitudes. Each of these loads corresponds to the bearing unit loads of

0.7, 1.4, 1.7, and 1.9 MPa respectively. As expected the trailing edge temperature located at 75% on pad 4 has the highest temperature. The temperature is also observed to increase with rotor speed, and unit load.

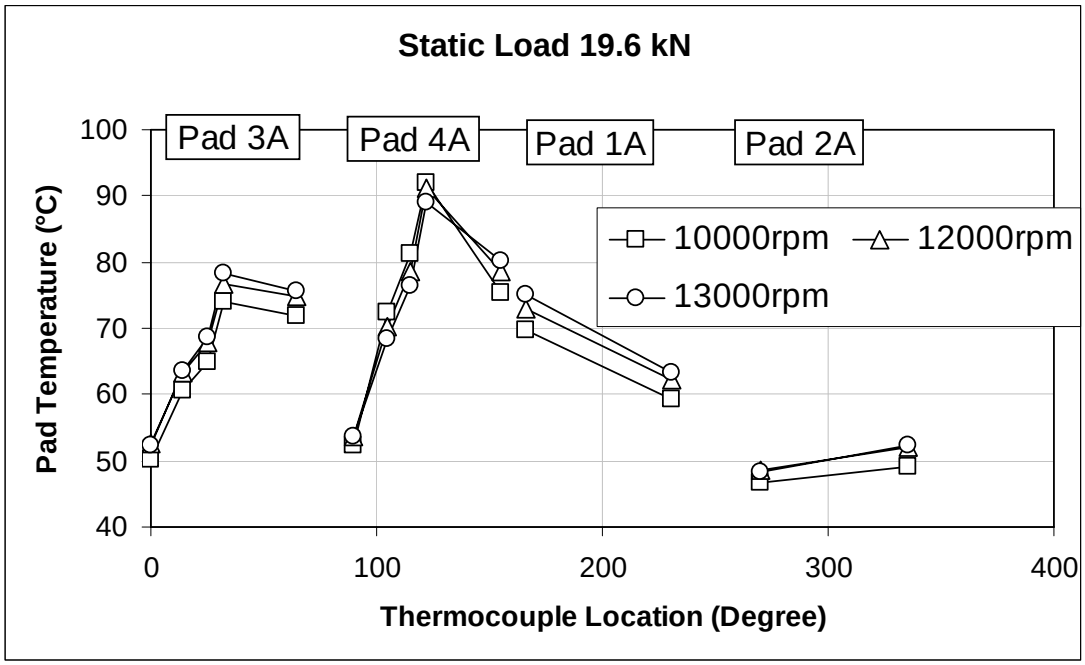

Figure 34: Pad Temperatures vs. Location at a Unit Load of 19.6 kN

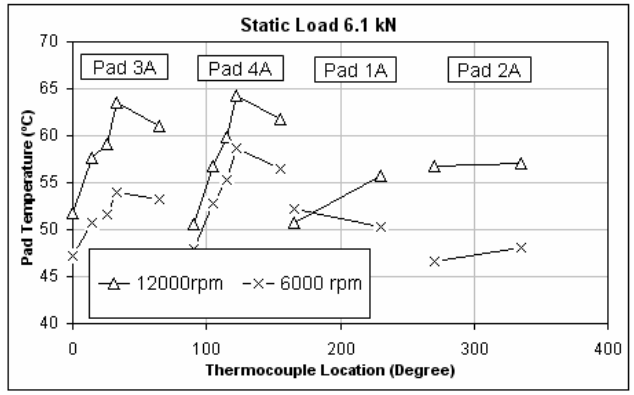

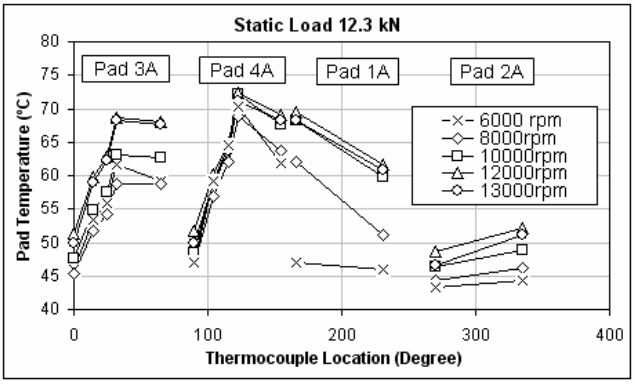

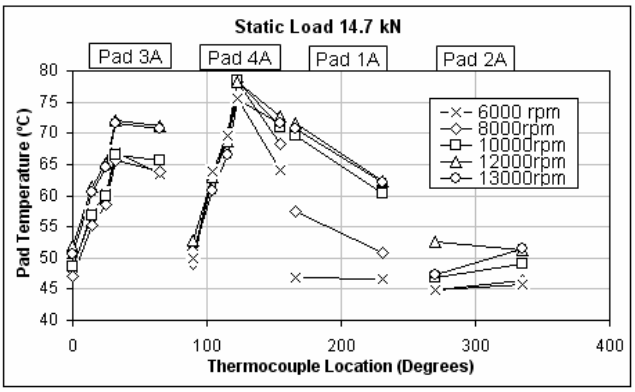

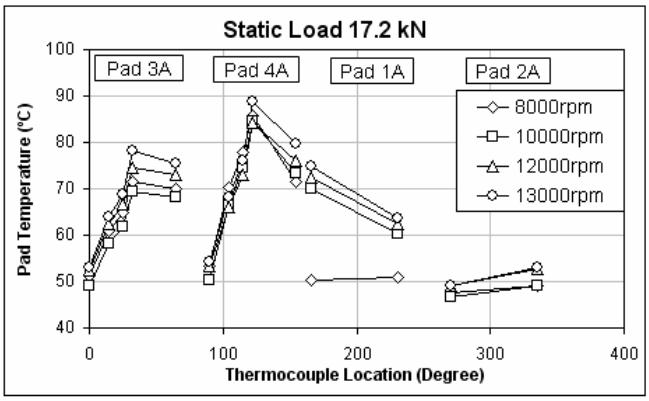

Figure 35: Pad Temperatures vs. Location at Varying Loads

Figures 36 and 37 respectively show the loaded and unloaded pad temperatures as a function of the load at a rotational speed of 13,000 rpm. Each set of pad temperatures is shown to increase with load. For both loaded pads the highest temperature is located at the 75% location. This tends to be common as the fresh oil that enters between the pads tends to cool the edges of the pads that it enters, thus the extremes of the pad are cooler. The increase in temperature as a function of unit loading remains true for every rotational speed tested, yet the unloaded pads decreased at lower speeds, such as 6,000. For the most part, the unloaded pad temperatures remain constant as a function of loading where the variation remains within approximately 5 °C.

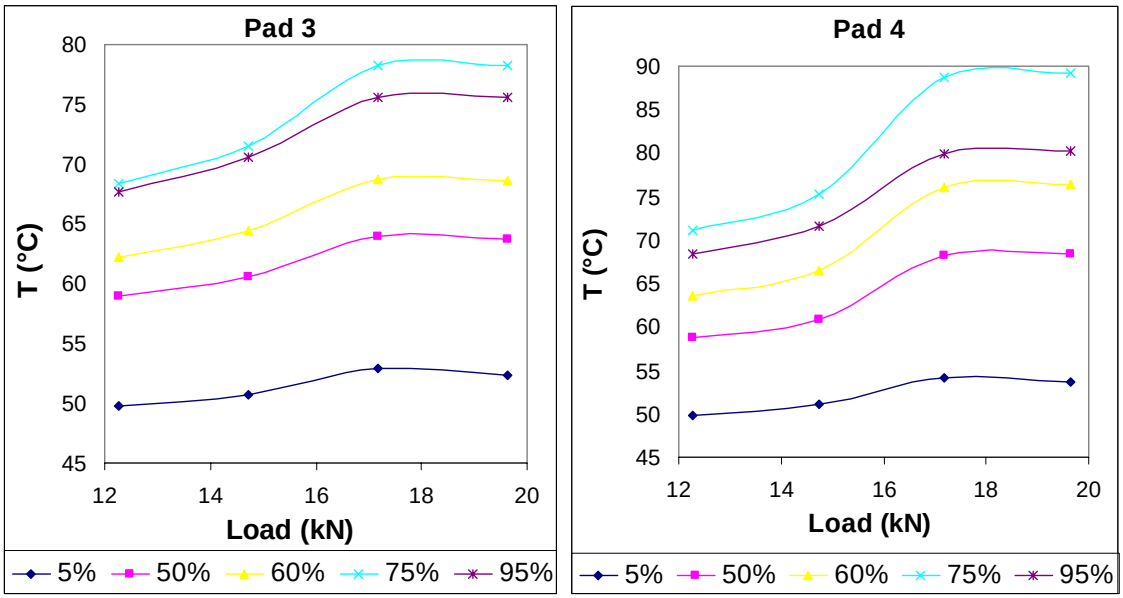

Figure 36: Loaded Pad Temperatures as a Function of Load at 13,000 rpm

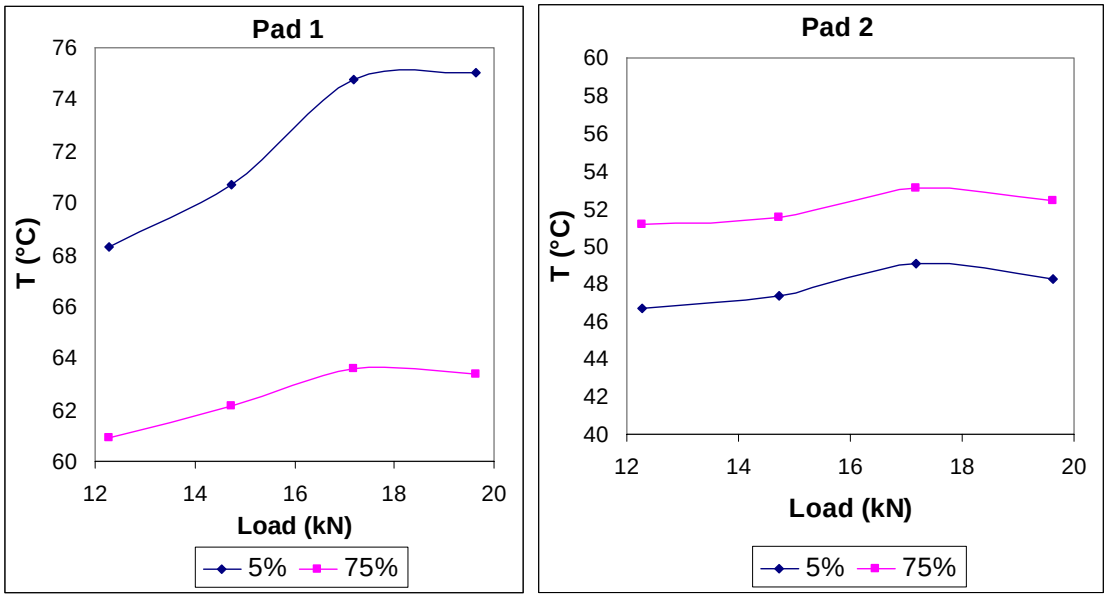

Figure 37: Unloaded Pad Temperatures as a Function of Load at 13,000 rpm

The 75% temperatures for pad 4 at both the drive end and non drive end locations are plotted against load for rotational speeds of 10,000, 12,000, and 13,000 rpm in Figure 38. These temperatures increase in a quadratic fashion, where the drive end temperatures exceed those at the non drive end.

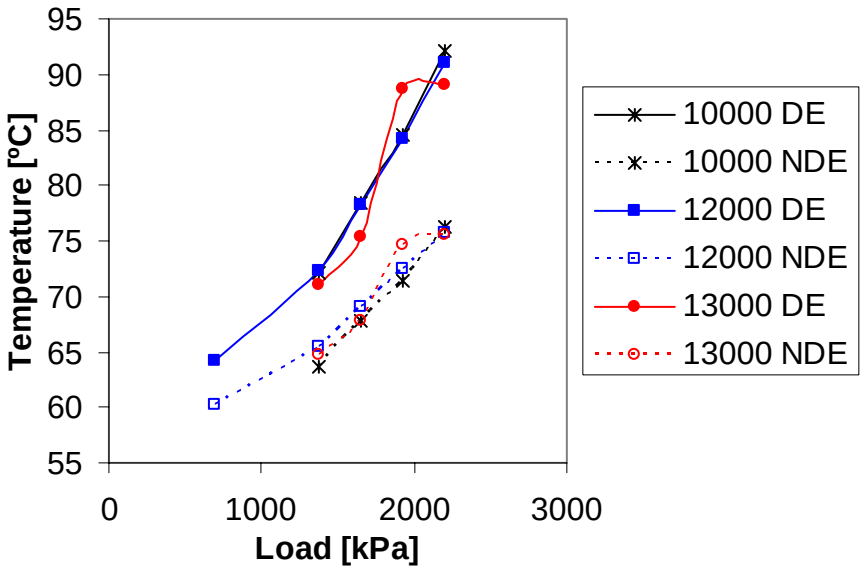

Figure 38: 75% Temperature [°F] vs. Load [psi] at Pad 4, DE and NDE

CONCLUSIONS

The experimental results presented were delivered to confirm the validity of the analytical model and to answer the question: *Are the rotordynamic coefficients of a FPB frequency dependent or not?* [3]. If the mass coefficients are included, all results for this thesis and Al-Ghasem's at lower loads may be said to be *frequency independent*. In the unit load range of 1 to 2.2 MPa, however, the resulting mass coefficients were generally negative and close to zero. Only in this range for the tests conducted could it be argued that stiffness coefficients are frequency independent without the inclusion of the mass coefficients.

The Bulk-Flow Governing equation was used as the analytical comparison for the experimental results rather than the Reynolds equation due to slightly better agreement. The stiffness, damping, and mass coefficients are commonly overpredicted by the model especially for the direct components of the impedance. The cross-coupled terms tend to be slightly overpredicted. The experimental results show orthotropy for both direct and cross-coupled terms; the model does not. This was especially significant for the direct components. The growing overprediction of the direct coefficients and absence of orthotropy in the analytical model were observed with increasing load for Al-Ghasem's experimental results and carry over into the present investigation. The overprediction might be to be due to the absence of the vertical flexure pivot stiffness in the analytical code.

Where experimental tests were performed at loads tested by Al-Ghasem the direct stiffness, damping, and mass coefficients were lower in magnitude. This is attributed to the increased radial bearing clearance associated with the present investigation over that of Al-Ghasem's. The following points are consistent with results produced by Al-Ghasem at lower loads, therefore supporting the reasonableness of the tested results:

- An infinite onset speed of instability is suggested by the resulting whirl-frequency ratios of 0 for the load range between 1.7 MPa (240 psi) and 2.2 MPa (320 psi).
- The local and dynamic stiffnesses are comparable.

- The attitude angle is less than 10 degrees for the applied static load range between 5 and 20 kN where it levels out around 1 degree at the higher values.
- Larger power losses are observed at higher rotational speeds. For the conditions tested, the effect of the load is dependent on the speed, but is nearly constant for each case with a variation under 6 kW.
- The 75% thermocouple location on pad 4 experienced the highest temperatures and increased with increasing load and rotational speed. The measured temperatures experienced at this location were greater at the DE than the NDE with an approximate 10 degree difference.

REFERENCES

[1] Rodriguez, L., 2004, "Experimental Frequency-Dependent Rotordynamic Coefficients for a Load-on-Pad, High Speed Flexible-Pivot Tilting-Pad Bearing," M.S. thesis, Mechanical Engineering, Texas A&M University, College Station, TX.

[2] Zeidan, F. Y., and Paquette, D. J., 1994, "Application of High Speed and High Performance Fluid Film Bearings in Rotating Machinery," *Proceedings of the 23th Turbomachinery Symposium*, Dallas, pp. 209-234.

[3] Al-Ghasem, A., 2004, "Measurement of Rotordynamic Coefficients for a High Speed Flexure-Pivot Tilting-Pad Bearing (Load Between Pad) Configuration," M.S. thesis, Mechanical Engineering, Texas A&M University, College Station, TX.

[4] Nicholas, J., 1994, "Tilt Pad Bearing Design", *Proceeding of the 23rd Turbomachinery Symposium*, Houston, pp. 179-194.

[5] Armentrout, R., and Paquette, D., 1993, "Rotordynamic Characteristics of Flexure-Pivot Tilting-Pad Journal Bearings," Tribology Transactions, **36**, 3, pp. 443-451.

[6] Lund, J., 1964, "Spring and Damping Coefficients for the Tilting Pad Journal Bearing," ASLE Transactions, **7**, pp. 342-352.

[7] Nicholas, J. C., Gunter, E. J., and Allaire, P. E., 1977, "Stiffness and Damping Coefficients for the Five-Pad Tilting-Pad bearing," ASLE Transactions, **22**, pp. 113-124.

[8] Barret, L., and Allaire, P., 1988, "The Eigenvalue Dependance of Reduced Tilting Pad Bearing Stiffness and Damping Coefficients," Tribology Transactions, **31**, 4, pp. 411-419.

[9] Reinhardt, E., and Lund, L., 1975, "The Influence of Fluid Inertia on the Dynamic Properties of Journal Bearings," ASME J. of Lubrication Technology, **97**, pp. 159-167.

[10] Rodriguez, L. and Childs, D., "Experimental Rotordynamic Coefficient Results for a Load-on-Pad Flexible-Pivot Tilting-Pad Bearing With Comparisons to Predictions From Bulk-Flow and Reynolds Equation Models," ASME paper TRIB2004-64042, Joint Triboloby Conference, Long Beach, CA, 24-27 October 2004, accepted for publication, ASME J. of Tribology.

[11] Al-Ghasem, A. and Childs, D., "Rotordynamic Coefficients; Measurements versus predictions for a High Speed Flexure-Pivot Tilting-Pad Bearing (Load-Between-Pad Configuration)," Paper No GT2005-68343, Proceedings of ASME Turbo Expo 2005 Power for Land, Sea and Air June 6-9, 2005, Nevada, USA, accepted for publication, ASME J. For Gas Turbines.

[12] DeChoudhury, P., Hill, M., and Paquette, D., 1992, "A Flexible Pad Bearing System for a High Speed Centrigugal Compressor," *Proceedings of the 21st Turbomachinery Symposium, Turbomachinery Laboratory*, Texas A&M University, pp. 57-64.

[13] Zeidan, F. Y., and Paquette, D. J., 1994, "Application of High Speed and High Performance Fluid Film Bearings in Rotating Machinery," *Proceedings of the 23rd Turbomachinery Symposium*, Dallas, pp. 209-234.

[14] San Andrés, L. A., 1996, "Turbulent Flow, Flexure-Pivot Hybrid Bearings for Cryogenic Applications," Transactions of the ASME, **118**, pp. 190-200.

[15] Parsell, J.K., Allaire, P.E., and Barrett, L.E., 1983, "Frequency Effects in Tilting-Pad Journal Bearing Dynamic Coefficients," ASLE Tran., **26**, pp. 222-227.

[16] Ha, Hyun Cheon, and Yang, Seong Heon, 1998, "Excitation Frequency Effects on the Stiffness and Damping Coefficients of a Five-Pad Tilting Pad Journal Bearing," ASME, Paper No. 98-TRIB-44.

[17] Kaul, A., 1999, "Design and Development of a Test Setup for the Experimental Determination of the Rotordynamic and Leakage Characteristics of Annular Bushing Oil Seals," M.S. thesis. Texas A&M University, College Station, TX.

[18] Childs, D., and Hale, K., 1994, "A Test Apparatus and Facility to Identify the Rotordynamic Coefficients of High-Speed Hydrostatic Bearings," ASME J. of Tribology, **116**, pp. 337-344.

[19] Montgomery, Douglas C., and Runger, George C.., 2003, *Applied Statistics and Probability for Engineers*., John Wiley & Sons, Inc., New York.

[20] San Andres, L.A., 1995, "Bulk-Flow Analysis of Flexure and Tilting Pad Fluid Film Bearings," TRC-B&C-3-95. Turbomachinery Laboratory, Texas A&M University, College Station, Texas.

[21] San Andres, Luis, "Modern Lubrication and Its Applications," Class Notes for MEEN 626. Texas A&M University, ch. 8, pp. 2.

[22] Childs, Dara W., "Rotordynamics of Turbomachinery..Looking Back..Looking Forward," *Proceedings, IFToMM 6th International Conference on Rotordynamics*, pp. 25-27, September 2002, Sydney, Australia.

[23] San Andres, L., 1991, "Effect of eccentricity on the Force Response of a Hybrid Bearing," Tribology Transactions, **34**, 4, pp. 537-544.

[24] Carter, C., Jughaiman, B., and Hensley J., "Experimental Rotordynamic Coefficient and Static Characteristics for a KMC Four-Pad Flexure Pivot Pad Tilting Pad Bearing with a 50% Offset and Load Between Pad Configuration," TRC Report, August 2005, Turbomachinery Laboratory, Texas A&M University.

APPENDIX

Table 6: Static Performance and Measurement Data

ω [RPM]	W [kN]	p [kPa]	e_{xNDE} [μm]	e_{yNDE} [μm]	e_{xDE} [μm]	e_{yDE} [μm]	ε	ϕ [degree]	$\dot{Q}$ [m3/s]	T_{in} [C°]	T_o [C°]	T_{ave} [C°]	S	P [kW]
6000	5.9	662.8	22.5	153	20.9	142	0.59	8.3864	53.95	44.6	48.7	46.7	0.17	6.18
6000	12.3	1377.9	13.5	208	11.7	219	0.84	3.371	53.76	41.5	45.9	43.7	0.09	6.61
6000	14.7	1649.9	11.9	222	9.99	238	0.91	2.7288	53.72	42.6	46.9	44.8	0.07	6.55
8000	8.8	985.0	13.8	175	13.4	163	0.67	4.5963	53.61	43.5	49.1	46.3	0.15	8.37
8000	12.2	1372.0	8.31	189	7.51	191	0.75	2.379	53.68	41.8	48.7	45.3	0.11	10.40
8000	14.7	1655.8	6.54	205	5.86	217	0.83	1.6844	53.64	42.0	48.8	45.4	0.09	10.21
8000	17.3	1938.2	2.5	222	5.55	225	0.88	1.0331	54.01	42.3	48.5	45.4	0.08	9.39
10000	12.2	1374.3	9.26	180	12.2	168	0.69	3.5301	53.84	42.8	51.7	47.2	0.13	13.22
10000	14.9	1674.6	8.01	195	7.92	194	0.77	2.3433	53.86	43.1	52.1	47.6	0.11	10.52
10000	17.2	1928.3	5.8	207	4.69	213	0.83	1.4338	53.83	43.1	52.1	47.6	0.09	10.14
10000	20.1	2253.2	4.74	217	2.19	231	0.88	0.8847	53.78	43.2	52.3	47.8	0.08	11.37
12000	5.9	657.1	12.5	94.8	1.56	98	0.38	4.1816	53.92	45.6	55.6	50.6	0.30	14.81
12000	12.0	1344.6	11.1	177	8.9	163	0.67	3.359	53.91	44.6	56.3	50.5	0.15	18.74
12000	14.7	1653.2	9.24	193	5.79	189	0.75	2.2533	54.83	44.8	56.8	50.8	0.12	19.41
12000	17.2	1927.0	7.66	205	3.43	209	0.82	1.5341	53.83	44.9	56.9	50.9	0.10	19.08
12000	20.1	2255.2	5.65	213	1.53	226	0.86	0.9376	53.78	44.1	56.4	50.2	0.09	19.58
13000	12.0	1349.9	11.8	164	5.84	160	0.64	3.1127	53.68	41.8	54.9	48.4	0.17	19.77
13000	14.7	1651.2	8.98	180	1.21	181	0.71	1.6165	53.69	42.4	55.9	49.1	0.14	20.30
13000	17.2	1930.6	9.43	197	0.4	204	0.79	1.4048	53.8	44.1	57.7	50.9	0.11	20.67
13000	20.1	2253.0	9.05	209	-0.72	223	0.85	1.104	53.81	43.9	57.8	50.8	0.09	21.00

Table 7: Pad Temperatures

ω [RPM]	W [kN]	T1	T2	T3	T4	T5	T6	T7	T8	T9	T10	T11	T12	T13	T14	T15	T16	T17	T18	T19
6000	6.1	47.3	50.8	51.6	54.0	53.2	47.9	52.8	55.3	58.7	56.5	52.2	50.3	46.6	48.1	47.1	52.7	53.8	53.7	54.0
6000	12.3	46.1	53.4	55.8	61.6	59.1	47.1	59.1	64.5	70.3	61.8	47.0	46.0	43.4	44.4	45.0	57.2	60.9	61.2	58.3
6000	14.7	48.5	57.3	60.3	66.9	63.5	49.9	63.9	69.7	75.6	64.1	46.9	46.7	44.9	45.8	47.2	62.1	65.9	66.0	61.5
8000	12.3	45.3	51.8	54.1	58.8	58.8	46.8	57.0	62.0	68.8	63.7	62.1	51.1	44.4	46.1	45.3	55.4	59.1	60.4	59.5
8000	14.7	47.0	55.4	58.5	65.7	63.8	49.1	63.5	70.0	78.3	68.4	57.5	50.9	44.9	46.5	46.5	61.1	66.1	67.1	63.4
8000	17.2	51.1	61.0	64.8	71.4	69.9	53.3	70.4	77.9	85.8	71.4	50.3	50.8	47.7	49.1	49.9	67.0	73.1	73.8	67.5
10000	12.3	47.7	54.9	57.5	63.1	62.7	48.5	59.0	64.4	72.1	67.5	68.2	59.9	46.4	49.0	46.9	57.7	61.7	63.7	63.2
10000	14.7	48.6	56.8	59.9	66.6	65.7	49.6	62.9	69.4	78.4	70.9	69.6	60.4	46.8	49.1	47.5	60.8	65.4	67.8	66.1
10000	17.2	49.0	58.1	61.7	69.5	68.2	50.2	66.8	74.5	84.6	73.3	70.0	60.2	46.6	49.0	48.0	63.4	63.8	71.4	68.5
10000	19.6	50.3	60.5	64.8	74.1	71.9	52.2	72.5	81.3	92.1	75.4	69.6	59.4	46.8	49.1	49.1	67.9	75.2	76.3	70.9
12000	6.1	51.7	57.7	59.1	63.5	61.0	50.5	56.8	59.8	64.2	61.7	50.8	55.7	56.8	57.1	49.2	56.8	58.7	60.2	61.2
12000	12.3	51.4	59.9	63.0	68.7	68.1	51.7	60.1	64.9	72.3	69.0	69.5	61.6	48.7	52.2	50.3	60.7	63.8	65.5	65.9
12000	14.7	52.0	61.4	65.2	72.1	71.1	52.8	62.9	68.7	78.2	72.6	71.6	62.2	49.1	52.6	51.3	62.6	66.6	69.1	68.6
12000	17.2	52.6	62.5	66.7	74.5	73.1	53.4	65.9	73.0	84.2	76.2	72.3	62.5	49.1	52.7	51.3	64.9	70.0	72.5	71.0
12000	19.6	52.6	63.2	67.9	76.8	74.7	53.6	70.2	78.6	91.1	78.7	73.1	62.2	48.5	52.0	50.9	67.6	73.8	75.8	72.9
13000	12.3	49.8	59.0	62.3	68.3	67.7	49.8	58.8	63.6	71.1	68.3	68.3	60.9	46.7	51.1	49.2	59.4	62.1	64.7	65.5
13000	14.7	50.7	60.6	64.4	71.6	70.6	51.0	60.8	66.4	75.3	71.7	70.7	62.2	47.4	51.6	50.8	61.5	65.3	67.8	67.9
13000	17.2	52.9	63.9	68.7	78.2	75.5	54.1	68.3	76.1	88.8	79.8	74.8	63.6	49.1	53.1	52.5	66.5	71.8	74.7	72.8
13000	19.6	52.3	63.7	68.6	78.2	75.5	53.7	68.4	76.3	89.1	80.2	75.1	63.4	48.2	52.4	51.9	67.1	72.7	75.6	73.1

Table 8: Thermocouple Numbers and Locations per Pad

Pad No. (Side)	Pad 3(DE)					Pad 4(DE)					Pad 1(DE)		Pad 2(DE)		Pad 4(NDE)				
Thermocouple	T1	T2	T3	T4	T5	T6	T7	T8	T9	T10	T11	T12	T13	T14	T15	T16	T17	T18	T19
% From Pad Arc Length	5	50	60	75	95	5	50	60	75	95	5	75	5	75	5	50	60	75	95
[Degree]	0	14.4	25.2	32.4	64.8	90	104	115	122	155	166	231	270	335	90	104	115	122	155

Table 9: Experimental Stiffness Coefficients, Related Uncertainties, and the Real Coefficients of Determination

		Experiment								Coefficient of Determination			
ω [RPM]	p [Mpa]	K_{xx} [MN/m]	K_{xy} [MN/m]	K_{yx} [MN/m]	K_{yy} [MN/m]	ΔK_{xx} [MN/m]	ΔK_{xy} [MN/m]	ΔK_{yx} [MN/m]	ΔK_{yy} [MN/m]	${R_{xx}}^2$	${R_{xy}}^2$	${R_{yx}}^2$	${R_{yy}}^2$
6000	0.7	51.26	3.31	18.84	59.80	3.50	1.44	4.14	5.35	0.1836	0.7474	0.5703	0.8165
6000	1.4	124.84	2.04	11.38	180.63	4.18	1.37	5.50	6.58	0.3914	0.9559	0.8476	0.9146
6000	1.7	152.49	-5.06	6.23	238.28	3.35	1.60	6.19	7.17	0.5349	0.9489	0.8217	0.9090
8000	1	83.64	-1.05	18.55	98.74	3.13	1.37	4.84	7.33	0.3569	0.9544	0.6601	0.6667
8000	1.4	115.29	-3.98	11.57	148.76	4.16	1.29	6.17	5.49	0.0403	0.9775	0.7641	0.8384
8000	1.7	147.59	-8.09	3.67	213.85	4.14	1.24	6.71	6.05	0.0819	0.9831	0.7975	0.8583
8000	1.9	167.39	-11.92	-4.83	264.45	3.99	1.57	7.28	9.26	0.1311	0.9736	0.8134	0.8263
10000	1.4	119.29	-15.28	10.16	145.35	4.55	2.40	7.70	4.80	0.0018	0.9390	0.5192	0.7853
10000	1.7	142.24	-18.79	5.60	185.78	4.27	2.66	8.82	5.53	0.0013	0.9459	0.5506	0.7405
10000	1.9	163.23	-22.80	-1.43	232.37	4.28	2.65	9.71	8.03	0.0472	0.9553	0.5820	0.6982
10000	2.2	187.29	-28.68	-12.17	291.85	4.32	2.67	10.04	9.06	0.2275	0.9577	0.6280	0.7007
12000	0.7	58.80	-18.78	7.24	66.50	3.02	1.55	2.76	3.11	0.7582	0.8111	0.8235	0.9197
12000	1.4	120.90	-25.97	5.12	147.60	4.87	3.34	7.90	4.34	0.0058	0.8265	0.3552	0.8737
12000	1.7	147.22	-33.76	0.31	191.17	4.85	2.17	9.23	4.76	0.0152	0.9552	0.3485	0.8511
12000	1.9	168.50	-39.33	-5.98	232.24	5.07	2.26	10.37	6.61	0.0532	0.9658	0.3590	0.7723
12000	2.2	188.51	-45.50	-10.75	273.61	5.51	2.29	11.43	7.95	0.1077	0.9745	0.3225	0.6519
13000	1.7	143.89	-32.62	1.59	175.21	4.62	3.26	7.54	4.24	0.0213	0.8833	0.4372	0.8794
13000	1.9	167.79	-40.22	-5.04	217.44	4.53	2.27	9.23	4.47	0.0029	0.9631	0.4075	0.8619
13000	2.2	192.29	-49.27	-11.24	266.71	5.15	2.51	11.59	7.80	0.0630	0.9681	0.3447	0.7195

Table 10: Experimental Damping Coefficients, Related Uncertainties, and the Imaginary Coefficients of Determination

		Experiment								Coefficient of Determination			
ω [RPM]	p [Mpa]	C_{xx} [kN.s/m]	C_{xy} [kN.s/m]	C_{yx} [kN.s/m]	C_{yy} [kN.s/m]	ΔC_{xx} [kN.s/m]	ΔC_{xy} [kN.s/m]	ΔC_{yx} [kN.s/m]	ΔC_{yy} [kN.s/m]	${R_{xx}}^2$	${R_{xy}}^2$	${R_{yx}}^2$	${R_{yy}}^2$
6000	0.7	106.13	11.20	26.98	127.62	3.11	2.61	5.67	10.59	0.9969	0.8349	0.8615	0.9755
6000	1.4	126.85	-7.57	-4.11	208.61	3.20	5.64	6.29	14.88	0.9977	0.3307	0.1049	0.9818
6000	1.7	123.92	-14.01	-21.92	226.56	3.21	7.26	6.68	17.08	0.9976	0.5051	0.7469	0.9797
8000	1	102.32	5.57	19.02	128.89	5.68	2.31	3.63	8.62	0.9881	0.5975	0.8755	0.9828
8000	1.4	100.07	-0.36	15.03	145.78	7.35	1.99	7.67	11.76	0.9793	0.0083	0.4959	0.9752
8000	1.7	102.84	-10.82	-1.26	169.42	5.18	2.55	7.96	15.60	0.9902	0.8221	0.0064	0.9680
8000	1.9	100.81	-14.67	-8.98	184.21	4.20	4.56	8.43	17.69	0.9933	0.7261	0.2253	0.9652
10000	1.4	80.36	14.91	12.64	119.08	6.71	1.98	11.34	11.95	0.9735	0.9357	0.2414	0.9622
10000	1.7	83.58	10.78	8.31	132.65	7.56	2.56	12.07	14.14	0.9691	0.8195	0.1082	0.9575
10000	1.9	86.20	3.86	3.26	147.89	7.32	3.00	12.72	15.56	0.9726	0.2981	0.0165	0.9586
10000	2.2	87.82	-5.55	-5.78	163.51	7.55	4.69	13.21	28.20	0.9720	0.2634	0.0468	0.8959
12000	0.7	63.33	-5.19	-2.29	79.31	2.62	2.85	3.74	7.75	0.9934	0.4585	0.0879	0.9641
12000	1.4	63.60	13.13	-5.05	115.28	6.55	2.27	6.80	10.05	0.9602	0.8958	0.1237	0.9712
12000	1.7	65.93	8.85	-12.87	132.06	6.56	2.06	8.39	13.67	0.9628	0.8259	0.3758	0.9598
12000	1.9	67.99	3.36	-17.96	148.38	6.67	3.36	10.33	15.16	0.9637	0.2041	0.4365	0.9608
12000	2.2	69.96	-0.97	-24.00	163.48	6.94	6.07	11.86	29.51	0.9630	0.0065	0.5120	0.8871
13000	1.7	59.67	14.33	-7.38	118.59	5.42	2.95	5.80	10.33	0.9668	0.8499	0.2800	0.9694
13000	1.9	60.53	9.69	-14.61	136.31	5.18	3.29	7.64	10.22	0.9704	0.6750	0.4676	0.9771
13000	2.2	67.05	4.89	-22.06	147.92	6.45	5.86	10.89	16.76	0.9629	0.1432	0.4963	0.9492

Table 11: Experimental Mass Coefficients and Related Uncertainties

ω [RPM]	p [MPa]	Experiment							
		M_{xx} [kg]	M_{xy} [kg]	M_{yx} [kg]	M_{yy} [kg]	ΔM_{xx} [kg]	ΔM_{xy} [kg]	ΔM_{yx} [kg]	ΔM_{yy} [kg]
6000	0.7	3.48	-5.18	-9.97	23.61	3.84	1.58	4.53	5.86
6000	1.4	-7.02	-13.40	-27.13	45.04	4.59	1.51	6.03	7.21
6000	1.7	-7.52	-14.43	-27.79	47.47	3.67	1.75	6.78	7.86
8000	1.0	4.83	-12.94	-13.96	21.44	3.28	1.43	5.07	7.67
8000	1.4	1.76	-17.65	-22.96	25.84	4.36	1.36	6.46	5.74
8000	1.7	-2.56	-19.49	-27.54	30.79	4.34	1.29	7.02	6.33
8000	1.9	-3.21	-19.69	-31.43	41.77	4.18	1.64	7.62	9.69
10000	1.4	-0.42	-20.06	-17.03	19.53	4.90	2.59	8.30	5.17
10000	1.7	-0.33	-23.68	-20.78	19.86	4.60	2.87	9.50	5.95
10000	1.9	-2.03	-26.07	-24.37	25.99	4.61	2.85	10.45	8.65
10000	2.2	-4.99	-27.03	-27.76	29.50	4.66	2.87	10.81	9.76
12000	0.7	11.86	-7.11	-13.24	23.35	3.39	1.74	3.10	3.49
12000	1.4	0.83	-16.19	-13.01	25.33	5.47	3.75	8.87	4.87
12000	1.7	-1.34	-22.20	-14.98	25.25	5.44	2.43	10.37	5.34
12000	1.9	-2.67	-26.69	-17.23	27.02	5.70	2.54	11.65	7.43
12000	2.2	-4.25	-31.40	-17.50	24.15	6.19	2.57	12.84	8.93
13000	1.7	1.48	-19.41	-14.41	24.80	4.90	3.46	8.01	4.50
13000	1.9	0.53	-25.10	-16.60	24.17	4.81	2.41	9.81	4.74
13000	2.2	-2.89	-30.01	-18.22	27.06	5.47	2.67	12.31	8.28

Table 12: Theoretical Stiffness, Damping and Mass Coefficients for Rotational Speeds 6 and 8 krpm

		Theory (bulk-flow)											
ω [RPM]	p [MPa]	K_{xx} [MN/m]	K_{xy} [MN/m]	K_{yx} [MN/m]	K_{yy} [MN/m]	C_{xx} [kN.s/m]	C_{xy} [kN.s/m]	C_{yx} [kN.s/m]	C_{yy} [kN.s/m]	M_{xx} [kg]	M_{xy} [kg]	M_{yx} [kg]	M_{yy} [kg]
6000	0.0	38.48	-7.32	7.42	38.48	105.76	1.36	-1.35	105.76	27.58	-3.02	3.24	27.58
6000	0.2	35.11	4.08	17.28	31.19	82.62	31.50	29.81	84.18	20.64	5.24	11.03	21.12
6000	0.3	54.74	7.16	16.90	51.07	113.38	28.69	26.57	113.95	28.93	5.41	9.13	27.79
6000	0.5	80.68	8.62	17.65	77.15	147.43	27.71	25.55	148.08	36.30	5.56	8.83	35.34
6000	0.7	102.26	10.92	18.26	99.84	165.72	22.81	20.93	166.15	37.40	5.43	7.36	37.41
6000	0.9	143.39	11.40	19.57	140.12	220.78	27.07	24.95	221.50	51.65	5.88	8.62	50.97
6000	1.0	178.71	12.65	20.53	175.54	258.51	26.99	24.91	259.22	59.55	6.06	8.63	58.97
6000	1.4	250.35	20.71	27.29	248.09	330.88	25.24	23.60	331.21	63.53	5.21	6.86	63.68
6000	1.6	312.78	26.07	32.24	310.78	396.12	27.22	25.81	396.19	71.45	4.40	5.81	71.76
8000	0.0	42.24	-7.88	7.89	42.24	72.91	2.04	-2.03	72.91	23.73	-2.45	2.45	23.73
8000	0.2	59.30	-6.84	9.08	59.51	99.98	2.82	-1.15	99.97	30.23	-2.48	2.86	30.42
8000	0.3	60.14	11.02	22.15	56.02	87.84	27.13	24.25	88.61	26.24	6.01	9.56	25.12
8000	0.5	83.42	11.25	21.71	79.26	109.38	25.12	22.33	110.24	31.29	5.67	8.86	30.20
8000	0.7	110.41	11.96	21.92	106.33	132.64	24.00	21.27	133.55	36.65	5.60	8.51	35.67
8000	0.9	140.37	12.86	22.42	136.36	156.98	23.23	20.57	157.91	42.24	5.58	8.28	41.33
8000	1.0	172.95	13.76	23.00	169.04	182.08	22.72	20.11	182.93	48.00	5.63	8.17	47.18
8000	1.4	233.19	19.93	27.31	230.58	226.33	18.76	16.83	226.66	52.03	5.16	6.44	52.23
8000	1.7	293.57	24.51	31.63	291.05	272.89	19.81	18.01	273.16	59.73	5.03	6.21	59.99
8000	1.9	356.44	29.72	36.64	354.01	319.84	20.91	19.20	320.05	67.37	4.79	5.90	67.66

Table 13: Theoretical Stiffness, Damping and Mass Coefficients for Rotational Speeds 10, 12 and 13 krpm

		Theory (bulk-flow)											
ω [RPM]	p [MPa]	K_{xx} [MN/m]	K_{xy} [MN/m]	K_{yx} [MN/m]	K_{yy} [MN/m]	C_{xx} [kN.s/m]	C_{xy} [kN.s/m]	C_{yx} [kN.s/m]	C_{yy} [kN.s/m]	M_{xx} [kg]	M_{xy} [kg]	M_{yx} [kg]	M_{yy} [kg]
10000	0.0	67.56	-8.13	8.13	67.56	83.95	2.25	-2.25	83.95	28.02	-2.11	2.12	28.01
10000	0.2	71.35	-7.42	9.00	71.49	86.72	2.73	-1.78	86.68	28.60	-2.13	2.22	28.71
10000	0.3	64.90	14.98	26.96	60.65	71.47	25.11	21.86	72.33	23.25	6.15	9.51	22.32
10000	0.5	86.44	14.29	25.66	81.99	86.71	22.94	19.84	87.69	26.78	5.63	8.71	25.79
10000	0.7	111.53	14.36	25.26	107.06	103.40	21.60	18.60	104.43	30.56	5.35	8.20	29.60
10000	0.9	139.62	14.75	25.26	135.14	121.03	20.66	17.75	122.06	34.57	5.20	7.86	33.65
10000	1.0	170.10	15.32	25.51	165.69	139.21	20.02	17.18	140.25	38.73	5.14	7.65	37.88
10000	1.4	223.87	18.94	27.21	220.67	169.85	15.31	13.19	170.39	41.91	4.26	5.32	42.05
10000	1.7	284.12	23.44	31.33	281.08	205.67	15.77	13.81	206.08	48.90	4.41	5.35	49.10
10000	1.9	337.22	27.60	35.28	334.28	237.10	16.86	15.00	237.43	54.31	4.10	4.97	54.57
10000	2.2	407.99	33.7063	41.1526	405.153	278.14	17.84	16.08	278.35	61.27	4.02	4.81	61.57
12000	0.0	79.32	8.26	2.24	79.32	76.28	2.24	-2.24	76.28	26.06	-1.71	1.77	26.06
12000	0.2	82.68	8.92	2.57	82.78	78.22	2.57	-1.95	78.17	26.47	-1.75	1.81	26.53
12000	0.3	69.14	31.78	23.57	65.46	62.65	23.57	20.26	62.34	20.16	6.28	9.02	19.88
12000	0.5	89.41	29.76	21.73	84.85	72.97	21.73	18.57	73.96	23.18	5.56	8.17	22.35
12000	0.7	95.57	9.34	20.27	90.99	71.54	13.07	10.14	72.72	20.94	3.24	4.83	20.53
12000	0.9	139.28	28.33	19.30	134.52	99.41	19.30	16.33	100.51	28.88	4.94	7.28	28.01
12000	1.0	168.02	28.24	18.56	163.25	113.48	18.56	15.65	114.63	31.91	4.77	7.00	31.09
12000	1.4	212.75	18.15	27.11	209.08	132.28	13.09	10.94	132.94	33.38	3.73	4.56	33.54
12000	1.7	272.19	22.71	31.23	268.74	161.26	13.62	11.65	161.72	38.96	3.80	4.49	39.20
12000	1.9	327.29	26.88	35.10	323.97	187.27	13.90	12.06	187.59	44.01	3.86	4.48	44.30
12000	2.2	396.04	32.73	40.69	392.85	220.09	15.06	13.35	220.35	49.49	3.68	4.22	49.86
13000	1.7	261.47	21.47	30.73	257.49	145.95	13.36	11.15	146.70	35.33	3.37	4.19	35.42
13000	1.9	315.14	25.89	34.80	311.35	169.72	13.75	11.70	170.35	39.86	3.49	4.19	40.05
13000	2.2	376.57	30.88	39.44	372.88	199.77	14.24	12.33	200.32	47.48	3.80	4.47	47.70

Table 14: Experimental Added-Mass Coefficients and Uncertainties with Theoretical Added-Mass Coefficients

ω [RPM]	p [MPa]	Theory (bulk-flow) K_{xx} [MN/m]	K_{xy} [MN/m]	K_{yx} [MN/m]	K_{yy} [MN/m]	C_{xx} [kN.s/m]	C_{xy} [kN.s/m]	C_{yx} [kN.s/m]	C_{yy} [kN.s/m]	M_{xx} [kg]	M_{xy} [kg]	M_{yx} [kg]	M_{yy} [kg]
10000	0.0	67.56	-8.13	8.13	67.56	83.95	2.25	-2.25	83.95	28.02	-2.11	2.12	28.01
10000	0.2	71.35	-7.42	9.00	71.49	86.72	2.73	-1.78	86.68	28.60	-2.13	2.22	28.71
10000	0.3	64.90	14.98	26.96	60.65	71.47	25.11	21.86	72.33	23.25	6.15	9.51	22.32
10000	0.5	86.44	14.29	25.66	81.99	86.71	22.94	19.84	87.69	26.78	5.63	8.71	25.79
10000	0.7	111.53	14.36	25.26	107.06	103.40	21.60	18.60	104.43	30.56	5.35	8.20	29.60
10000	0.9	139.62	14.75	25.26	135.14	121.03	20.66	17.75	122.06	34.57	5.20	7.86	33.65
10000	1.0	170.10	15.32	25.51	165.69	139.21	20.02	17.18	140.25	38.73	5.14	7.65	37.88
10000	1.4	223.87	18.94	27.21	220.67	169.85	15.31	13.19	170.39	41.91	4.26	5.32	42.05
10000	1.7	284.12	23.44	31.33	281.08	205.67	15.77	13.81	206.08	48.90	4.41	5.35	49.10
10000	1.9	337.22	27.60	35.28	334.28	237.10	16.86	15.00	237.43	54.31	4.10	4.97	54.57
10000	2.2	407.99	33.7063	41.1526	405.153	278.14	17.84	16.08	278.35	61.27	4.02	4.81	61.57
12000	0.0	79.32	8.26	2.24	79.32	76.28	2.24	-2.24	76.28	26.06	-1.71	1.77	26.06
12000	0.2	82.68	8.92	2.57	82.78	78.22	2.57	-1.95	78.17	26.47	-1.75	1.81	26.53
12000	0.3	69.14	31.78	23.57	65.46	62.65	23.57	20.26	62.34	20.16	6.28	9.02	19.88
12000	0.5	89.41	29.76	21.73	84.85	72.97	21.73	18.57	73.96	23.18	5.56	8.17	22.35
12000	0.7	95.57	9.34	20.27	90.99	71.54	13.07	10.14	72.72	20.94	3.24	4.83	20.53
12000	0.9	139.28	28.33	19.30	134.52	99.41	19.30	16.33	100.51	28.88	4.94	7.28	28.01
12000	1.0	168.02	28.24	18.56	163.25	113.48	18.56	15.65	114.63	31.91	4.77	7.00	31.09
12000	1.4	212.75	18.15	27.11	209.08	132.28	13.09	10.94	132.94	33.38	3.73	4.56	33.54
12000	1.7	272.19	22.71	31.23	268.74	161.26	13.62	11.65	161.72	38.96	3.80	4.49	39.20
12000	1.9	327.29	26.88	35.10	323.97	187.27	13.90	12.06	187.59	44.01	3.86	4.48	44.30
12000	2.2	396.04	32.73	40.69	392.85	220.09	15.06	13.35	220.35	49.49	3.68	4.22	49.86
13000	1.7	261.47	21.47	30.73	257.49	145.95	13.36	11.15	146.70	35.33	3.37	4.19	35.42
13000	1.9	315.14	25.89	34.80	311.35	169.72	13.75	11.70	170.35	39.86	3.49	4.19	40.05
13000	2.2	376.57	30.88	39.44	372.88	199.77	14.24	12.33	200.32	47.48	3.80	4.47	47.70

Table 15: Experimental Dynamic Stiffness at 6,000 rpm and 0.7 MPa

Ω Hz	Ω/ω	Experiment: Dynamic Stiffness Re(H_{xx})	Im(H_{xx})	Re(H_{xy})	Im(H_{xy})	Re(H_{yx})	Im(H_{yx})	Re(H_{yy})	Im(H_{yy})	Uncertainty Re(U_{xx})	Im(U_{xx})	Re(U_{xy})	Im(U_{xy})	Re(U_{yx})	Im(U_{yx})	Re(U_{yy})	Im(U_{yy})
20	0.2	56.1	3.3	5.4	-0.3	24.5	-5.0	65.8	12.4	1.7	1.3	0.9	0.9	2.6	3.1	1.2	0.9
30	0.3	54.0	11.1	4.2	-2.1	21.7	-3.5	64.1	15.4	1.4	0.9	0.7	0.4	1.9	1.7	1.2	0.6
40	0.4	53.6	18.4	2.7	-1.2	18.8	1.5	60.7	25.9	1.3	0.8	0.5	0.4	1.6	0.8	1.3	0.7
50	0.5	54.0	25.1	2.3	-1.3	17.3	-2.1	62.5	29.2	1.4	1.0	0.4	0.4	2.2	0.9	1.0	0.8
70	0.7	52.2	35.8	2.9	0.5	23.1	7.0	56.8	47.7	1.5	0.9	0.4	0.3	1.9	1.3	0.5	1.4
80	0.8	51.8	41.7	5.2	1.9	20.3	4.8	47.1	66.5	1.3	0.9	0.4	0.4	0.9	1.1	1.1	1.2
90	0.9	50.9	48.0	4.4	3.1	19.5	8.4	50.7	72.1	1.6	1.3	0.7	0.5	0.4	0.7	1.0	1.6
110	1.1	46.8	60.7	3.2	3.4	18.4	8.6	39.6	72.3	1.3	1.7	0.6	0.6	0.6	1.3	0.6	1.9
130	1.3	43.2	73.4	5.4	3.9	25.4	8.8	43.6	85.1	1.2	2.1	0.7	0.8	1.2	0.5	1.3	1.6
140	1.4	40.8	80.2	9.2	7.7	32.7	16.9	31.4	112.1	1.6	2.5	0.8	0.6	1.4	0.8	1.0	2.1
150	1.5	40.5	86.8	10.0	4.1	36.6	12.8	45.9	107.5	1.1	2.5	1.0	1.0	1.9	1.0	1.4	2.0
160	1.6	44.7	96.1	8.6	6.5	19.7	21.2	30.9	117.2	1.1	1.9	1.3	0.9	1.6	1.4	1.4	2.4
170	1.7	46.0	105.7	12.4	7.4	19.3	14.1	22.0	135.0	2.6	3.0	1.6	1.2	1.1	1.2	1.4	2.7
190	1.9	44.9	119.0	10.9	5.6	32.7	17.8	39.4	141.7	1.6	3.1	1.8	1.3	1.4	1.5	1.2	3.0
210	2.1	50.9	126.9	13.7	10.8	38.8	38.7	17.5	180.6	2.5	2.6	1.2	1.0	1.3	2.1	1.0	3.6
220	2.2	51.5	140.8	9.5	16.8	42.2	29.2	18.9	159.1	2.6	3.1	1.4	0.6	2.7	1.6	0.8	3.2

Table 16: Experimental Dynamic Stiffnesses at 6,000 rpm and 1.4 MPa

Ω	Ω/ω	Experiment															
		Dynamic Stiffness								Uncertainty							
Hz		$Re(H_{xx})$	$Im(H_{xx})$	$Re(H_{xy})$	$Im(H_{xy})$	$Re(H_{yx})$	$Im(H_{yx})$	$Re(H_{yy})$	$Im(H_{yy})$	$Re(U_{xx})$	$Im(U_{xx})$	$Re(U_{xy})$	$Im(U_{xy})$	$Re(U_{yx})$	$Im(U_{yx})$	$Re(U_{yy})$	$Im(U_{yy})$
20	0.2	127.8	10.6	1.8	-0.7	18.0	-15.0	190.7	17.6	1.7	1.3	0.9	0.9	2.6	3.1	1.2	0.9
30	0.3	128.1	19.5	2.0	-2.4	14.9	-12.4	186.5	22.0	1.4	0.9	0.7	0.4	1.9	1.7	1.2	0.6
40	0.4	128.4	27.8	3.0	-4.9	10.3	-7.7	178.5	43.8	1.3	0.8	0.5	0.4	1.6	0.8	1.3	0.7
50	0.5	134.0	35.0	2.2	-6.3	0.0	-13.7	179.7	47.5	1.4	1.0	0.4	0.4	2.2	0.9	1.0	0.8
70	0.7	128.1	47.3	3.9	-9.7	22.2	-8.2	174.3	78.2	1.5	0.9	0.4	0.3	1.9	1.3	0.5	1.4
80	0.8	125.9	56.2	8.1	-10.3	16.6	-13.4	154.7	96.1	1.3	0.9	0.4	0.4	0.9	1.1	1.1	1.2
90	0.9	125.7	62.6	7.2	-12.5	19.1	-8.6	168.8	123.8	1.6	1.3	0.7	0.5	0.4	0.7	1.0	1.6
110	1.1	128.0	78.7	7.2	-9.9	20.2	-7.9	148.6	122.0	1.3	1.7	0.6	0.6	0.6	1.3	0.6	1.9
130	1.3	121.9	96.6	9.4	-10.7	34.9	-15.8	147.5	138.9	1.2	2.1	0.7	0.8	1.2	0.5	1.3	1.6
140	1.4	122.6	107.0	16.0	-14.9	41.6	-18.8	137.1	178.4	1.6	2.5	0.8	0.6	1.4	0.8	1.0	2.1
150	1.5	121.6	114.3	12.5	-14.9	47.2	-23.8	148.8	171.9	1.1	2.5	1.0	1.0	1.9	1.0	1.4	2.0
160	1.6	128.5	122.2	17.0	-13.9	35.8	-10.0	125.6	194.6	1.1	1.9	1.3	0.9	1.6	1.4	1.4	2.4
170	1.7	131.7	134.5	18.3	-18.3	29.2	-22.5	122.3	221.4	2.6	3.0	1.6	1.2	1.1	1.2	1.4	2.7
190	1.9	133.7	145.9	17.5	-15.2	45.9	-18.0	133.1	231.5	1.6	3.1	1.8	1.3	1.4	1.5	1.2	3.0
210	2.1	140.2	156.6	26.8	-14.1	60.8	-8.6	101.9	286.4	2.5	2.6	1.2	1.0	1.3	2.1	1.0	3.6
220	2.2	148.5	171.5	27.5	-2.1	64.3	-14.6	95.9	262.0	2.6	3.1	1.4	0.6	2.7	1.6	0.8	3.2

Table 17: Experimental Dynamic Stiffnesses at 6,000 rpm and 1.7 MPa

Ω	Ω/ω	Experiment															
		Dynamic Stiffness								Uncertainty							
Hz		$Re(H_{xx})$	$Im(H_{xx})$	$Re(H_{xy})$	$Im(H_{xy})$	$Re(H_{yx})$	$Im(H_{yx})$	$Re(H_{yy})$	$Im(H_{yy})$	$Re(U_{xx})$	$Im(U_{xx})$	$Re(U_{xy})$	$Im(U_{xy})$	$Re(U_{yx})$	$Im(U_{yx})$	$Re(U_{yy})$	$Im(U_{yy})$
20	0.2	155.2	7.8	-4.3	-1.4	9.5	-13.0	250.1	17.8	1.7	1.3	0.9	0.9	2.6	3.1	1.2	0.9
30	0.3	153.4	18.6	-3.8	-3.9	3.4	-13.8	246.3	21.6	1.4	0.9	0.7	0.4	1.9	1.7	1.2	0.6
40	0.4	154.5	29.4	-3.3	-7.7	1.8	-9.6	238.4	46.2	1.3	0.8	0.5	0.4	1.6	0.8	1.3	0.7
50	0.5	161.4	35.7	-3.9	-10.0	-8.4	-16.9	238.4	49.7	1.4	1.0	0.4	0.4	2.2	0.9	1.0	0.8
70	0.7	155.4	49.8	-3.0	-15.0	20.9	-13.9	231.2	83.4	1.5	0.9	0.4	0.3	1.9	1.3	0.5	1.4
80	0.8	152.6	59.6	0.7	-16.5	17.2	-20.6	215.5	102.4	1.3	0.9	0.4	0.4	0.9	1.1	1.1	1.2
90	0.9	153.5	65.2	-0.4	-19.5	22.4	-16.1	226.6	134.1	1.6	1.3	0.7	0.5	0.4	0.7	1.0	1.6
110	1.1	157.7	79.7	0.1	-17.3	14.4	-14.6	198.7	133.4	1.3	1.7	0.6	0.6	0.6	1.3	0.6	1.9
130	1.3	152.1	97.5	2.4	-18.5	30.5	-27.1	196.5	152.9	1.2	2.1	0.7	0.8	1.2	0.5	1.3	1.6
140	1.4	153.6	108.7	8.6	-25.2	36.8	-34.3	189.7	201.4	1.6	2.5	0.8	0.6	1.4	0.8	1.0	2.1
150	1.5	151.5	114.7	6.0	-22.3	41.8	-39.3	198.8	187.8	1.1	2.5	1.0	1.0	1.9	1.0	1.4	2.0
160	1.6	157.4	120.4	10.9	-27.1	35.5	-25.6	184.7	226.6	1.1	1.9	1.3	0.9	1.6	1.4	1.4	2.4
170	1.7	160.7	132.5	10.9	-28.3	25.5	-37.6	178.9	246.9	2.6	3.0	1.6	1.2	1.1	1.2	1.4	2.7
190	1.9	161.6	142.7	10.4	-22.0	41.0	-36.2	186.7	251.2	1.6	3.1	1.8	1.3	1.4	1.5	1.2	3.0
210	2.1	166.8	154.1	20.9	-21.6	55.0	-31.5	159.8	299.5	2.5	2.6	1.2	1.0	1.3	2.1	1.0	3.6
220	2.2	175.4	167.3	25.9	-11.5	58.4	-34.4	149.1	276.3	2.6	3.1	1.4	0.6	2.7	1.6	0.8	3.2

Table 18: Experimental Dynamic Stiffnesses at 8,000 rpm and 1 MPa

Ω	Ω/ω	Experiment															
		Dynamic Stiffness								Uncertainty							
Hz		$Re(H_{xx})$	$Im(H_{xx})$	$Re(H_{xy})$	$Im(H_{xy})$	$Re(H_{yx})$	$Im(H_{yx})$	$Re(H_{yy})$	$Im(H_{yy})$	$Re(U_{xx})$	$Im(U_{xx})$	$Re(U_{xy})$	$Im(U_{xy})$	$Re(U_{yx})$	$Im(U_{yx})$	$Re(U_{yy})$	$Im(U_{yy})$
20	0.2	84.9	5.8	0.6	0.3	27.9	-11.4	103.1	15.0	1.7	1.3	0.9	0.9	2.6	3.1	1.2	0.9
30	0.2	84.2	10.9	0.7	-0.4	24.8	-13.0	108.4	19.5	1.4	0.9	0.7	0.4	1.9	1.7	1.2	0.6
40	0.3	82.7	18.2	-0.1	-1.0	20.9	-8.4	100.5	29.0	1.3	0.8	0.5	0.4	1.6	0.8	1.3	0.7
50	0.4	85.6	25.2	-1.0	-0.7	15.9	-11.6	101.4	38.7	1.4	1.0	0.4	0.4	2.2	0.9	1.0	0.8
70	0.5	82.7	40.1	-0.1	0.0	21.7	-3.5	96.9	51.9	1.5	0.9	0.4	0.3	1.9	1.3	0.5	1.4
80	0.6	85.4	43.7	4.2	1.7	15.6	-2.3	70.4	79.9	1.3	0.9	0.4	0.4	0.9	1.1	1.1	1.2
90	0.7	84.9	49.5	2.0	1.7	17.7	-0.3	93.5	76.3	1.6	1.3	0.7	0.5	0.4	0.7	1.0	1.6
110	0.8	84.0	53.0	2.1	2.3	25.4	0.4	89.4	82.6	1.3	1.7	0.6	0.6	0.6	1.3	0.6	1.9
130	1.0	82.5	58.1	2.4	3.0	20.4	2.9	84.2	83.2	1.2	2.1	0.7	0.8	1.2	0.5	1.3	1.6
140	1.1	75.5	70.4	8.3	7.6	35.3	4.7	78.8	118.7	1.6	2.5	0.8	0.6	1.4	0.8	1.0	2.1
150	1.1	72.4	76.9	11.7	3.7	39.9	1.2	94.0	115.5	1.1	2.5	1.0	1.0	1.9	1.0	1.4	2.0
160	1.2	75.5	90.8	13.6	7.8	22.6	10.1	60.8	133.0	1.1	1.9	1.3	0.9	1.6	1.4	1.4	2.4
170	1.3	71.6	102.7	17.8	6.4	24.4	3.0	70.8	145.1	2.6	3.0	1.6	1.2	1.1	1.2	1.4	2.7
190	1.4	72.0	115.7	18.2	3.1	38.3	6.5	76.2	148.5	1.6	3.1	1.8	1.3	1.4	1.5	1.2	3.0
210	1.6	76.2	122.9	18.5	5.8	37.5	14.2	54.7	152.1	2.5	2.6	1.2	1.0	1.3	2.1	1.0	3.6
220	1.7	78.2	127.7	21.7	2.1	52.9	12.9	73.0	181.7	2.6	3.1	1.4	0.6	2.7	1.6	0.8	3.2

Table 19: Experimental Dynamic Stiffnesses at 8,000 rpm and 1.4 MPa

Ω	Ω/ϖ	Experiment															
		Dynamic Stiffness								Uncertainty							
Hz		Re(H_{xx})	Im(H_{xx})	Re(H_{xy})	Im(H_{xy})	Re(H_{yx})	Im(H_{yx})	Re(H_{yy})	Im(H_{yy})	Re(U_{xx})	Im(U_{xx})	Re(U_{xy})	Im(U_{xy})	Re(U_{yx})	Im(U_{yx})	Re(U_{yy})	Im(U_{yy})
20	0.2	112.8	15.5	-4.3	-0.4	24.9	-25.7	151.0	16.4	1.7	1.3	0.9	0.9	2.6	3.1	1.2	0.9
30	0.2	113.9	20.6	-3.8	-1.5	19.2	-22.7	153.9	25.5	1.4	0.9	0.7	0.4	1.9	1.7	1.2	0.6
40	0.3	112.8	26.5	-0.8	-1.8	15.0	-17.6	143.6	36.4	1.3	0.8	0.5	0.4	1.6	0.8	1.3	0.7
50	0.4	117.1	34.9	-2.5	-5.4	4.0	-24.2	145.8	45.6	1.4	1.0	0.4	0.4	2.2	0.9	1.0	0.8
70	0.5	116.5	45.0	-0.9	-2.4	20.2	-9.6	144.2	69.0	1.5	0.9	0.4	0.3	1.9	1.3	0.5	1.4
80	0.6	120.1	49.3	3.3	-1.1	9.0	-10.2	130.6	83.1	1.3	0.9	0.4	0.4	0.9	1.1	1.1	1.2
90	0.7	120.6	53.5	2.5	-3.3	9.7	-4.4	143.3	102.2	1.6	1.3	0.7	0.5	0.4	0.7	1.0	1.6
110	0.8	120.5	57.3	1.7	-3.4	20.5	-2.1	137.6	106.2	1.3	1.7	0.6	0.6	0.6	1.3	0.6	1.9
130	1.0	118.7	59.8	2.5	-3.0	15.6	1.2	127.3	104.6	1.2	2.1	0.7	0.8	1.2	0.5	1.3	1.6
140	1.1	109.3	76.3	7.7	0.7	37.2	-8.0	127.4	143.7	1.6	2.5	0.8	0.6	1.4	0.8	1.0	2.1
150	1.1	104.2	81.1	10.4	-3.5	44.7	-8.9	142.8	133.3	1.1	2.5	1.0	1.0	1.9	1.0	1.4	2.0
160	1.2	106.5	92.7	12.3	-1.7	32.3	3.3	124.0	157.8	1.1	1.9	1.3	0.9	1.6	1.4	1.4	2.4
170	1.3	106.8	108.5	20.0	-1.7	23.5	-10.1	119.3	173.4	2.6	3.0	1.6	1.2	1.1	1.2	1.4	2.7
190	1.4	108.7	120.4	21.3	-3.8	40.9	-6.0	121.9	169.2	1.6	3.1	1.8	1.3	1.4	1.5	1.2	3.0
210	1.6	112.0	130.7	22.3	-0.9	45.7	0.5	98.0	178.5	2.5	2.6	1.2	1.0	1.3	2.1	1.0	3.6
220	1.7	114.2	134.0	28.5	-5.2	61.0	-1.7	107.8	208.9	2.6	3.1	1.4	0.6	2.7	1.6	0.8	3.2

Table 20: Experimental Dynamic Stiffnesses at 8,000 rpm and 1.7 MPa

Ω	Ω/ϖ	Experiment															
		Dynamic Stiffness								Uncertainty							
Hz		Re(H_{xx})	Im(H_{xx})	Re(H_{xy})	Im(H_{xy})	Re(H_{yx})	Im(H_{yx})	Re(H_{yy})	Im(H_{yy})	Re(U_{xx})	Im(U_{xx})	Re(U_{xy})	Im(U_{xy})	Re(U_{yx})	Im(U_{yx})	Re(U_{yy})	Im(U_{yy})
20	0.2	144.0	16.9	-8.3	-2.7	19.6	-23.8	217.7	24.3	1.7	1.3	0.9	0.9	2.6	3.1	1.2	0.9
30	0.2	147.3	23.6	-8.3	-2.1	10.0	-23.2	211.0	25.2	1.4	0.9	0.7	0.4	1.9	1.7	1.2	0.6
40	0.3	144.2	29.9	-5.4	-4.5	7.7	-19.8	210.2	49.0	1.3	0.8	0.5	0.4	1.6	0.8	1.3	0.7
50	0.4	151.7	38.6	-9.4	-5.5	-7.0	-28.5	208.0	51.7	1.4	1.0	0.4	0.4	2.2	0.9	1.0	0.8
70	0.5	151.8	48.5	-4.7	-6.9	13.0	-16.5	208.9	79.7	1.5	0.9	0.4	0.3	1.9	1.3	0.5	1.4
80	0.6	153.4	53.9	-0.9	-7.7	0.4	-17.2	199.4	95.3	1.3	0.9	0.4	0.4	0.9	1.1	1.1	1.2
90	0.7	153.5	57.2	0.6	-10.9	2.2	-11.0	207.4	126.4	1.6	1.3	0.7	0.5	0.4	0.7	1.0	1.6
110	0.8	153.0	62.4	-1.3	-10.4	14.4	-10.2	204.1	120.1	1.3	1.7	0.6	0.6	0.6	1.3	0.6	1.9
130	1.0	153.1	65.1	-0.2	-10.3	11.1	-5.5	186.6	125.8	1.2	2.1	0.7	0.8	1.2	0.5	1.3	1.6
140	1.1	143.1	86.0	8.0	-9.6	33.7	-22.8	185.5	168.9	1.6	2.5	0.8	0.6	1.4	0.8	1.0	2.1
150	1.1	139.5	92.0	8.9	-11.4	41.9	-21.7	193.5	156.4	1.1	2.5	1.0	1.0	1.9	1.0	1.4	2.0
160	1.2	143.5	101.1	12.6	-15.3	34.9	-10.4	193.6	199.1	1.1	1.9	1.3	0.9	1.6	1.4	1.4	2.4
170	1.3	146.4	116.5	16.8	-17.4	20.6	-26.2	186.8	203.2	2.6	3.0	1.6	1.2	1.1	1.2	1.4	2.7
190	1.4	148.0	126.6	17.7	-17.0	39.5	-24.2	182.7	196.6	1.6	3.1	1.8	1.3	1.4	1.5	1.2	3.0
210	1.6	151.4	134.9	22.4	-16.5	47.2	-17.8	154.7	217.8	2.5	2.6	1.2	1.0	1.3	2.1	1.0	3.6
220	1.7	153.5	139.0	24.5	-15.7	58.8	-23.7	165.9	235.5	2.6	3.1	1.4	0.6	2.7	1.6	0.8	3.2

Table 21: Experimental Dynamic Stiffnesses at 8,000 rpm and 1.9 MPa

Ω	Ω/ϖ	Experiment															
		Dynamic Stiffness								Uncertainty							
Hz		Re(H_{xx})	Im(H_{xx})	Re(H_{xy})	Im(H_{xy})	Re(H_{yx})	Im(H_{yx})	Re(H_{yy})	Im(H_{yy})	Re(U_{xx})	Im(U_{xx})	Re(U_{xy})	Im(U_{xy})	Re(U_{yx})	Im(U_{yx})	Re(U_{yy})	Im(U_{yy})
20	0.2	163.3	17.2	-11.5	-2.4	12.3	-24.4	267.9	25.2	1.7	1.3	0.9	0.9	2.6	3.1	1.2	0.9
30	0.2	167.3	25.0	-11.2	-3.7	3.2	-25.6	258.6	27.8	1.4	0.9	0.7	0.4	1.9	1.7	1.2	0.6
40	0.3	163.3	31.1	-8.9	-5.0	0.2	-21.4	259.8	50.0	1.3	0.8	0.5	0.4	1.6	0.8	1.3	0.7
50	0.4	172.2	39.3	-11.6	-8.1	-17.3	-30.2	255.3	52.7	1.4	1.0	0.4	0.4	2.2	0.9	1.0	0.8
70	0.5	172.6	49.2	-8.6	-10.9	4.4	-21.3	255.8	82.4	1.5	0.9	0.4	0.3	1.9	1.3	0.5	1.4
80	0.6	172.7	55.7	-3.9	-12.4	-8.5	-20.9	247.6	99.0	1.3	0.9	0.4	0.4	0.9	1.1	1.1	1.2
90	0.7	172.8	58.6	-4.7	-16.0	-6.8	-15.6	256.0	133.7	1.6	1.3	0.7	0.5	0.4	0.7	1.0	1.6
110	0.8	172.5	64.0	-5.2	-15.2	7.7	-14.3	249.3	126.7	1.3	1.7	0.6	0.6	0.6	1.3	0.6	1.9
130	1.0	173.6	66.2	-3.4	-13.4	5.0	-8.8	230.4	132.0	1.2	2.1	0.7	0.8	1.2	0.5	1.3	1.6
140	1.1	163.1	88.1	2.7	-11.8	28.3	-32.0	227.6	169.2	1.6	2.5	0.8	0.6	1.4	0.8	1.0	2.1
150	1.1	160.4	94.2	4.5	-15.7	37.6	-29.7	232.3	165.5	1.1	2.5	1.0	1.0	1.9	1.0	1.4	2.0
160	1.2	164.7	101.6	8.4	-24.9	32.7	-17.9	242.7	227.6	1.1	1.9	1.3	0.9	1.6	1.4	1.4	2.4
170	1.3	168.1	115.8	11.0	-24.8	16.0	-33.2	229.6	216.4	2.6	3.0	1.6	1.2	1.1	1.2	1.4	2.7
190	1.4	168.8	125.5	13.0	-22.0	37.0	-32.7	218.2	210.0	1.6	3.1	1.8	1.3	1.4	1.5	1.2	3.0
210	1.6	172.3	134.1	18.6	-22.5	46.4	-28.4	192.4	233.2	2.5	2.6	1.2	1.0	1.3	2.1	1.0	3.6
220	1.7	173.9	137.8	19.6	-21.9	55.5	-36.5	205.4	248.6	2.6	3.1	1.4	0.6	2.7	1.6	0.8	3.2

Table 22: Experimental Dynamic Stiffnesses at 10,000 rpm and 1.4 MPa

Ω	Ω/ϖ	Experiment															
		Dynamic Stiffness								Uncertainty							
Hz		$Re(H_{xx})$	$Im(H_{xx})$	$Re(H_{xy})$	$Im(H_{xy})$	$Re(H_{yx})$	$Im(H_{yx})$	$Re(H_{yy})$	$Im(H_{yy})$	$Re(U_{xx})$	$Im(U_{xx})$	$Re(U_{xy})$	$Im(U_{xy})$	$Re(U_{yx})$	$Im(U_{yx})$	$Re(U_{yy})$	$Im(U_{yy})$
20	0.1	112.8	10.4	-7.6	-4.5	15.2	-3.0	143.9	19.3	1.7	1.3	0.9	0.9	2.6	3.1	1.2	0.9
30	0.2	107.6	24.1	-9.3	-6.1	32.6	-4.4	140.7	22.3	1.4	0.9	0.7	0.4	1.9	1.7	1.2	0.6
40	0.2	117.3	25.7	-10.8	-5.3	21.7	-4.1	141.4	38.8	1.3	0.8	0.5	0.4	1.6	0.8	1.3	0.7
50	0.3	131.6	37.7	-14.8	-6.9	-0.1	-35.2	145.0	43.0	1.4	1.0	0.4	0.4	2.2	0.9	1.0	0.8
70	0.4	121.8	43.0	-13.9	-3.7	17.4	-20.7	143.9	64.0	1.5	0.9	0.4	0.3	1.9	1.3	0.5	1.4
80	0.5	126.0	38.0	-10.4	-0.9	-1.4	-10.3	132.4	73.4	1.3	0.9	0.4	0.4	0.9	1.1	1.1	1.2
90	0.5	126.7	37.2	-12.3	1.0	-0.9	3.0	145.6	92.8	1.6	1.3	0.7	0.5	0.4	0.7	1.0	1.6
110	0.7	114.7	52.1	-10.8	0.5	8.7	-4.7	140.3	92.1	1.3	1.7	0.6	0.6	0.6	1.3	0.6	1.9
130	0.8	117.8	48.7	-9.2	3.7	8.6	6.4	128.5	90.3	1.2	2.1	0.7	0.8	1.2	0.5	1.3	1.6
140	0.8	113.8	70.0	-4.8	4.8	28.0	-3.8	133.8	101.5	1.6	2.5	0.8	0.6	1.4	0.8	1.0	2.1
150	0.9	125.6	70.7	-0.9	6.9	26.0	-8.3	129.6	132.1	1.1	2.5	1.0	1.0	1.9	1.0	1.4	2.0
160	1.0	118.8	77.3	2.3	6.8	38.8	-7.4	136.3	118.7	1.1	1.9	1.3	0.9	1.6	1.4	1.4	2.4
170	1.0	123.3	84.9	2.2	6.3	29.8	0.7	128.9	143.1	2.6	3.0	1.6	1.2	1.1	1.2	1.4	2.7
190	1.1	114.8	98.5	12.6	7.9	30.4	-3.8	131.9	143.9	1.6	3.1	1.8	1.3	1.4	1.5	1.2	3.0
210	1.3	119.0	107.4	18.2	10.5	34.5	0.6	108.0	155.3	2.5	2.6	1.2	1.0	1.3	2.1	1.0	3.6
220	1.3	116.8	108.9	22.2	8.6	40.1	8.1	112.9	176.9	2.6	3.1	1.4	0.6	2.7	1.6	0.8	3.2

Table 23: Experimental Dynamic Stiffnesses at 10,000 rpm and 1.7 MPa

Ω	Ω/ϖ	Experiment															
		Dynamic Stiffness								Uncertainty							
Hz		$Re(H_{xx})$	$Im(H_{xx})$	$Re(H_{xy})$	$Im(H_{xy})$	$Re(H_{yx})$	$Im(H_{yx})$	$Re(H_{yy})$	$Im(H_{yy})$	$Re(U_{xx})$	$Im(U_{xx})$	$Re(U_{xy})$	$Im(U_{xy})$	$Re(U_{yx})$	$Im(U_{yx})$	$Re(U_{yy})$	$Im(U_{yy})$
20	0.1	137.2	13.0	-10.4	-6.0	18.2	-12.5	182.4	24.2	1.7	1.3	0.9	0.9	2.6	3.1	1.2	0.9
30	0.2	132.2	25.2	-12.1	-7.6	30.4	-9.2	177.7	26.7	1.4	0.9	0.7	0.4	1.9	1.7	1.2	0.6
40	0.2	140.3	28.1	-14.1	-6.9	18.3	-10.5	181.2	45.5	1.3	0.8	0.5	0.4	1.6	0.8	1.3	0.7
50	0.3	154.0	39.3	-17.7	-8.1	-7.7	-40.1	183.5	48.4	1.4	1.0	0.4	0.4	2.2	0.9	1.0	0.8
70	0.4	147.2	44.8	-17.2	-6.1	9.2	-27.9	184.3	74.0	1.5	0.9	0.4	0.3	1.9	1.3	0.5	1.4
80	0.5	147.8	39.1	-13.4	-3.0	-7.2	-14.5	175.9	84.0	1.3	0.9	0.4	0.4	0.9	1.1	1.1	1.2
90	0.5	148.1	37.2	-15.1	-1.1	-5.2	1.3	188.7	106.4	1.6	1.3	0.7	0.5	0.4	0.7	1.0	1.6
110	0.7	140.5	51.9	-14.2	-1.3	3.3	-5.0	182.3	104.3	1.3	1.7	0.6	0.6	0.6	1.3	0.6	1.9
130	0.8	140.5	49.6	-11.2	2.2	5.5	3.7	167.7	104.3	1.2	2.1	0.7	0.8	1.2	0.5	1.3	1.6
140	0.8	134.4	71.8	-5.7	3.0	27.0	-9.4	174.0	116.7	1.6	2.5	0.8	0.6	1.4	0.8	1.0	2.1
150	0.9	146.4	73.2	0.2	3.0	24.2	-15.0	167.6	151.1	1.1	2.5	1.0	1.0	1.9	1.0	1.4	2.0
160	1.0	139.1	81.1	2.1	4.0	38.9	-16.5	176.3	133.9	1.1	1.9	1.3	0.9	1.6	1.4	1.4	2.4
170	1.0	144.6	88.7	2.3	2.3	28.9	-8.6	175.5	167.9	2.6	3.0	1.6	1.2	1.1	1.2	1.4	2.7
190	1.1	137.4	103.2	13.3	2.5	30.6	-11.5	172.1	163.1	1.6	3.1	1.8	1.3	1.4	1.5	1.2	3.0
210	1.3	142.1	112.6	20.5	5.8	37.3	-9.3	151.0	175.0	2.5	2.6	1.2	1.0	1.3	2.1	1.0	3.6
220	1.3	141.0	114.1	25.2	1.6	42.3	-3.7	149.3	195.1	2.6	3.1	1.4	0.6	2.7	1.6	0.8	3.2

Table 24: Experimental Dynamic Stiffnesses at 10,000 rpm and 1.9 MPa

Ω	Ω/ϖ	Experiment															
		Dynamic Stiffness								Uncertainty							
Hz		$Re(H_{xx})$	$Im(H_{xx})$	$Re(H_{xy})$	$Im(H_{xy})$	$Re(H_{yx})$	$Im(H_{yx})$	$Re(H_{yy})$	$Im(H_{yy})$	$Re(U_{xx})$	$Im(U_{xx})$	$Re(U_{xy})$	$Im(U_{xy})$	$Re(U_{yx})$	$Im(U_{yx})$	$Re(U_{yy})$	$Im(U_{yy})$
20	0.1	156.6	15.5	-14.5	-7.4	16.1	-16.8	226.0	28.6	1.7	1.3	0.9	0.9	2.6	3.1	1.2	0.9
30	0.2	153.7	26.1	-16.4	-8.5	24.9	-13.1	221.9	29.7	1.4	0.9	0.7	0.4	1.9	1.7	1.2	0.6
40	0.2	160.2	30.7	-18.0	-7.8	14.0	-15.7	225.5	50.9	1.3	0.8	0.5	0.4	1.6	0.8	1.3	0.7
50	0.3	174.0	40.1	-21.4	-9.3	-15.2	-43.6	227.1	54.6	1.4	1.0	0.4	0.4	2.2	0.9	1.0	0.8
70	0.4	171.5	48.5	-20.7	-9.4	-0.6	-35.8	228.5	82.9	1.5	0.9	0.4	0.3	1.9	1.3	0.5	1.4
80	0.5	168.9	43.0	-17.0	-6.1	-16.5	-19.0	223.0	93.6	1.3	0.9	0.4	0.4	0.9	1.1	1.1	1.2
90	0.5	168.9	40.5	-18.6	-4.5	-11.2	-2.8	235.3	117.7	1.6	1.3	0.7	0.5	0.4	0.7	1.0	1.6
110	0.7	164.5	54.2	-17.2	-4.4	-4.4	-7.9	228.3	115.6	1.3	1.7	0.6	0.6	0.6	1.3	0.6	1.9
130	0.8	162.9	53.1	-13.3	-0.6	0.7	-1.5	210.0	117.7	1.2	2.1	0.7	0.8	1.2	0.5	1.3	1.6
140	0.8	157.0	76.5	-7.2	-0.6	22.1	-16.5	216.3	129.2	1.6	2.5	0.8	0.6	1.4	0.8	1.0	2.1
150	0.9	168.3	76.9	-1.4	-2.3	19.4	-23.5	213.5	163.3	1.1	2.5	1.0	1.0	1.9	1.0	1.4	2.0
160	1.0	160.6	86.7	0.4	-2.6	34.9	-24.4	215.6	147.6	1.1	1.9	1.3	0.9	1.6	1.4	1.4	2.4
170	1.0	166.7	94.5	-0.1	-6.5	25.2	-16.9	223.4	195.4	2.6	3.0	1.6	1.2	1.1	1.2	1.4	2.7
190	1.1	160.7	107.3	13.3	-4.8	28.2	-19.7	210.5	179.5	1.6	3.1	1.8	1.3	1.4	1.5	1.2	3.0
210	1.3	165.7	117.7	18.3	-3.4	36.5	-17.5	191.0	200.0	2.5	2.6	1.2	1.0	1.3	2.1	1.0	3.6
220	1.3	165.5	118.9	23.3	-6.8	43.3	-15.6	192.6	208.6	2.6	3.1	1.4	0.6	2.7	1.6	0.8	3.2

Table 25: Experimental Dynamic Stiffnesses at 10,000 rpm and 2.2 MPa

Ω	Ω/ϖ	Experiment															
		Dynamic Stiffness								Uncertainty							
Hz		$Re(H_{xx})$	$Im(H_{xx})$	$Re(H_{xy})$	$Im(H_{xy})$	$Re(H_{yx})$	$Im(H_{yx})$	$Re(H_{yy})$	$Im(H_{yy})$	$Re(U_{xx})$	$Im(U_{xx})$	$Re(U_{xy})$	$Im(U_{xy})$	$Re(U_{yx})$	$Im(U_{yx})$	$Re(U_{yy})$	$Im(U_{yy})$
20	0.1	180.1	19.2	-20.6	-9.7	9.4	-21.1	284.4	33.3	1.7	1.3	0.9	0.9	2.6	3.1	1.2	0.9
30	0.2	179.0	27.6	-22.7	-9.6	13.0	-15.5	280.1	32.1	1.4	0.9	0.7	0.4	1.9	1.7	1.2	0.6
40	0.2	182.4	34.8	-24.3	-11.5	4.4	-21.4	285.7	57.5	1.3	0.8	0.5	0.4	1.6	0.8	1.3	0.7
50	0.3	197.0	43.4	-29.4	-14.4	-26.3	-46.8	287.0	62.1	1.4	1.0	0.4	0.4	2.2	0.9	1.0	0.8
70	0.4	199.3	52.4	-26.9	-14.6	-13.3	-42.1	287.4	93.1	1.5	0.9	0.4	0.3	1.9	1.3	0.5	1.4
80	0.5	194.8	47.4	-23.8	-12.5	-29.0	-23.6	282.8	104.1	1.3	0.9	0.4	0.4	0.9	1.1	1.1	1.2
90	0.5	192.1	43.5	-23.8	-9.6	-19.1	-7.6	297.8	129.2	1.6	1.3	0.7	0.5	0.4	0.7	1.0	1.6
110	0.7	192.2	56.0	-22.3	-10.6	-14.0	-12.4	286.7	127.8	1.3	1.7	0.6	0.6	0.6	1.3	0.6	1.9
130	0.8	187.8	57.7	-18.2	-6.5	-6.1	-9.2	264.0	131.3	1.2	2.1	0.7	0.8	1.2	0.5	1.3	1.6
140	0.8	184.6	82.2	-11.0	-8.9	12.3	-25.7	271.3	145.2	1.6	2.5	0.8	0.6	1.4	0.8	1.0	2.1
150	0.9	192.1	82.2	-4.5	-14.3	11.4	-34.4	270.0	182.3	1.1	2.5	1.0	1.0	1.9	1.0	1.4	2.0
160	1.0	185.9	93.6	-2.9	-11.5	26.7	-35.9	268.8	163.8	1.1	1.9	1.3	0.9	1.6	1.4	1.4	2.4
170	1.0	193.7	100.9	-1.7	-24.2	17.6	-26.4	285.1	257.6	2.6	3.0	1.6	1.2	1.1	1.2	1.4	2.7
190	1.1	190.1	111.9	5.5	-18.0	21.3	-31.0	264.1	199.2	1.6	3.1	1.8	1.3	1.4	1.5	1.2	3.0
210	1.3	194.2	123.0	13.9	-17.6	30.7	-29.5	238.9	220.9	2.5	2.6	1.2	1.0	1.3	2.1	1.0	3.6
220	1.3	195.5	123.5	18.2	-18.4	41.1	-30.2	251.1	229.9	2.6	3.1	1.4	0.6	2.7	1.6	0.8	3.2

Table 26: Experimental Dynamic Stiffnesses at 12,000 rpm and 0.7 MPa

Ω	Ω/ϖ	Experiment															
		Dynamic Stiffness								Uncertainty							
Hz		$Re(H_{xx})$	$Im(H_{xx})$	$Re(H_{xy})$	$Im(H_{xy})$	$Re(H_{yx})$	$Im(H_{yx})$	$Re(H_{yy})$	$Im(H_{yy})$	$Re(U_{xx})$	$Im(U_{xx})$	$Re(U_{xy})$	$Im(U_{xy})$	$Re(U_{yx})$	$Im(U_{yx})$	$Re(U_{yy})$	$Im(U_{yy})$
20	0.1	60.9	1.4	-16.0	-4.4	8.1	7.1	68.9	10.0	1.7	1.3	0.9	0.9	2.6	3.1	1.2	0.9
30	0.2	67.3	2.5	-18.8	-7.0	2.8	8.0	67.1	11.4	1.4	0.9	0.7	0.4	1.9	1.7	1.2	0.6
40	0.2	60.7	9.5	-18.0	-5.7	4.9	4.9	67.5	17.5	1.3	0.8	0.5	0.4	1.6	0.8	1.3	0.7
50	0.3	58.3	15.3	-16.8	-8.5	5.0	-1.9	67.0	17.8	1.4	1.0	0.4	0.4	2.2	0.9	1.0	0.8
70	0.4	55.6	19.6	-17.4	-8.8	12.7	4.3	61.8	30.9	1.5	0.9	0.4	0.3	1.9	1.3	0.5	1.4
80	0.4	58.2	21.6	-16.0	-8.4	9.4	4.6	51.8	54.3	1.3	0.9	0.4	0.4	0.9	1.1	1.1	1.2
90	0.5	52.1	27.3	-18.3	-7.3	11.2	4.6	60.8	45.8	1.6	1.3	0.7	0.5	0.4	0.7	1.0	1.6
110	0.6	52.4	29.8	-17.8	-8.4	14.8	4.0	58.0	51.6	1.3	1.7	0.6	0.6	0.6	1.3	0.6	1.9
130	0.7	49.1	34.7	-18.2	-11.6	11.8	5.8	47.4	50.9	1.2	2.1	0.7	0.8	1.2	0.5	1.3	1.6
140	0.7	49.8	43.0	-14.2	-13.2	21.5	0.8	49.9	59.2	1.6	2.5	0.8	0.6	1.4	0.8	1.0	2.1
150	0.8	45.5	46.1	-14.0	-8.9	24.3	1.8	46.5	73.7	1.1	2.5	1.0	1.0	1.9	1.0	1.4	2.0
160	0.8	44.2	49.3	-9.1	-11.7	25.3	-0.7	43.5	68.1	1.1	1.9	1.3	0.9	1.6	1.4	1.4	2.4
170	0.9	41.0	52.2	-14.2	-16.1	21.4	5.9	48.9	82.7	2.6	3.0	1.6	1.2	1.1	1.2	1.4	2.7
190	1.0	43.1	57.9	-11.9	-8.9	17.2	-0.3	42.9	88.9	1.6	3.1	1.8	1.3	1.4	1.5	1.2	3.0
210	1.1	41.0	68.4	-4.6	-13.2	25.0	-1.1	39.1	87.9	2.5	2.6	1.2	1.0	1.3	2.1	1.0	3.6
220	1.1	41.9	78.2	-8.8	-8.5	28.7	5.4	25.2	111.4	2.6	3.1	1.4	0.6	2.7	1.6	0.8	3.2

Table 27: Experimental Dynamic Stiffnesses at 12,000 rpm and 1.4 MPa

Ω	Ω/ϖ	Experiment															
		Dynamic Stiffness								Uncertainty							
Hz		$Re(H_{xx})$	$Im(H_{xx})$	$Re(H_{xy})$	$Im(H_{xy})$	$Re(H_{yx})$	$Im(H_{yx})$	$Re(H_{yy})$	$Im(H_{yy})$	$Re(U_{xx})$	$Im(U_{xx})$	$Re(U_{xy})$	$Im(U_{xy})$	$Re(U_{yx})$	$Im(U_{yx})$	$Re(U_{yy})$	$Im(U_{yy})$
20	0.1	111.5	19.0	-17.5	-4.9	20.2	-3.8	146.8	13.9	1.7	1.3	0.9	0.9	2.6	3.1	1.2	0.9
30	0.2	113.2	23.9	-17.2	-5.6	17.3	-12.3	143.3	17.2	1.4	0.9	0.7	0.4	1.9	1.7	1.2	0.6
40	0.2	121.5	23.3	-21.2	-7.9	3.7	-5.2	146.6	32.0	1.3	0.8	0.5	0.4	1.6	0.8	1.3	0.7
50	0.3	137.0	21.9	-24.4	-6.3	-18.1	-6.0	149.9	31.2	1.4	1.0	0.4	0.4	2.2	0.9	1.0	0.8
70	0.4	123.1	36.6	-23.7	-6.9	5.8	-4.2	145.2	49.7	1.5	0.9	0.4	0.3	1.9	1.3	0.5	1.4
80	0.4	122.4	33.5	-22.2	-3.2	3.0	-6.8	132.3	59.7	1.3	0.9	0.4	0.4	0.9	1.1	1.1	1.2
90	0.5	126.3	34.7	-27.4	-5.0	4.9	0.6	145.2	77.8	1.6	1.3	0.7	0.5	0.4	0.7	1.0	1.6
110	0.6	117.3	44.7	-23.3	-4.0	6.7	-5.6	139.4	76.5	1.3	1.7	0.6	0.6	0.6	1.3	0.6	1.9
130	0.7	121.1	39.3	-22.6	-1.6	4.5	4.4	127.6	76.7	1.2	2.1	0.7	0.8	1.2	0.5	1.3	1.6
140	0.7	120.9	54.5	-18.0	-0.4	26.9	-3.3	127.2	88.0	1.6	2.5	0.8	0.6	1.4	0.8	1.0	2.1
150	0.8	119.0	52.4	-16.9	3.8	18.4	-17.1	125.7	112.5	1.1	2.5	1.0	1.0	1.9	1.0	1.4	2.0
160	0.8	120.7	63.5	-12.9	2.2	34.2	-15.5	125.6	106.2	1.1	1.9	1.3	0.9	1.6	1.4	1.4	2.4
170	0.9	117.6	66.8	-14.9	1.8	24.9	-8.2	126.0	126.8	2.6	3.0	1.6	1.2	1.1	1.2	1.4	2.7
190	1.0	114.2	73.2	-8.6	3.5	7.0	-15.0	124.4	133.7	1.6	3.1	1.8	1.3	1.4	1.5	1.2	3.0
210	1.1	113.7	84.0	-2.2	5.5	22.2	-11.5	124.2	131.1	2.5	2.6	1.2	1.0	1.3	2.1	1.0	3.6
220	1.1	115.7	93.1	6.8	7.2	25.2	-8.4	100.7	160.4	2.6	3.1	1.4	0.6	2.7	1.6	0.8	3.2

Table 28: Experimental Dynamic Stiffnesses at 12,000 rpm and 1.7 MPa

Ω	Ω/ϖ	Experiment															
		Dynamic Stiffness								Uncertainty							
Hz		$\mathrm{Re}(H_{xx})$	$\mathrm{Im}(H_{xx})$	$\mathrm{Re}(H_{xy})$	$\mathrm{Im}(H_{xy})$	$\mathrm{Re}(H_{yx})$	$\mathrm{Im}(H_{yx})$	$\mathrm{Re}(H_{yy})$	$\mathrm{Im}(H_{yy})$	$\mathrm{Re}(U_{xx})$	$\mathrm{Im}(U_{xx})$	$\mathrm{Re}(U_{xy})$	$\mathrm{Im}(U_{xy})$	$\mathrm{Re}(U_{yx})$	$\mathrm{Im}(U_{yx})$	$\mathrm{Re}(U_{yy})$	$\mathrm{Im}(U_{yy})$
20	0.1	137.4	21.5	-27.5	-4.7	13.9	-3.7	190.3	17.5	1.7	1.3	0.9	0.9	2.6	3.1	1.2	0.9
30	0.2	139.4	25.5	-28.1	-5.2	13.9	-15.5	185.6	22.9	1.4	0.9	0.7	0.4	1.9	1.7	1.2	0.6
40	0.2	147.1	26.3	-30.4	-5.1	1.4	-9.3	188.8	37.4	1.3	0.8	0.5	0.4	1.6	0.8	1.3	0.7
50	0.3	159.4	27.4	-32.8	-4.6	-21.5	-13.3	193.2	38.2	1.4	1.0	0.4	0.4	2.2	0.9	1.0	0.8
70	0.4	150.8	41.4	-31.1	-5.2	-0.2	-13.2	189.3	60.8	1.5	0.9	0.4	0.3	1.9	1.3	0.5	1.4
80	0.4	149.9	39.1	-27.8	-2.7	-6.2	-13.7	178.7	72.9	1.3	0.9	0.4	0.4	0.9	1.1	1.1	1.2
90	0.5	152.8	38.3	-30.0	-2.0	-1.6	-7.0	188.3	91.7	1.6	1.3	0.7	0.5	0.4	0.7	1.0	1.6
110	0.6	146.9	49.6	-28.3	-1.9	-1.5	-10.9	183.7	90.0	1.3	1.7	0.6	0.6	0.6	1.3	0.6	1.9
130	0.7	148.5	46.1	-26.1	1.4	-2.6	-4.9	171.0	90.5	1.2	2.1	0.7	0.8	1.2	0.5	1.3	1.6
140	0.7	152.2	57.9	-20.9	2.7	26.5	-4.4	170.4	100.0	1.6	2.5	0.8	0.6	1.4	0.8	1.0	2.1
150	0.8	146.6	56.8	-16.3	2.6	19.5	-29.9	167.1	136.4	1.1	2.5	1.0	1.0	1.9	1.0	1.4	2.0
160	0.8	150.1	65.3	-13.5	2.0	36.9	-25.7	168.7	122.3	1.1	1.9	1.3	0.9	1.6	1.4	1.4	2.4
170	0.9	147.4	70.6	-15.0	-1.8	28.0	-18.9	173.0	155.0	2.6	3.0	1.6	1.2	1.1	1.2	1.4	2.7
190	1.0	142.7	78.3	-8.4	1.6	4.9	-27.8	167.6	158.6	1.6	3.1	1.8	1.3	1.4	1.5	1.2	3.0
210	1.1	142.0	90.0	-3.6	3.7	18.3	-22.6	169.5	150.4	2.5	2.6	1.2	1.0	1.3	2.1	1.0	3.6
220	1.1	142.3	99.3	6.7	3.3	21.2	-22.0	145.2	183.3	2.6	3.1	1.4	0.6	2.7	1.6	0.8	3.2

Table 29: Experimental Dynamic Stiffnesses at 12,000 rpm and 1.9 MPa

Ω	Ω/ϖ	Experiment															
		Dynamic Stiffness								Uncertainty							
Hz		$\mathrm{Re}(H_{xx})$	$\mathrm{Im}(H_{xx})$	$\mathrm{Re}(H_{xy})$	$\mathrm{Im}(H_{xy})$	$\mathrm{Re}(H_{yx})$	$\mathrm{Im}(H_{yx})$	$\mathrm{Re}(H_{yy})$	$\mathrm{Im}(H_{yy})$	$\mathrm{Re}(U_{xx})$	$\mathrm{Im}(U_{xx})$	$\mathrm{Re}(U_{xy})$	$\mathrm{Im}(U_{xy})$	$\mathrm{Re}(U_{yx})$	$\mathrm{Im}(U_{yx})$	$\mathrm{Re}(U_{yy})$	$\mathrm{Im}(U_{yy})$
20	0.1	159.0	21.2	-33.8	-4.6	5.9	-5.3	229.9	21.5	1.7	1.3	0.9	0.9	2.6	3.1	1.2	0.9
30	0.2	160.5	26.8	-33.7	-5.4	9.6	-18.4	224.3	27.3	1.4	0.9	0.7	0.4	1.9	1.7	1.2	0.6
40	0.2	167.0	28.3	-35.6	-4.9	-3.4	-12.4	228.1	44.4	1.3	0.8	0.5	0.4	1.6	0.8	1.3	0.7
50	0.3	178.9	29.4	-37.9	-4.2	-26.3	-17.7	231.8	45.6	1.4	1.0	0.4	0.4	2.2	0.9	1.0	0.8
70	0.4	174.1	44.6	-36.4	-5.6	-6.9	-20.9	228.8	71.0	1.5	0.9	0.4	0.3	1.9	1.3	0.5	1.4
80	0.4	172.3	41.9	-31.9	-3.5	-15.0	-18.1	220.3	82.3	1.3	0.9	0.4	0.4	0.9	1.1	1.1	1.2
90	0.5	175.3	40.4	-34.1	-2.6	-10.6	-10.6	230.5	105.2	1.6	1.3	0.7	0.5	0.4	0.7	1.0	1.6
110	0.6	171.3	52.2	-32.8	-2.4	-10.9	-13.9	226.2	103.4	1.3	1.7	0.6	0.6	0.6	1.3	0.6	1.9
130	0.7	170.0	48.5	-29.6	1.5	-7.0	-8.7	210.1	104.3	1.2	2.1	0.7	0.8	1.2	0.5	1.3	1.6
140	0.7	174.4	58.8	-22.9	2.2	25.6	-5.8	210.1	113.9	1.6	2.5	0.8	0.6	1.4	0.8	1.0	2.1
150	0.8	167.8	59.4	-16.6	2.3	15.9	-38.2	208.0	148.5	1.1	2.5	1.0	1.0	1.9	1.0	1.4	2.0
160	0.8	172.0	68.2	-13.2	0.1	36.4	-33.4	208.0	137.3	1.1	1.9	1.3	0.9	1.6	1.4	1.4	2.4
170	0.9	169.7	74.1	-15.9	-7.6	27.4	-26.8	220.3	185.1	2.6	3.0	1.6	1.2	1.1	1.2	1.4	2.7
190	1.0	165.2	81.9	-9.1	-3.3	1.5	-36.4	208.8	176.7	1.6	3.1	1.8	1.3	1.4	1.5	1.2	3.0
210	1.1	164.3	94.8	-3.6	-2.1	13.6	-30.3	207.6	170.3	2.5	2.6	1.2	1.0	1.3	2.1	1.0	3.6
220	1.1	165.2	102.8	6.8	-2.0	17.4	-32.0	188.2	202.4	2.6	3.1	1.4	0.6	2.7	1.6	0.8	3.2

Table 30: Experimental Dynamic Stiffnesses at 12,000 rpm and 2.2 MPa

Ω	Ω/ϖ	Experiment															
		Dynamic Stiffness								Uncertainty							
Hz		$\mathrm{Re}(H_{xx})$	$\mathrm{Im}(H_{xx})$	$\mathrm{Re}(H_{xy})$	$\mathrm{Im}(H_{xy})$	$\mathrm{Re}(H_{yx})$	$\mathrm{Im}(H_{yx})$	$\mathrm{Re}(H_{yy})$	$\mathrm{Im}(H_{yy})$	$\mathrm{Re}(U_{xx})$	$\mathrm{Im}(U_{xx})$	$\mathrm{Re}(U_{xy})$	$\mathrm{Im}(U_{xy})$	$\mathrm{Re}(U_{yx})$	$\mathrm{Im}(U_{yx})$	$\mathrm{Re}(U_{yy})$	$\mathrm{Im}(U_{yy})$
20	0.1	178.6	23.2	-39.9	-5.0	0.7	-5.5	270.1	24.7	1.7	1.3	0.9	0.9	2.6	3.1	1.2	0.9
30	0.2	180.5	27.5	-40.7	-5.0	6.7	-20.6	263.5	31.6	1.4	0.9	0.7	0.4	1.9	1.7	1.2	0.6
40	0.2	186.1	30.3	-41.6	-5.3	-5.2	-17.8	268.8	51.2	1.3	0.8	0.5	0.4	1.6	0.8	1.3	0.7
50	0.3	197.3	32.3	-44.1	-5.1	-28.2	-24.0	273.1	54.4	1.4	1.0	0.4	0.4	2.2	0.9	1.0	0.8
70	0.4	193.8	47.1	-41.3	-6.9	-10.3	-29.1	270.8	82.8	1.5	0.9	0.4	0.3	1.9	1.3	0.5	1.4
80	0.4	196.0	46.5	-38.3	-4.9	-24.9	-28.0	262.6	95.2	1.3	0.9	0.4	0.4	0.9	1.1	1.1	1.2
90	0.5	198.6	40.7	-39.7	-3.5	-19.6	-17.0	275.6	118.6	1.6	1.3	0.7	0.5	0.4	0.7	1.0	1.6
110	0.6	195.0	53.7	-37.7	-2.7	-20.0	-21.5	270.0	117.3	1.3	1.7	0.6	0.6	0.6	1.3	0.6	1.9
130	0.7	187.6	51.6	-33.2	1.1	-12.1	-18.1	252.7	119.5	1.2	2.1	0.7	0.8	1.2	0.5	1.3	1.6
140	0.7	194.8	60.7	-24.7	3.0	20.4	-9.1	253.0	129.1	1.6	2.5	0.8	0.6	1.4	0.8	1.0	2.1
150	0.8	188.4	63.0	-17.5	0.6	13.7	-48.2	250.1	166.4	1.1	2.5	1.0	1.0	1.9	1.0	1.4	2.0
160	0.8	192.5	70.4	-14.4	-1.7	34.9	-42.7	251.0	154.6	1.1	1.9	1.3	0.9	1.6	1.4	1.4	2.4
170	0.9	191.7	79.4	-17.3	-18.4	25.8	-34.8	272.6	250.8	2.6	3.0	1.6	1.2	1.1	1.2	1.4	2.7
190	1.0	186.3	85.9	-7.3	-8.2	-2.7	-46.8	251.6	199.2	1.6	3.1	1.8	1.3	1.4	1.5	1.2	3.0
210	1.1	186.6	99.3	-3.5	-8.2	7.0	-40.0	250.7	190.4	2.5	2.6	1.2	1.0	1.3	2.1	1.0	3.6
220	1.1	187.2	105.3	9.6	-5.1	15.3	-44.8	237.8	222.2	2.6	3.1	1.4	0.6	2.7	1.6	0.8	3.2

Table 31: Experimental Dynamic Stiffnesses at 13,000 rpm and 1.7 MPa

Ω	Ω/ϖ	Experiment															
		Dynamic Stiffness								Uncertainty							
Hz		$Re(H_{xx})$	$Im(H_{xx})$	$Re(H_{xy})$	$Im(H_{xy})$	$Re(H_{yx})$	$Im(H_{yx})$	$Re(H_{yy})$	$Im(H_{yy})$	$Re(U_{xx})$	$Im(U_{xx})$	$Re(U_{xy})$	$Im(U_{xy})$	$Re(U_{yx})$	$Im(U_{yx})$	$Re(U_{yy})$	$Im(U_{yy})$
20	0.1	135.7	18.4	-23.1	-5.3	20.9	-8.0	169.8	14.3	1.7	1.3	0.9	0.9	2.6	3.1	1.2	0.9
30	0.1	133.5	22.7	-24.2	-5.2	16.4	-14.3	172.8	21.6	1.4	0.9	0.7	0.4	1.9	1.7	1.2	0.6
40	0.2	143.8	23.4	-27.8	-8.3	1.1	-13.3	171.3	36.7	1.3	0.8	0.5	0.4	1.6	0.8	1.3	0.7
50	0.2	157.8	25.7	-31.0	-7.4	-17.4	-14.4	177.9	40.2	1.4	1.0	0.4	0.4	2.2	0.9	1.0	0.8
70	0.3	144.2	38.4	-29.8	-7.2	-0.8	-13.2	173.7	57.1	1.5	0.9	0.4	0.3	1.9	1.3	0.5	1.4
80	0.4	146.2	37.1	-28.7	-3.5	-5.5	-11.2	161.9	67.0	1.3	0.9	0.4	0.4	0.9	1.1	1.1	1.2
90	0.4	148.0	35.8	-33.2	-3.8	-0.6	-5.4	174.7	84.3	1.6	1.3	0.7	0.5	0.4	0.7	1.0	1.6
110	0.5	144.0	44.2	-29.9	-3.8	2.2	-10.2	166.2	85.7	1.3	1.7	0.6	0.6	0.6	1.3	0.6	1.9
130	0.6	141.8	38.3	-26.5	-1.3	1.5	-3.6	156.4	83.7	1.2	2.1	0.7	0.8	1.2	0.5	1.3	1.6
140	0.6	143.4	57.8	-22.6	-0.3	17.5	-3.9	155.0	93.5	1.6	2.5	0.8	0.6	1.4	0.8	1.0	2.1
150	0.7	145.4	50.8	-22.0	3.8	18.4	-15.7	153.7	123.3	1.1	2.5	1.0	1.0	1.9	1.0	1.4	2.0
160	0.7	147.3	63.6	-15.1	2.8	31.8	-18.3	157.6	113.3	1.1	1.9	1.3	0.9	1.6	1.4	1.4	2.4
170	0.8	141.8	66.9	-18.6	0.3	23.5	-10.5	156.9	136.1	2.6	3.0	1.6	1.2	1.1	1.2	1.4	2.7
190	0.9	133.5	67.8	-10.6	4.4	9.6	-21.0	150.9	144.4	1.6	3.1	1.8	1.3	1.4	1.5	1.2	3.0
210	1.0	134.9	82.1	-4.1	4.6	21.5	-19.6	151.9	145.0	2.5	2.6	1.2	1.0	1.3	2.1	1.0	3.6
220	1.0	143.1	88.0	-0.3	7.2	24.4	-20.9	130.8	146.4	2.6	3.1	1.4	0.6	2.7	1.6	0.8	3.2

Table 32: Experimental Dynamic Stiffnesses at 13,000 rpm and 1.9 MPa

Ω	Ω/ϖ	Experiment															
		Dynamic Stiffness								Uncertainty							
Hz		$Re(H_{xx})$	$Im(H_{xx})$	$Re(H_{xy})$	$Im(H_{xy})$	$Re(H_{yx})$	$Im(H_{yx})$	$Re(H_{yy})$	$Im(H_{yy})$	$Re(U_{xx})$	$Im(U_{xx})$	$Re(U_{xy})$	$Im(U_{xy})$	$Re(U_{yx})$	$Im(U_{yx})$	$Re(U_{yy})$	$Im(U_{yy})$
20	0.1	157.4	21.4	-33.1	-5.1	16.8	-9.6	210.9	17.6	1.7	1.3	0.9	0.9	2.6	3.1	1.2	0.9
30	0.1	158.1	24.6	-33.8	-5.2	10.6	-15.4	213.4	24.7	1.4	0.9	0.7	0.4	1.9	1.7	1.2	0.6
40	0.2	166.4	25.3	-36.6	-6.2	-3.9	-17.5	212.9	42.0	1.3	0.8	0.5	0.4	1.6	0.8	1.3	0.7
50	0.2	176.7	26.6	-38.8	-4.6	-21.7	-19.7	219.1	47.1	1.4	1.0	0.4	0.4	2.2	0.9	1.0	0.8
70	0.3	171.0	40.9	-37.6	-6.0	-8.4	-22.9	216.5	68.4	1.5	0.9	0.4	0.3	1.9	1.3	0.5	1.4
80	0.4	170.8	38.9	-34.0	-2.5	-14.0	-18.6	205.3	77.8	1.3	0.9	0.4	0.4	0.9	1.1	1.1	1.2
90	0.4	173.0	38.2	-35.8	-2.8	-13.2	-11.3	218.6	95.0	1.6	1.3	0.7	0.5	0.4	0.7	1.0	1.6
110	0.5	169.6	46.5	-34.3	-1.5	-8.6	-17.1	211.0	97.5	1.3	1.7	0.6	0.6	0.6	1.3	0.6	1.9
130	0.6	168.2	43.2	-31.4	1.2	-8.0	-9.7	200.1	96.6	1.2	2.1	0.7	0.8	1.2	0.5	1.3	1.6
140	0.6	169.4	58.6	-25.5	2.0	13.0	-5.0	199.1	104.9	1.6	2.5	0.8	0.6	1.4	0.8	1.0	2.1
150	0.7	169.7	53.3	-21.0	3.8	16.2	-23.4	193.5	136.3	1.1	2.5	1.0	1.0	1.9	1.0	1.4	2.0
160	0.7	172.1	62.9	-17.8	2.1	32.9	-24.7	199.5	125.9	1.1	1.9	1.3	0.9	1.6	1.4	1.4	2.4
170	0.8	169.0	69.2	-19.4	-2.3	27.3	-18.4	203.8	159.9	2.6	3.0	1.6	1.2	1.1	1.2	1.4	2.7
190	0.9	158.4	73.6	-10.0	0.0	7.8	-30.7	192.6	163.0	1.6	3.1	1.8	1.3	1.4	1.5	1.2	3.0
210	1.0	160.0	85.2	-4.4	1.2	16.4	-30.8	193.0	161.5	2.5	2.6	1.2	1.0	1.3	2.1	1.0	3.6
220	1.0	169.7	90.9	0.4	3.8	21.6	-34.0	172.2	167.0	2.6	3.1	1.4	0.6	2.7	1.6	0.8	3.2

Table 33: Experimental Dynamic Stiffnesses at 13,000 rpm and 2.2 MPa

Ω	Ω/ϖ	Experiment															
		Dynamic Stiffness								Uncertainty							
Hz		$Re(H_{xx})$	$Im(H_{xx})$	$Re(H_{xy})$	$Im(H_{xy})$	$Re(H_{yx})$	$Im(H_{yx})$	$Re(H_{yy})$	$Im(H_{yy})$	$Re(U_{xx})$	$Im(U_{xx})$	$Re(U_{xy})$	$Im(U_{xy})$	$Re(U_{yx})$	$Im(U_{yx})$	$Re(U_{yy})$	$Im(U_{yy})$
20	0.1	182.0	22.9	-43.3	-5.9	12.4	-14.0	256.5	24.4	3.2	3.4	1.4	1.7	6.3	5.2	5.3	1.7
30	0.1	183.5	23.2	-43.4	-4.2	5.3	-15.2	260.6	28.1	3.8	2.8	1.1	1.6	4.7	2.9	5.8	2.1
40	0.2	189.0	28.5	-44.7	-5.7	-6.2	-22.7	258.2	50.4	4.0	1.9	0.8	0.7	2.9	0.8	4.5	1.7
50	0.2	198.4	30.6	-46.9	-5.2	-24.5	-27.6	264.7	56.4	4.4	2.0	1.7	1.1	3.6	1.6	4.2	2.1
70	0.3	196.4	44.0	-45.8	-7.0	-12.9	-33.2	262.6	81.5	4.2	2.5	0.9	1.5	2.5	1.6	4.1	2.5
80	0.4	197.7	47.2	-41.5	-6.3	-24.6	-32.2	254.3	93.0	3.1	2.0	1.4	1.4	1.1	1.2	5.5	1.8
90	0.4	201.7	41.5	-43.4	-4.8	-29.2	-18.4	271.4	111.6	3.0	2.1	1.7	1.4	1.0	1.1	6.0	2.5
110	0.5	198.4	50.7	-42.2	-3.1	-21.2	-26.9	260.6	115.9	3.9	2.1	1.5	1.4	0.8	1.4	3.7	3.6
130	0.6	194.8	43.9	-37.8	1.2	-14.3	-11.3	245.7	113.9	3.0	3.3	1.3	1.9	1.7	1.3	4.9	5.5
140	0.6	193.4	65.2	-30.1	0.7	4.2	-7.2	247.6	123.8	3.2	3.3	1.1	2.4	2.3	1.3	4.8	5.7
150	0.7	198.1	58.5	-24.8	1.1	17.3	-31.0	243.0	158.7	3.2	3.3	2.0	2.2	2.8	1.7	7.0	6.4
160	0.7	198.4	69.4	-20.3	-1.6	34.1	-32.2	248.9	144.7	4.6	3.6	2.1	2.7	1.9	1.7	7.1	6.6
170	0.8	196.2	78.6	-24.5	-10.9	30.6	-29.5	262.0	197.0	3.7	3.5	3.1	4.0	1.5	1.4	7.1	6.2
190	0.9	185.1	81.7	-12.9	-6.6	5.0	-44.0	240.7	186.8	5.0	4.2	3.7	3.6	1.7	2.7	3.9	8.7
210	1.0	188.2	97.2	-8.2	-7.1	11.5	-43.9	238.4	182.8	4.1	3.4	2.7	2.5	3.0	3.3	4.2	7.9
220	1.0	202.6	101.2	-3.9	-2.6	17.5	-47.3	219.0	195.4	4.5	2.8	2.0	1.8	2.4	3.0	2.4	6.5

VITA

Name:	John Eric Hensley
Address:	Well Dynamics Inc. 445 Woodline Drive Spring, TX 77386
Email Address:	j.eric.hensley@gmail.com
Education:	B.S., Mechanical Engineering, Texas A&M University, 2003 M.S., Mechanical Engineering, Texas A&M University, 2006